THESIS

UNDERSTANDING THE MOLECULAR BASIS OF INSECT PEST RESISTANCE IN *TRITICUM AESTIVUM* USING MASS SPECTROMETRY

Submitted by

Florent D. Lavergne

Department of Horticulture and Landscape Architecture

In partial fulfillment of the requirements

For the Degree of Master of Science

Colorado State University

Fort Collins, Colorado

Fall 2018

Master's Committee:

Advisor: Adam Heuberger

Corey Broeckling
Stephen Pearce
Courtney Jahn

ABSTRACT

UNDERSTANDING THE MOLECULAR BASIS OF INSECT PEST RESISTANCE IN *TRITICUM AESTIVUM* USING MASS SPECTROMETRY

Bread wheat (*Triticum aestivum* L.) is a global staple crop and controlling for environmental stress that impacts grain yield is critical. Recently, Wheat Stem Sawfly (*Cephus cinctus*, hereafter WSS) has emerged as a new pest of wheat and is expanding across the Great Plains and southern United States. WSS is difficult to control using chemical, cultural or biological pest management methods. Currently, wheat breeders utilize a solid-stem trait to inhibit larval feeding and reduce lodging, however this trait only confers partial resistance and is thought to reduce grain yield. Models of metabolic-based resistance with demonstrated impact on reduction of insect pest fitness have been documented. Here, I investigate the broader hypothesis that wheat resistance to WSS is mediated by shifts in metabolism that promote avoidance and toxicity towards WSS. Four cultivars with contrasting phenotypes are used in our studies: Hatcher (resistant to WSS, hollow-stem, winter wheat); Conan (resistant, semi-solid-stem, spring); Denali (susceptible, hollow-stem, winter); and Reeder (susceptible, hollow-stem, spring).

The first part of this work involved gas chromatography-mass spectrometry (GC-MS) metabolomics methods to provide a comprehensive characterization of the chemical composition of wheat cuticular waxes. A total of 263 putative compounds were detected among the four abovementioned wheat cultivars and comprised 58 wax compounds including alkanes and fatty acids. Many of the detected wax metabolites have known associations to important biological functions such as insect pest and drought resistance. Uni- and multivariate statistics were used to

evaluate metabolite distribution between tissue types (leaf, stem) and cultivars. Leaves contained more primary alcohols than stems such as 6-methylheptacosan-1-ol and octacosan-1-ol. The metabolite data were complemented using scanning electron microscopy of epicuticular wax crystals which detected wax tubules and platelets. Conan (resistant to WSS) was the only cultivar to display alcohol-associated platelet-shaped crystals on its abaxial leaf surface.

The second part of this study aimed at evaluating a selection of wheat cultivars in a WSS-infested field. Cultivars with increased yield and reduced WSS infestation values were found. The molecular basis of this resistance was evaluated in a greenhouse study that characterized proteomic and metabolomic signatures of wheat stems associated with WSS infestation. Stem proteins (1832) and metabolites (1823) were detected in the same four wheat cultivars using liquid chromatography-mass spectrometry. During infestation with WSS, 62 proteins and 29 metabolites were differentially regulated in the hollow-stem resistant cultivar Hatcher. Metabolic processes that were associated with resistance included enzymatic detoxification, proteinase inhibition, and anti-herbivory compound production, specifically the benzoxazinoids, neolignans, and phenolics. Compared to the semi-solid and resistant cultivar Conan, hollow-stem Hatcher had increased abundance of proteins and metabolites with known roles in plant defense against insects.

These results will be invaluable to plant breeders as they contribute to the understanding of wax composition and metabolic regulation associated with important phenotypic traits in a major crop, including passive and active defense mechanisms to WSS.

ACKNOWLEDGEMENTS

First, I wish to thank all my committee members, Adam L. Heuberger, Courtney E. Jahn, Corey D. Broeckling, and Stephen Pearce, for their unlimited support and for providing all the help I needed to achieve my goals. Adam and Courtney both greatly contributed to making this journey a reality and graduate from CSU, and I am profusely grateful for their support and investment. Likewise, I want to thank the Colorado Wheat Research Foundation, the Colorado State University Agricultural Experiment Station, and more specifically Scott D. Haley who provided funding and supported my research.

These years spend in Fort Collins have been punctuated with beautiful encounters with people from all horizons, both professionally and in my personal life. These people include my lab/research teammates, Harmonie M. Bettenhausen, Nate M. Sindt, Sahar Bagheri Toulabi, Jackie M. Chaparro, and many others. I also had the chance to mingle with foreigners from various cultures and I would like to thank Denis, Eliakim, Tom, and Marc for opening my mind and helping me see things from a different perspective. And all those I have met during the last three years and will always have a place in my heart and memories, thank you.

I wish to acknowledge all members of my family, specifically my mom and dad, Martine and Francis, who always have and always will support my decisions should I decide to leave hometown for a place far, far away. My childhood friends also, especially Morgan that I might soon rejoin with in Germany. This work is dedicated to my passed grandmother, Paulette, whom nothing would give greater joy than witnessing our personal achievements.

TABLE OF CONTENTS

LIST OF TABLES

LIST OF FIGURES

CHAPTER 1 – INTRODUCTION

1.1. Bread Wheat Is an Important Global Food Crop

Managing pest outbreaks is a critical component of national food security. Bread wheat (*Triticum aestivum* L., Poaceae) is a widely grown staple crop that provides approximately 20% of a typical daily caloric intake [1,2]. As of 2017, *T. aestivum* ranks third among United States (US) field crops in planted acreage, production, and gross farm receipts, with annual outputs that reach 700 million metric tons [3]. The United States Department of Agriculture (USDA) annual statistical bulletin ranked the state of Colorado as the sixth largest winter wheat producer, representing nearly 6% of national production [3]. To continue a steady food production in the face of projected population growth, it is however critical to understand how to achieve optimal grain yield in the presence of biotic and abiotic stresses [4,5]. Wheat is indeed affected by biotic and abiotic pressure that reduces grain yield, with insect pest infestations representing up to 20% of annual losses [6].

1.2. The Wheat Stem Sawfly Is a Major Pest of *Triticum aestivum*

1.2.1. Wheat Stem Sawfly Rapid Expansion Is Associated with Severe Wheat Yield Losses

An important economic insect pest of wheat is the Wheat Stem Sawfly (WSS hereafter), *Cephus cinctus* Norton (Hymenoptera: Cephidae). *C. cinctus* infestations were first described in 1872 from specimens of native grass in Colorado [7]. A host jump to spring wheat (i.e., varieties that do not need to vernalize, are planted in the spring and harvested in late summer of the same year), more than a century ago, resulted in dramatic expansion of the grass feeding insect distribution across the Northern Great Plains and South Canada [8,9]. For clarification, the term "variety" will be used throughout the manuscript to designate both "cultivars" (also termed

cultivated varieties, including the four wheat cultivars evaluated in our studies) and “advanced breeding lines”. Vernalization describes the induction of a plant's flowering process by exposure to the prolonged cold of winter. Cultivars and advanced breeding lines are obtained using distinct breeding techniques that will not be detailed here. Spring wheat is extensively grown in North America but remains difficult to produce in dryland areas such as Colorado, where farmers typically grow winter varieties (i.e., varieties planted in the autumn, remain in the vegetative phase and vernalize during the winter, resume growth in early spring and are harvested in the summer of the following year). Benefits of growing winter wheat over spring wheat in Colorado include superior management of soil moisture under dry climates, reduced soil erosion, and improved out-competition of weed varieties. While WSS exclusively infested spring wheat in early periods of expansion, a second episode of host jump, that affected winter wheat this time, was reported in the early 1980s. Winter wheat phenology differs from that of spring varieties, and it is believed that *C. cinctus* adaptation to winter wheat was enabled by synchronization of emergence patterns to exploit this host. Research indicates rich genetic diversity among specimens of WSS from across the world, and distinct haplotypes identified in North America suggest phenotypic variation that promotes rapid adaptation to new hosts, and potential signs of expansion across the continent [10]. Recent field studies conducted on winter wheat in Colorado indicate southward expansion of the WSS habitat and support its ability to colonize both spring and winter wheat at an alarming pace, which breeders and growers are poorly prepared for (Figure 1A,B) [11].

Most of the WSS life cycle is spent in larval stages, and larval feeding causes major tissue damage (Figure 1C). Pupated individuals emerge and mate in the spring, and females oviposit (i.e., deposit eggs) shortly thereafter (within 10 days) on wheat stems [12]. Females use

their saw-like ovipositor to cut through the stem and insert a single egg. Selection of plant host relies upon a number of attributes as suggested by Buteler et al. (2009), that includes stem diameter and height, and emission of attracting volatile compounds (i.e., semiochemicals) [13]. By the sixth or seventh day after oviposition, larvae break free of their egg sac and enter the stem cavity [14]. Over the course of the summer season, hatched WSS larvae chew through inner stem tissue, otherwise known as stem-boring activity, downwards to reach soil level [15]. A V-shaped notch is sliced inside the stem at crown level and used as protection by the overwintering insect. Larvae pupate during the next spring season and adults leave stubs to start a new cycle (Figure 1C).

Stem-cutting and boring activities are responsible for most damage from WSS larvae in wheat, causing annual yield losses up to 350 million US dollars in North America [8]. Indeed, newly hatched larvae feed upon wheat parenchyma tissue and vascular bundles, causing major reduction in photosynthetic capacity and subsequent decrease in kernel weight [16]. Stem cutting induces further yield loss as plant lodging hampers mechanical harvesting [17,18].

1.2.2. Development of Larvae Inside Stems Limits the Efficacy of Control Strategies

The life cycle of *C. cinctus* involves an extended period of up to ten months per year spent within the host stem. Early control tactics thus aimed at targeting larvae through destruction of wheat stubble (i.e., cut parts left sticking aboveground after the grain is harvested) [14]. However, burning of wheat stubble results in little to no WSS larval death, increased soil erosion due to removal of residue, and decreased numbers of WSS natural enemies (i.e., parasitoids) that are usually housed within aboveground parts of the plant. Tillage through ploughing of infested stubble does not offer complete control on WSS adult emergence either,

promotes erosion of soils, and threatens the developments of WSS parasitoids *Bracon cephi* and *Bracon lissogaster* [14,19].

Cropping practices have been explored to limit WSS infestations and include the use of trap crops in fallow lands. The large variety of suitable hosts for WSS includes rye (*Lolium perenne*), brome (*Bromus inermis*), and barley (*Hordeum vulgare*) grasses. Sawfly adults in a field of mixed species show little to no preference for a specific host and wheat infestations are hence diluted. However, many producers still favor continuous cropping practices and do not wish to fallow their fields. Alternatively, trap crops can be sown at field borders to intercept WSS, however, success of this strategy remains limited under high sawfly pressure [8]. Wheat row spacing and seeding rates also influence WSS numbers. Variation in canopy density modifies light penetration and thus alters stem pith expression (a phenotypic trait related to WSS resistance that will be discussed further) and moisture levels, yet again, studies report insufficient results in the field [20]. Other cultural practices include delayed seeding dates and crop nutrient management. While altering sowing dates lowers exposure to WSS due to plants being immature and unsuitable hosts at periods of high sawfly pressure, this practice can be detrimental as delayed planting correlates with less efficient use of soil moisture, resulting in reduced grain yield [21]. Likewise, the stochastic nature of soil-plant fertility dynamics prevents the reproducibility of studies on nutrient supplemented wheat to control WSS attacks [22]. Success of control management that relies on pesticides and pest parasitism is diminished by the extended WSS adult emergence (three to six weeks) and the time larvae spend inside wheat stems [8]. Heptachlor is the only chemical that induces consistent death of larvae upon application. However, due to an extended persistence in the environment and potential harm to ecosystems, this organochlorine-based insecticide was banned from the US more than 30 years

ago. As previously mentioned, natural enemies of WSS in wheat include *B. cephi* and *B. lissogaster*. Although studies have shown significant reduction in yield losses upon parasitic activity, other means of control (e.g., cultural practices, pesticides) contribute to great reduction of parasitoid numbers [13]. Plant phenology, and environmental conditions that include temperature and soil moisture, also contribute to the success of WSS parasitoid development and may explain the relative absence of *B. cephi* and *B. lissogaster* in Colorado fields.

1.2.3. The Widely Used Solid-Stem Trait Is Associated with Inconsistent Field Performance

Mitigation of *C. cinctus* populations often relies upon host genetic resistance using solid-stemmed cultivars [23,24]. A great majority of spring and winter wheat cultivars with solid stems derive from S-615, the first wheat line to exhibit the qualitative solid-stem trait [25]. Comparative studies on hollow- and solid-stem cultivars reveal an anti-herbivory potential for this trait [26]. Mechanical pressure induced by pith development as well as excessive moisture levels within solid stems increase egg mortality. Moreover, high expression of pith filling appears to have a deterring effect as it affects host preference and reduces WSS oviposition [27].

The major quantitative trait locus (QTL) for stem solidness (i.e., *Qss.msub-3BL*) has been identified and shown to control most of the variation in stem pith formation [28]. A study conducted on a population of recombinant inbred lines (RIL) derived from a solid- by hollow-stemmed winter wheat cross indicated that *Qss.msub-3BL* was responsible for 76% of the variation in stem pith expression. However, wheat plants that carry the major stem solidness locus show relative inconsistency in pith expression and yield performance under fluctuating weather conditions [29]. While intense sunlight offers maximum pith expression, cloudy conditions or shading elements decrease stem pith development. It is believed that the solid-stem

trait itself is accompanied by yield reduction, as a fitness penalty is observed in plants that allocate high amounts of energy for pith expression instead of grain filling.

1.3. Wheat Molecular Resistance to Biotic Stress Is Both Passive and Active

1.3.1. The Plant Cuticle as a Natural Barrier: Composition, Structure and Function

In plants, changes in the chemical composition of tissues facilitate stress tolerance. Insects and pathogens create physical contact with the plant through organ surfaces (e.g., leaves and stems). The outermost layer of leaf and stem cells is known as the cuticle and controls water retention during episodes of fluctuating atmospheric humidity, soil moisture, and temperature (Figure 2A) [30-32]. The cuticle is an extracellular matrix that contains high levels of the simple polymer cutin and a variety of lipids. The lipids are herein referred to as "waxes" and usually termed epicuticular waxes in the literature [33]. Waxes result from the metabolism of long-chain lipids and include alkanes, fatty acids, primary and secondary alcohols, and ketones (Figure 2B) [34].

The role of waxes in biotic stress tolerance is critical as they create a natural barrier against pest and pathogen penetration through passive resistance (i.e., constitutive presence of structural barriers that also includes trichomes, hairs and resins) [33-35]. A deterring potential for cuticular alcohols and fatty acids has been observed in the cabbage (*Brassica oleracea*)/ Diamondback Moth (*Plutella xylostella*) system, and resistance to the pest is facilitated by increased biosynthesis of these lipids [36]. Likewise, abiotic stress, including drought episodes, is mitigated by the glaucousness levels of the cuticle (i.e., bluish-green appearance on the surface). Wax composition (e.g., proportions of ketones and primary alcohols) and content have been demonstrated to correlate with glaucousness [37-41].

Scanning electron microscopy (SEM) studies reveal the three-dimensional crystal micromorphology of waxes, and the "platelet" and "tubule" types are distributed among all major groups of plants, including the Poaceae (Figure 2C) [39,42]. The chemical composition of waxes is associated with the type of wax crystal, and platelets are mostly composed of primary alcohols [39], whereas tubules are high in content of β-diketones in *Triticum* species [42,43].

1.3.2. Enzymes and Metabolites Are Critical Actors of the Molecular Defense Response

Genetic and molecular responses that relate to plant–insect interactions have been largely explored. Direct defenses aim at reducing host suitability and insect fitness through mechanical protection (i.e., passive resistance, with epicuticular waxes as an example) and production of toxic and repelling compounds (i.e., active resistance, includes direct and indirect defenses) such as alkaloids, phenolics, benzoxazinoids, and volatile organic compounds (VOCs; Figure 3) [44,45]. Induced indirect defenses promote parasitism of pest herbivores through release of attractants such as VOCs, production of nectar and housing of natural enemies [44,46]. Upon selection of a suitable host, herbivorous pests make physical contact with the plant epicuticle and often puncture tissue to either feed or deposit eggs. Insect activity is perceived through release of damage- and herbivore-associated molecular patterns (DAMPs and HAMPs; Figure 3). Triggered immunity is set up once insect effectors have been recognized by plant receptors (e.g., NBS-LRR domain-containing proteins), and both direct and indirect defenses may be elicited [47,48]. The hypersensitive response has been documented for a variety of plant–insect interactions and aims at restricting foreign tissue at the wounding site through local necrosis [49,50]. Simultaneous and subsequent events involve signaling cascades and modulation of metabolism including increased calcium fluxes, oxidative burst and detoxification activities, and up-regulation of wound-induced protein kinases (WIPK), products of specialized metabolism

(formerly known as secondary metabolism; e.g., phytohormones, anti-herbivory compounds), and proteinase inhibitors, among others [44,51]. In the case of chewing insects that attack vascular tissues, the plant's ability to propagate defense signals beyond the initial wounding site (i.e., the oviposition site) is critical to prepare intact areas for potential infestation [52,53]. In addition, insect manipulation of host defenses is documented for many plant/pest systems including the interaction of wheat and WSS. The role of small non-coding RNA (snRNA) sequences in suppressing the wheat response to WSS larval feeding is currently being investigated [54].

Complex molecular networks that involve protein and small molecule actors of plant defense to herbivores have been described. Up-regulation of pathogenesis-related (PR) proteins (e.g., proteinase inhibitors), detoxification enzymes (e.g., peroxidases, glutathiones), and other defense-related proteins (e.g., lectins, remorins) is observed during the incompatible interaction (i.e., unsuccessful infection/infestation by the pathogen/pest; Figure 3) [44,55-57]. However, enzymatic shifts are not restricted to defense-related compounds but also impact pathways involved in energy production and allocation of assimilates [58]. Hence, enzymes with activities related to production of primary and specialized metabolites (e.g., hydroxypyruvate reductases, enzymes of the phenylpropanoid pathway), energy production and allocation (e.g., enzymes involved in photosynthesis and gluconeogenesis), and protein anabolism/catabolism (e.g., tRNA synthetases, ubiquitin-proteasome complexes) are also key factors in the defense response [53,58-60]. Likewise, products of metabolism are differentially regulated in defense to phytophagous insects. Both primary (e.g., amino acids and carbohydrates) and specialized metabolism (e.g., bioactive compounds such as anti-herbivory metabolites) are differentially regulated in this context [44,53]. Anti-herbivory compounds include phytotoxins that are

classified based on their mode of action. The phytoanticipins are constitutively stored in their inactive form in the plant and become toxic upon insect attack through cleavage of a glycosidic bond. Example phytoanticipins are the benzoxazinoid glycosides found in the Poaceae and down-regulation of their inactive form upon biotic stress correlates with overexpression of their toxic variant [61]. Phytoalexins are synthesized de novo upon biotic stress and include a wide range of chemical structures (e.g., alkaloids, benzenoids, phenolics) [53]. Other specialized metabolites are critical to the deployment of the stress response and include phytohormones (e.g., jasmonates, ethylene) and VOCs [47].

1.4. Mass Spectrometry-Based Methods Enable the Detection of Defense Compounds

1.4.1. Detection of Semi-Volatile Waxes Using Gas Chromatography-Mass Spectrometry

In plants, metabolomics is the comprehensive analysis of small molecules (~50–1200 Da), typically involved in primary or specialized metabolism. While waxes are in fact end products of metabolism (they are exuded from leaf and stem cells), they are amenable to analysis by metabolomics methods due to their chemical properties. A common method to evaluate primary metabolites in plants is to extract, derivatize via silylation, and detect metabolites using gas chromatography coupled to mass spectrometry (GC-MS) [62]. Many plant waxes are small and semi-volatile and are also detected using GC-MS [38,40,63-66]. Further, many contain hydroxyl groups that allow for derivatization to improve volatility and detection by GC-MS.

1.4.2. Detection of Proteins and Metabolites Using Liquid Chromatography-Mass Spectrometry

Compared to cuticular waxes, plant anti-herbivory metabolites and peptide compounds usually have a higher mass and are less amenable to volatilization and detection using GC-MS. Metabolomics and proteomics methods to detect anti-herbivory metabolites and enzymes rather rely upon the use of liquid chromatography coupled to mass spectrometry (LC-MS). LC-MS

methods are invaluable for precise determination of metabolite structures and have been applied to research on plant defense compounds and related enzymes [60,61,67].

1.5. Preliminary Studies

1.5.1. Wheat Cultivars Assessed in Preliminary Studies and Further Explored in the Present Work

Hard red spring wheat cultivars "Conan" (PI 607549) and "Reeder" (PI 613586), and hard red winter wheat cultivars "Hatcher" (PI 638512) [68] and "Denali" (PI 664256) [69] were used in both research works described in this manuscript. Spring cultivar Conan displays semi-solid stems (stem pith is expressed at its maximum during early stages of development and regresses as the plant matures) that appear to provide relatively good tolerance to WSS attacks [26,27,70]. It is therefore referred to as a resistant semi-solid spring cultivar. Genotypic/phenotypic details for all four cultivars of interest are provided in Table 1. Conversely to Conan, spring cultivar Reeder has poor stem pith expression throughout the growing season and higher host suitability. Reeder is thus defined as a susceptible hollow-stem cultivar. Both these spring cultivars are largely grown in the Northern Great Plains but unsuitable for production in dryland areas such as Colorado. Hollow-stem winter wheat Hatcher was released in Colorado in 2004, is now widely grown in the state, and a 3-year field study described in Chapter 3 suggests low WSS infestation rates for this cultivar. Denali, also a hollow-stem winter cultivar of wheat, was released in Colorado in 2011 and is susceptible to *C. cinctus*.

Selection of these wheat cultivars was based on the following genotypic and phenotypic traits: (1) degree of resistance to WSS, (2) degree of stem pith expression (stem solidness), (3) growth habit (spring or winter type), and (4) degree of surface glaucousness (bluish-green appearance of the plant surface associated with chemical; Table 1).

1.5.2. Behavior of WSS on a Resistant Cultivar Suggests Presence of Repelling Cuticular Structures and/or Volatile Emissions

Previous research on WSS behavior in response to volatile attractants from wheat, conducted at the Montana State University, indicated oviposition preference on the susceptible cultivar Reeder, over resistant Conan (see Table 1 for cultivar phenotype details) [66]. Similar test conditions were reproduced in our lab using a Y-tube system, but no significance for oviposition preference between the two cultivars was observed. However, a unique grooming behavior pattern was noticed when WSS were residing on Conan. Insects were compulsively cleaning themselves instead of depositing eggs, possibly indicating the presence of a wax surface or volatile irritant. Part one (Chapter 2) of the present study aims at elucidating the chemical composition of wheat cuticular waxes. The *hypothesis* is that WSS resistant Conan has a unique blend of surface metabolites that contribute to defense to insect pests and complement the semi-solid-stem trait.

1.5.3. Wheat Active Responses to WSS Involve Complex Molecular Networks

Literature on the molecular aspects of plant pathology for the wheat/WSS system is relatively scarce. A recent study on the molecular response of wheat to WSS feeding described protein and metabolite variation in the phenylpropanoid and pentose phosphate pathways in wheat cultivars with different levels of resistance to the insect [71]. Reallocation of carbohydrates may, however, be the downstream result of intense damage in susceptible plants rather than an active response that aims at strengthening tissues. In part two (Chapter 3) of the present study, particular interest is pointed towards Hatcher, that displays low stem pith levels during the WSS flight period, yet shows consistent resistance and high yields under sawfly pressure (Table 1). We *hypothesize* that critical metabolic variation occurs in Hatcher in response

to WSS pressure and that it does not rely on the solid-stem trait. Mass spectrometry data supports the quantitative nature of wheat genetic resistance to WSS and provides avenues to breed for resistant phenotypes that do not depend on stem solidness. We also describe a potential model for metabolic resistance in Hatcher.

1.6. Overview

In this study, we combine the amenability of GC- and LC-MS for wax and anti-herbivory metabolites, and proteins, with non-targeted metabolomics and proteomics data processing methods to enable comparisons of four wheat cultivars that differ for resistance to WSS and other phenotypic traits. We provide a comprehensive characterization of the wheat metabolome and proteome and demonstrate variation among cultivars. The data supports the potential to breed for wax traits with demonstrated effects on a variety of biologically relevant phenotypes, including resistance to biotic stress.

Table 1. Cultivars used in our study.

Cultivar	Stem solidness	Response to WSS	Growth habit	Glaucousness level
Conan	Semi-solid	Resistant	Spring wheat	High
Reeder	Hollow	Susceptible	Spring wheat	Low
Hatcher	Hollow	Resistant	Winter wheat	Low
Denali	Hollow	Susceptible	Winter wheat	Low

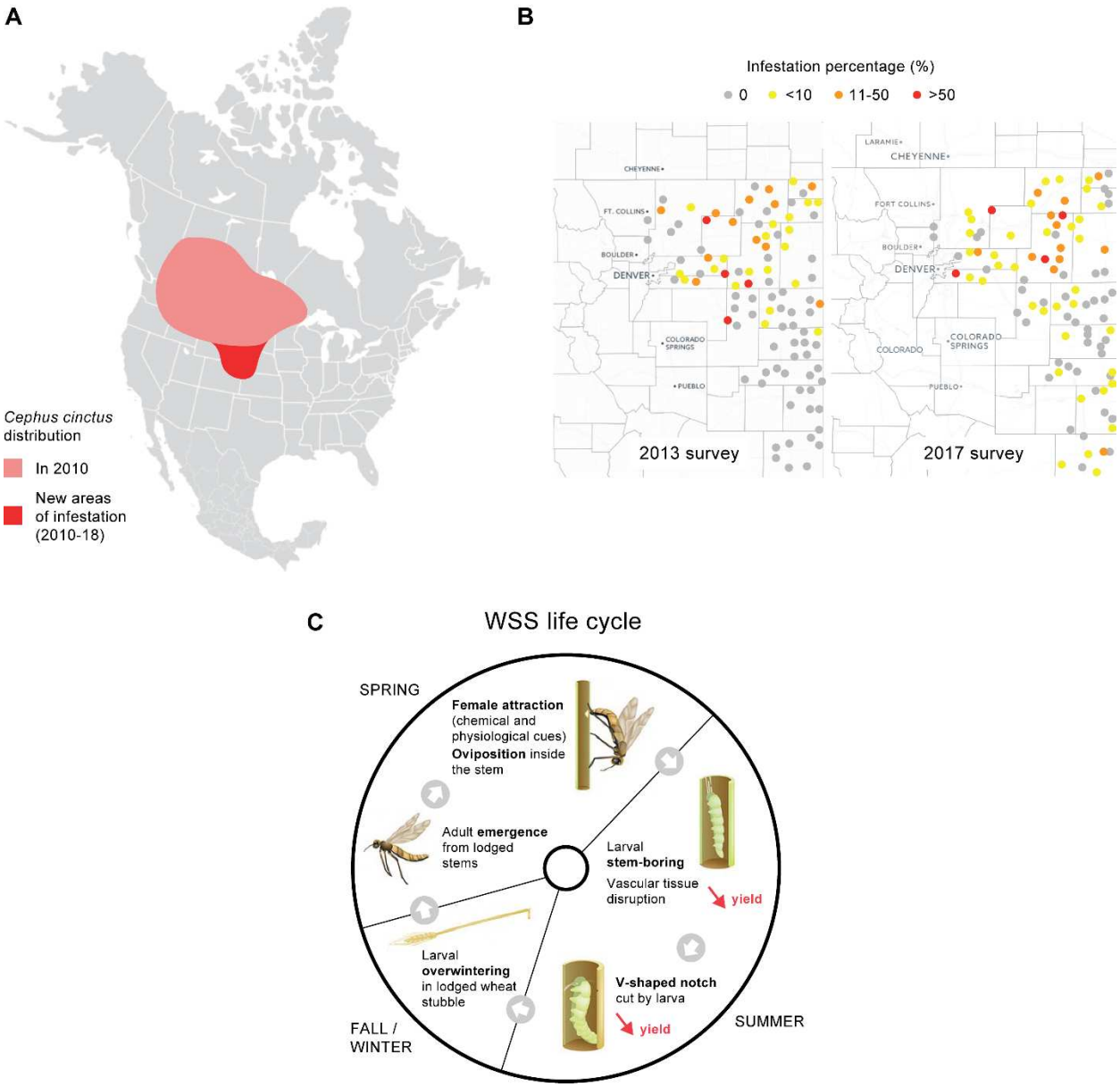

Figure 1. *Cephus cinctus* distribution and life cycle. **(A)** Map of the North American continent showing a widespread distribution of WSS across the Northern Great Plains. Light red indicates area of WSS distribution as of 2010, bright red indicates the most recent southward expansion. **(B)** Comparative maps of WSS progression in Colorado (2013 and 2017 field surveys). Each colored dot represents a different wheat field, and infestation percentages illustrate the proportion of infested wheat plants within a field. **(C)** Diagram of the WSS life cycle that includes the major stages of WSS development, and which are responsible for wheat yield losses (indicated in red). Figures **1A** and **1C** are modified versions of diagrams prepared by Phillip Glogoza, Jochum Wiersma, and Ian McRae [72]. Figure **1B** is a modified version of a map created by Darren M. Cockrell, Frank B. Peairs, and Paul J. Ode upon field observations of WSS infestation in wheat. Notation: ↘ = reduction.

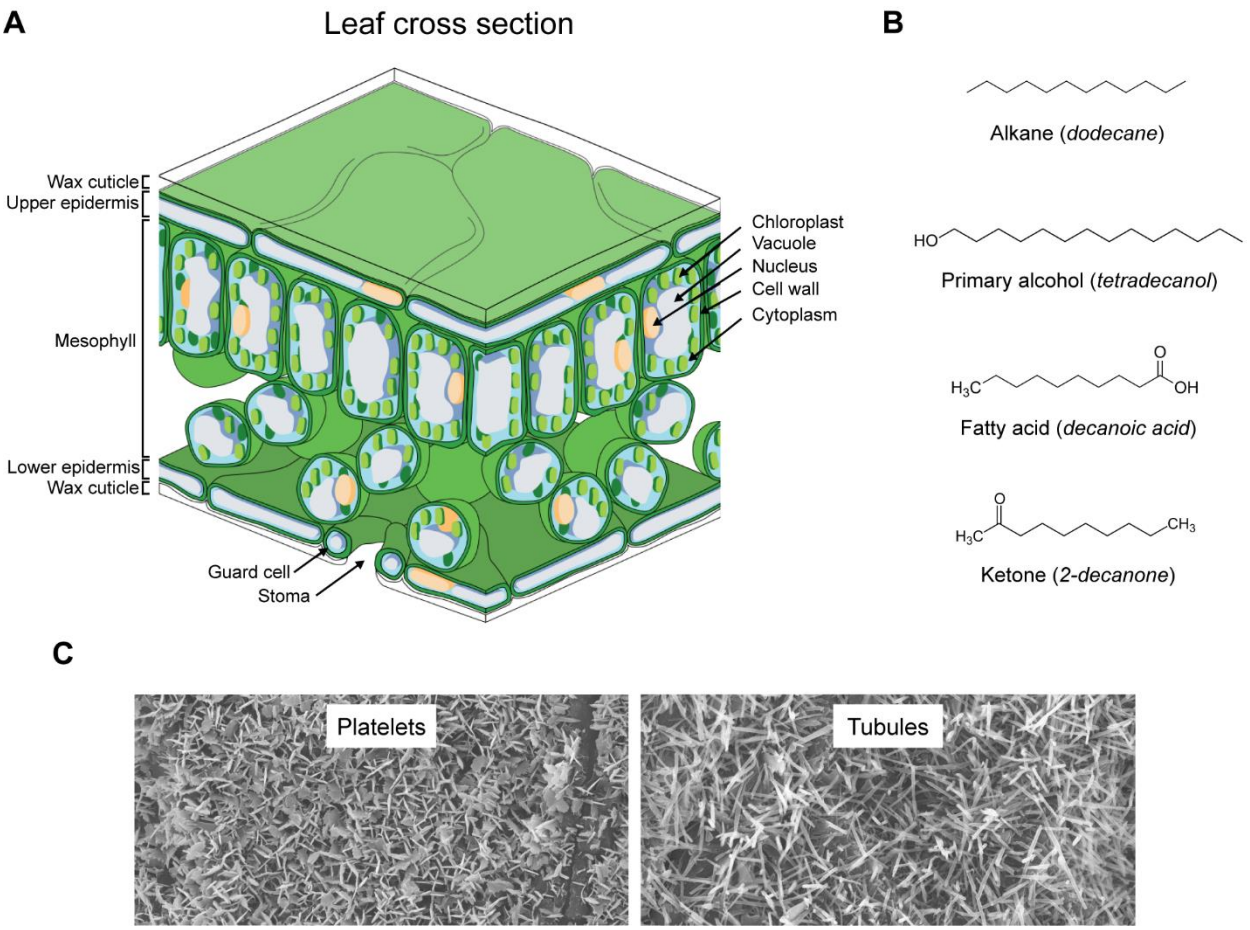

Figure 2. Micromorphology and chemical composition of the plant cuticle. **(A)** Diagram of a leaf cross section. Different compartments and cell types are indicated. This is a modified version of the diagram obtained from [73]. **(B)** Example waxes typically found on plant cuticles. **(C)** Scanning electron micrographs of two types of wax crystals: platelets and tubules.

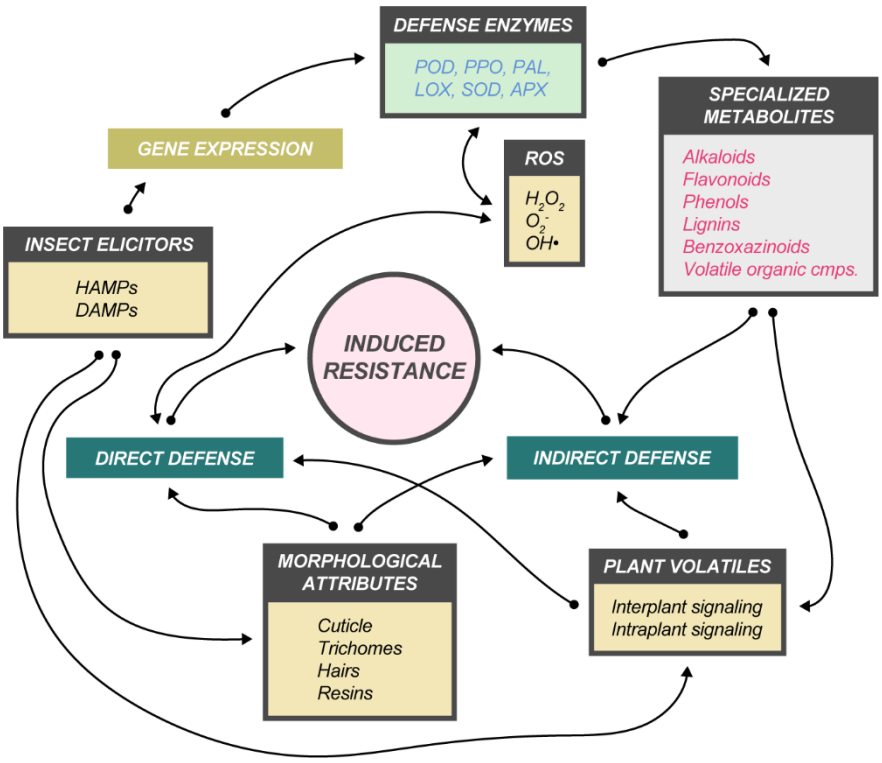

Figure 3. Simplified model for molecular resistance in plants. Resistance is induced upon recognition of insect elicitors and relies on both direct and indirect defenses. Molecular responses include overexpression of defense enzymes (e.g., detoxicating SOD) and metabolites. Abbreviations/Notations: HAMPs = herbivore-associated molecular patterns; DAMPs = damage-associated molecular patterns; POD = peroxidase; PPO = polyphenol oxidase; PAL = phenylalanine ammonia lyase; LOX = lipoxygenase; SOD = superoxide dismutase; APX = ascorbate peroxidase; cmps. = compounds.

REFERENCES

1. Food and Agriculture Organization of the United Nations website. Available online: http://faostat3.fao.org/.
2. Shiferaw, B.; Smale, M.; Braun, H.-J.; Duveiller, E.; Reynolds, M.; Muricho, G. Crops that feed the world 10. Past successes and future challenges to the role played by wheat in global food security. *Food Sec.* **2013**, *5*, 291–317.
3. United States Department of Agriculture website. Available online: https://www.usda.gov/.
4. Godfray, H.C.J.; Beddington, J.R.; Crute, I.R.; Haddad, L.; Lawrence, D.; Muir, J.F.; Pretty, J.; Robinson, S.; Thomas, S.M.; Toulmin, C. Food security: the challenge of feeding 9 billion people. *Science* **2010**, *327*, 812–818.
5. Tester, M.; Langridge, P. Breeding technologies to increase crop production in a changing world. *Science* **2010**, *327*, 818–822.
6. Pandey, P.; Irulappan, V.; Bagavathiannan, M.V.; Senthil-Kumar, M. Impact of combined abiotic and biotic stresses on plant growth and avenues for crop improvement by exploiting physio-morphological traits. *Front. Plant Sci.* **2017**, *8*, 537.
7. Norton, E. Notes on North American Tenthredinidae, with descriptions of new species. *T. A. Entomol. Soc.* **1872**, *4*, 77–86.
8. Beres, B.L.; Dosdall, L.M.; Weaver, D.K.; Cárcamo, H.A.; Spaner, D.M. Biology and integrated management of wheat stem sawfly and the need for continuing research. *Can. Entomol.* **2011**, *143*, 105–125.
9. Shanower, T.G.; Hoelmer, K.A. Biological control of wheat stem sawflies: past and future. *J. Agric. Urban Entomol.* **2004**, *21*, 197–221.
10. Lesieur, V.; Martin, J.F.; Weaver, D.K.; Hoelmer, K.A.; Smith, D.R.; Morrill, W.L.; Kadiri, N.; Peairs, F.B.; Cockrell, D.M.; Randolph, T.L.; Waters, D.K.; Bon, M.C. Phylogeography of the Wheat Stem Sawfly, *Cephus cinctus* Norton (Hymenoptera: Cephidae): implications for pest management. *PLoS One* **2016**, *11*, e0168370.
11. Cockrell, D.M.; Griffin-Nolan, R.J.; Rand, T.A.; Altilmisani, N.; Ode, P.J.; Peairs, F. Host plants of the wheat stem sawfly (Hymenoptera: Cephidae). *Environ. Entomol.* **2017**, *46*, 847–854.
12. Nilsen, K.T.; Clarke, J.M.; Beres, B.L.; Pozniak, C.J. Sowing density and cultivar effects on pith expression in solid-stemmed durum wheat. *Agron. J.* **2016**, *108*, 219–228.
13. Buteler, M.; Weaver, D.K.; Peterson, R.K.D. Oviposition behavior of the wheat stem sawfly when encountering plants infested with cryptic conspecifics. *Environ. Entomol.* **2009**, *38*, 1707–1715.
14. Ainslie, C.N. The western grass-stem sawfly: a pest of small grains. **1929**, USDA Technical Bulletin No. 157.
15. Holmes, N.D. The effect of light on the resistance of hard red spring wheats to the wheat stem sawfly, *Cephus cinctus* (Hymenoptera: Cephidae). *Can. Entomol.* **1984**, *116*, 677–684.

16. Macedo, T.B.; Weaver, D.K.; Peterson, R.K.D. Photosynthesis in wheat at the grain filling stage is altered by larval wheat stem sawfly (Hymenoptera: Cephidae) injury and reduced water availability. *J. Entomol. Sci.* **2007**, *42*, 228–238.

17. Morrill, W.L.; Gabor, J.W.; Kushnak, G.D. Wheat stem sawfly (Hymenoptera: Cephidae): damage and detection. *J. Econ. Entomol.* **1992**, *85*, 2413–2417.

18. Weiss, M.J.; Morrill, W.L. Wheat stem sawfly (Hymenoptera: Cephidae) revisited. *Am. Entomol.* **1992**, *38*, 241–245.

19. Runyon, J.B.; Morrill, W.L.; Weaver, D.K.; Miller, P.R. Parasitism of the wheat stem sawfly (Hymenoptera Cephidae) by *Bracon cephi* and *B. lissogaster* (Hymenoptera Braconidae) in wheat fields bordering tilled and untilled fallow in Montana. *J. Econ. Entomol.* **2002**, *95*, 1130–1134.

20. Luginbill, P.; McNeal, F.H. Influence of seeding density and row spacings on the resistance of spring wheats to the wheat stem sawfly. *J. Econ. Entomol.* **1958**, *51*, 804–808.

21. Morrill, W.L.; Kushnak, G.D. Planting date influence on the wheat stem sawfly (Hymenoptera: Cephidae) in spring wheat. *J. Agr. Urban Entomol.* **1999**, *16*, 123–128.

22. DePauw, R.M.; Read, D.W.L. The effect of nitrogen and phosphorus on the expression of stem solidness in Canuck wheat at four locations in southwestern Saskatchewan. *Can. J. Plant Sci.* **1982**, *62*, 593–598.

23. Sherman, J.D.; Blake, N.K.; Martin, J.M.; Kephart, K.D.; Smith, J.; Clark, D.R.; Hofland, M.L.; Weaver, D.K.; Lanning, S.P.; Heo, H.-Y.; Pumphrey, M.; Chen, J.; Talbert, L.E. Agronomic impact of a stem solidness gene in near-isogenic lines of wheat. *Crop Sci.* **2015**, *55*, 514–520.

24. Szczepaniec, A.; Glover, K.D.; Berzonsky, W. Impact of solid and hollow varieties of winter and spring wheat on severity of wheat stem sawfly (Hymenoptera: Cephidae) infestations and yield and quality of grain. *J. Econ. Entomol.* **2015**, *108*, 2316–2323.

25. Larson, R.I.; MacDonald, M.D. Cytogenetics of solid stem on chromosomes 3B, 3D, 5A, 5B, and 5D affecting stem in common wheat. II. Stem solidness of monosomic lines of the variety S-615. *Can. J. Bot.* **1959**, *37*, 368–378.

26. Varella, A.C.; Talbert, L.E.; Hofland, M.L.; Buteler, M.; Sherman, J.D.; Blake, N.K.; Heo, H.-Y.; Martin, J.M.; Weaver, D.K. Alleles at a quantitative trait locus for stem solidness in wheat affect temporal patterns of pith expression and level of resistance to the wheat stem sawfly. *Plant Breeding* **2016**, *135*, 546–551.

27. Varella, A.C.; Weaver, D.K.; Peterson, R.K.; Sherman, J.D.; Hofland, M.L.; Blake, N.K.; Martin, J.M.; Talbert, L.E. Host plant quantitative trait loci affect specific behavioral sequences in oviposition by a stem-mining insect. *Theor. Appl. Genet.* **2017**, *130*, 187–197.

28. Cook, J.P.; Wichman, D.M.; Martin, J.M.; Bruckner, P.L.; Talbert, L.E. Identification of microsatellite markers associated with a stem solidness locus in wheat. *Crop Sci.* **2004**, *44*, 1397–1402.

29. Holmes, N.D. The effect of the wheat stem sawfly, *Cephus cinctus* (Hymenoptera: Cephidae), on the yield and quality of wheat. *Can. Entomol.* **1977**, *109*, 1591–1598.

30. Riederer, M.; Schreiber, L. Protecting against water loss: analysis of the barrier properties of plant cuticles. *J. Exp. Bot.* **2001**, *52*, 2023–2032.

31. Bi, H.; Luang, S.; Li, Y.; Bazanova, N.; Morran, S.; Song, Z.; Perera, M.A.; Hrmova, M.; Borisjuk, N.; Lopato, S. Identification and characterization of wheat drought-responsive MYB transcription factors involved in the regulation of cuticle biosynthesis. *J. Exp. Bot.* **2016**, *67*, 5363–5380.

32. Baur, P.; Buchholz, A.; Schönherr, J. Diffusion in plant cuticles as affected by temperature and size of organic solutes: similarity and diversity among species. *Plant Cell Environ.* **1997**, *20*, 982–994.

33. Yeats, T.H.; Rose, J.K. The formation and function of plant cuticles. *Plant Physiol.* **2013**, *163*, 5–20.

34. Kunst, L.; Samuels, L. Plant cuticles shine: advances in wax biosynthesis and export. *Curr. Opin. Plant Biol.* **2009**, *12*, 721–727.

35. Serrano, M.; Coluccia, F.; Torres, M.; L'Haridon, F.; Metraux, J.P. The cuticle and plant defense to pathogens. *Front. Plant Sci.* **2014**, *5*, 274.

36. Eigenbrode, S.D.; Espelie, K.E.; Shelton, A.M. Behavior of neonate Diamondback moth larvae [*Plutella xylostella* (L.)] on leaves and on extracted leaf waxes of resistant and susceptible cabbages. *J. Chem. Ecol.* **1991**, *17*, 1691–1704.

37. Cervantes, D.E.; Eigenbrode, S.D.; Ding, H.-J.; Bosque-Pérez, N.A. Oviposition responses by Hessian fly, *Mayetiola destructor*, to wheats varying in surfaces waxes. *J. Chem. Ecol.* **2002**, *28*, 193–210.

38. Jenks, M.A.; Gaston, C.H.; Goodwin, M.S.; Keith, J.A.; Teusink, R.S. Seasonal variation in cuticular waxes on *Hosta* genotypes differing in leaf surface glaucousness. *HortScience* **2002**, *37*, 673–677.

39. von Wettstein-Knowles, P. *Plant waxes*. Publisher: John Wiley & Sons, Ltd., Chichester, UK, 2012.

40. Wang, Y.; Wang, J.; Chai, G.; Li, C.; Hu, Y.; Chen, X.; Wang, Z. Developmental changes in composition and morphology of cuticular waxes on leaves and spikes of glossy and glaucous wheat (*Triticum aestivum* L.). *PLoS One* **2015**, *10*, e0141239.

41. Hen-Avivi, S.; Savin, O.; Racovita, R.C.; Lee, W.S.; Adamski, N.M.; Malitsky, S.; Almekias-Siegl, E.; Levy, M.; Vautrin, S.; Berges, H.; Friedlander, G.; Kartvelishvily, E.; Ben-Zvi, G.; Alkan, N.; Uauy, C.; Kanyuka, K.; Jetter, R.; Distelfeld, A.; Aharoni, A. A metabolic gene cluster in the wheat *W1* and the barley *Cer-cqu* loci determines β-diketone biosynthesis and glaucousness. *Plant Cell* **2016**, *28*, 1440–1460.

42. Barthlott, W.; Neinhuis, C.; Cutler, D.; Ditsch, F.; Meusel, I.; Theisen, I.; Wilhelmi, H. Classification and terminology of plant epicuticular waxes. *Bot. J. Linn. Soc.* **1998**, *126*, 237–260.

43. Chambers, T.C.; Ritchie, I.M.; Booth, M.A. Chemical models for plant wax morphogenesis. *New Phytol.* **1976**, *77*, 43–49.

44. War, A.R.; Paulraj, M.G.; Ahmad, T.; Buhroo, A.A.; Hussain, B.; Ignacimuthu, S.; Sharma, H.C. Mechanisms of plant defense against insect herbivores. *Plant Signal Behav.* **2012**, *7*, 1306–1320.

45. Braccini, C.L.; Vega, A.S.; Coll Aráos, M.V.; Teal, P.E.; Cerrillo, T.; Zavala, J.A.; Fernandez, P.C. Both volatiles and cuticular plant compounds determine oviposition of the willow sawfly *Nematus oligospilus*. *J. Chem. Ecol.* **2015**, *41*, 985–996.

46. Baldwin, I.T.; Halitschke, R.; Kessler, A.; Schittko, U. Merging molecular and ecological approaches in plant–insect interactions. *Curr. Opin. Plant Biol.* **2001**, *4*, 351–358.

47. Hogenhout, S.A.; Bos, J.I. Effector proteins that modulate plant–insect interactions. *Curr. Opin. Plant Biol.* **2011**, *14*, 422–428.

48. Acevedo, F.E.; Rivera-Vega, L.J.; Chung, S.H.; Ray, S.; Felton, G.W. Cues from chewing insects — the intersection of DAMPs, HAMPs, MAMPs and effectors. *Curr. Opin. Plant Biol.* **2015**, *26*, 80–86.

49. Reymond, P. Perception, signaling and molecular basis of oviposition-mediated plant responses. *Planta* **2013**, *238*, 247–258.

50. Bonaventure, G. Perception of insect feeding by plants. *Plant Biol.* **2012**, *14*, 872–880.

51. Stotz, H.U.; Kroymann, J.; Mitchell-Olds, T. Plant–insect interactions. *Curr. Opin. Plant Biol.* **1999**, *2*, 268–272.

52. Moreira, X.; Lundborg, L.; Zas, R.; Carrillo-Gavilán, A.; Borg-Karlson, A.-K.; Sampedro, L. Inducibility of chemical defences by two chewing insect herbivores in pine trees is specific to targeted plant tissue, particular herbivore and defensive trait. *Phytochemistry* **2013**, *94*, 113–122.

53. Fürstenberg-Hägg, J.; Zagrobelny, M.; Bak, S. Plant defense against insect herbivores. *Int. J. Mol. Sci.* **2013**, *14*, 10242–10297.

54. Cagirici, H.B.; Biyiklioglu, S.; Budak, H. Assembly and annotation of transcriptome provided evidence of miRNA mobility between wheat and wheat stem sawfly. *Front. Plant Sci.* **2017**, *8*, 1653.

55. Dubreuil-Maurizi, C.; Poinssot, B. Role of glutathione in plant signaling under biotic stress. *Plant Signal Behav.* **2012**, *7*, 210–212.

56. Vandenborre, G.; Smagghe, G.; Van Damme, E.J. Plant lectins as defense proteins against phytophagous insects. *Phytochemistry* **2011**, *72*, 1538–1550.

57. Lefebvre, B.; Timmers, T.; Mbengue, M.; Moreau, S.; Herve, C.; Toth, K.; Bittencourt-Silvestre, J.; Klaus, D.; Deslandes, L.; Godiard, L.; Murray, J.D.; Udvardi, M.K.; Raffaele, S.; Mongrand, S.; Cullimore, J.; Gamas, P.; Niebel, A.; Ott, T. A remorin protein interacts with symbiotic receptors and regulates bacterial infection. *Proc. Natl. Acad. Sci. USA* **2010**, *107*, 2343–2348.

58. Schwachtje, J.; Baldwin, I.T. Why does herbivore attack reconfigure primary metabolism? *Plant Physiol.* **2008**, *146*, 845–851.

59. Dixon, R.A.; Achnine, L.; Kota, P.; Liu, C.-J.; Srinivasa Reddy, M.S.; Wang, L. The phenylpropanoid pathway and plant defence — a genomics perspective. *Mol. Plant Pathol.* **2002**, *3*, 371–390.

60. Tzin, V.; Hojo, Y.; Strickler, S.R.; Bartsch, L.J.; Archer, C.M.; Ahern, K.R.; Zhou, S.; Christensen, S.A.; Galis, I.; Mueller, L.A.; Jander, G. Rapid defense responses in maize leaves induced by *Spodoptera exigua* caterpillar feeding. *J. Exp. Bot.* **2017**, *68*, 4709–4723.

61. Wouters, F.C.; Blanchette, B.; Gershenzon, J.; Vassão, D.G. Plant defense and herbivore counter-defense: benzoxazinoids and insect herbivores. *Phytochem. Rev.* **2016**, *15*, 1127–1151.

62. Osorio, S.; Thi Do, P.; Fernie, A.R. Profiling primary metabolites of tomato fruit with gas chromatography/mass spectrometry. In *Plant metabolomics: methods and protocols*; Hardy, N.W., Hall R.D., Eds.; Publisher: Springer/Humana Press, New York City, NY, USA, 2012; pp. 101–109; 9761617795947.

63. Bush, R.T.; McInerney, F.A. Leaf wax *n*-alkane distributions in and across modern plants: implications for paleoecology and chemotaxonomy. *Geochim. Cosmochim. Acta* **2013**, *117*, 161–179.

64. Racovita, R.C.; Hen-Avivi, S.; Fernandez-Moreno, J.P.; Granell, A.; Aharoni, A.; Jetter, R. Composition of cuticular waxes coating flag leaf blades and peduncles of *Triticum aestivum* cv. Bethlehem. *Phytochemistry* **2016**, *130*, 182–192.

65. Steinbauer, M.J.; Davies, N.W.; Gaertner, C.; Derridj, S. Epicuticular waxes and plant primary metabolites on the surfaces of juvenile *Eucalyptus globulus* and *E. nitens* (Myrtaceae) leaves. *Aust. J. Bot.* **2009**, *57*, 474–485.

66. Weaver, D.K.; Buteler, M.; Hofland, M.L.; Runyon, J.B.; Nansen, C.; Talbert, L.E.; Lamb, P.; Carlson, G.R. Cultivar preferences of ovipositing wheat stem sawflies as influenced by the amount of volatile attractant. *J. Econ. Entomol.* **2009**, *102*, 1009–1017.

67. Truong, D.-H.; Nguyen, H.C.; Bauwens, J.; Mazzucchelli, G.; Lognay, G.; Francis, F. Plant defense in response to chewing insects: proteome analysis of *Arabidopsis thaliana* damaged by *Plutella xylostella*. *J. Plant Interact.* **2018**, *13*, 30–36.

68. Haley, S.D.; Quick, J.S.; Johnson, J.J.; Peairs, F.B.; Stromberger, A.; Clayshulte, S.R.; Clifford, B.L.; Rudolf, J.B.; Seabourn, B.W.; Chung, O.K.; Jin, Y.; Kolmer, J. Registration of 'Hatcher' wheat. *Crop Sci.* **2005**, *45*, 2654–2656.

69. Haley, S.D.; Johnson, J.J.; Peairs, F.B.; Stromberger, J.A.; Hudson, E.E.; Seifert, S.A.; Kottke, R.A.; Valdez, V.A.; Rudolph, J.B.; Martin, T.J.; Bai, G.; Chen, X.; Bowden, R.L.; Jin, Y.; Kolmer, J.A.; Chen, M.-S.; Seabourn, B.W. Registration of 'Denali' wheat. *J. Plant Regist.* **2012**, *6*, 311–314.

70. Talbert, L.E.; Sherman, J.D.; Hofland, M.L.; Lanning, S.P.; Blake, N.K.; Grabbe, R.; Lamb, P.F.; Martin, J.M.; Weaver, D.K.; Bürstmayr, H. Resistance to *Cephus cinctus* Norton, the wheat stem sawfly, in a recombinant inbred line population of wheat derived from two resistance sources. *Plant Breeding* **2014**, *133*, 427–432.

71. Biyiklioglu, S.; Alptekin, B.; Akpinar, B.A.; Varella, A.C.; Hofland, M.L.; Weaver, D.K.; Bothner, B.; Budak, H. A large-scale multiomics analysis of wheat stem solidness and the wheat stem sawfly feeding response, and syntenic associations in barley, *Brachypodium*, and rice. *Funct. Integr. Genomics* **2018**, *18*, 241–259.

72. Minnesota crop news website. Available online: http://blog-crop-news.extension.umn.edu/.

73. Wikimedia Commons website. Availale online: https://commons.wikimedia.org/.

CHAPTER 2 – GC-MS METABOLOMICS TO EVALUATE THE COMPOSITION OF PLANT CUTICULAR WAXES FOR FOUR *TRITICUM AESTIVUM* CULTIVARS[a,b,c]

2.1. Summary

Wheat (*Triticum aestivum* L.) is an important food crop, and biotic and abiotic stresses significantly impact grain yield. Wheat leaf and stem surface waxes are associated with traits of biological importance, including stress resistance. Past studies have characterized the composition of wheat cuticular waxes, however protocols can be relatively low-throughput and narrow in the range of metabolites detected. Here, gas chromatography-mass spectrometry (GC-MS) metabolomics methods were utilized to provide a comprehensive characterization of the chemical composition of cuticular waxes in wheat leaves and stems. Further, waxes from four wheat cultivars were assayed to evaluate the potential for GC-MS metabolomics to describe wax composition attributed to differences in wheat genotype. A total of 263 putative compounds were detected and included 58 wax compounds that can be classified (e.g., alkanes and fatty acids). Many of the detected wax metabolites have known associations to important biological functions. Principal component analysis and ANOVA were used to evaluate metabolite distribution, which was attributed to both tissue type (leaf, stem) and cultivar differences. Leaves contained more primary alcohols than stems such as 6-methylheptacosan-1-ol and

---

[a]This chapter is adapted from a research article that was published in the International Journal of Molecular Sciences on Jan. 23, 2018, with minor modifications.
[b]Article citation: Lavergne, Florent D., et al. "GC-MS Metabolomics to Evaluate the Composition of Plant Cuticular Waxes for Four *Triticum aestivum* Cultivars." *International journal of molecular sciences* 19.2 (2018): 249.
[c]Authors: Florent D. Lavergne, Corey D. Broeckling, Darren M. Cockrell, Scott D. Haley, Frank B. Peairs, Courtney E. Jahn, Adam L. Heuberger.

octacosan-1-ol. The metabolite data were complemented using scanning electron microscopy of epicuticular wax crystals which detected wax tubules and platelets. Conan was the only cultivar to display alcohol-associated platelet-shaped crystals on its abaxial leaf surface. Taken together, application of GC-MS metabolomics enabled the characterization of cuticular wax content in wheat tissues and provided relative quantitative comparisons among sample types, thus contributing to the understanding of wax composition associated with important phenotypic traits in a major crop.

2.2. Introduction

Common wheat (*Triticum aestivum* L.) is a widely grown staple crop, and is often affected by biotic and abiotic pressure that reduces grain yield [1]. In wheat, resistance to stress is associated with metabolic responses in various tissues and organs, changing the plant chemical composition of tissues that provide stress tolerance. The surface of leaf and stem organs is known as the cuticle, which is a primary point of contact with insects and pathogens, and regulates water retention during periods of high temperature, low atmospheric humidity, and low soil moisture [2-4]. The cuticle is an extracellular matrix of two main components: cutin (a simple polymer) and lipids, termed epicuticular waxes (herein referred to as “waxes”) [5]. Waxes are considered end products of long-chain lipid metabolism and include alkanes, fatty acids, primary and secondary alcohols, ketones, esters, and aldehydes [6].

Waxes are important to stress tolerance for their role in forming a physical barrier to prevent dust and debris accumulation on hydrophilic surfaces and form a natural obstacle to pathogen penetration [5,7]. Cuticular fatty acids and primary alcohols have been demonstrated to facilitate resistance of cabbage (*Brassica oleracea*) to Diamondback Moth larvae (*Plutella xylostella*), specifically through chemical deterrence [8]. Waxes can also act as photoprotectants

for ultraviolet light [9]. Likewise, wax composition (e.g., proportions of ketones and primary alcohols) and content correlate with glaucousness, a bluish-green appearance of the plant cuticle that is associated with drought tolerance [10-14].

Waxes assemble in the cuticle as three-dimensional crystals of 23 types based on micromorphology [15]. Scanning electron microscopy (SEM) studies reveal that the "platelet" and "tubule" types of epicuticular wax crystals are distributed among all major groups of plants [12,15]. Further, the wax composition (lipid class and abundance) is associated with the type of wax crystal. In *Triticum* species, platelets are mostly composed of primary alcohols [12], whereas tubules are high in content of β-diketones [15,16]. Here, these associations are used to verify the accuracy of a customized biochemical analysis workflow on wax detection.

Various methods have been developed to evaluate waxes. Leaf or stem samples are usually air- or freeze-dried and then immersed in a polar (e.g., methanol) or non-polar (e.g., hexane) solvent [17-20]. Rapid dips in hexane can solubilize wax alkanes, primary alcohols, fatty acids, ketones, and aldehydes that are often known for their agronomic importance [10,21-23]. Further, several studies have compared gas chromatography injection methods (e.g., split ratios) and oven temperatures necessary for wax compounds [24-26].

In plants, metabolomics is the comprehensive analysis of small molecules (~50–1200 Da), typically involved in primary or specialized (secondary) metabolism. While waxes are in fact end products of metabolism (they are exuded from leaf and stem cells), they are amenable to analysis by metabolomics methods due to their chemical properties. A common method to evaluate primary metabolites in plants is to extract, derivatize via silylation, and detect metabolites using gas chromatography coupled to mass spectrometry (GC-MS) [27]. Many plant waxes are small and semi-volatile and are also detected using GC-MS [11,13,24,28-30]. Further,

many contain hydroxyl groups that allow for derivatization to improve volatility and detection by GC-MS.

In MS-based non-targeted metabolomics, extracts from different samples are analyzed as metabolite "profiles", determined by a collection of molecular features that include chromatographic retention indices (RI, derived from retention times), mass-to-charge ratios (*m*/*z*) and the relative abundance of each metabolite [31,32]. Non-targeted metabolomics methods utilize data processing algorithms that attempt to align large datasets (chromatographic retention times can drift over time) and provide information on all detectable *m*/*z*. Due to the complexity of calculating absolute quantities for thousands of compounds, metabolite quantities are recorded as relative abundances [33,34], typically to the total chemical signal or an internal standard. The resulting data matrix is unique in that it allows for a comparison of chemical profiles to evaluate sources of variation in a biological system.

In this study, we combine the amenability of GC-MS for waxes with non-targeted metabolomics data processing methods to enable comparisons of wax composition on tissues (i.e., leaf and stem cuticles) of four wheat cultivars that differ for glaucousness and resistance to an insect pest. Further, micro-morphological features are evaluated using SEM to validate the relevance of our workflow. Here, we provide a comprehensive characterization of wheat waxes and demonstrate variation among tissues and cultivars. The data supports the potential to breed for wax traits with demonstrated effects on a variety of biologically relevant phenotypes, including stress resistance. Further, this method allows for high-throughput extraction, detection, and quantitation of waxes and is applicable to very large sample sets made up of thousands of metabolites.

2.3. Methodology

2.3.1. Plant Material

Hard red winter wheat (*Triticum aestivum* L., Poaceae) cultivars "Hatcher" (PI 638512) [35] and "Denali" (PI 664256) [36], and hard red spring wheat cultivars "Conan" (PI 607549) and "Reeder" (PI 613586) were used for comparisons of cuticular wax metabolites and epicuticular wax crystals. For metabolomics analyses, winter wheat cultivars were vernalized for eight weeks at 3 °C ± 2 °C. Spring wheat cultivars were vernalized for 10 d at 3 °C ± 2 °C to facilitate more synchronous development of the winter and spring wheat cultivars. Vernalized seedlings were planted in 5-inch circular pots in the following mix: seven parts Fafard professional metro mix (45–55% Canadian Sphagnum peat moss, vermiculite, bark, dolomite lime, and wetting agent; Sun Gro Horticulture, Agawam, MA, USA), two parts coarse perlite, one part Fort Collins loam soil supplemented with aged manure and Osmocote slow release fertilizer (Greenhouse Products Pty Ltd., Princess, South Africa) as per the manufacturer's recommendation. All plants were grown at the Colorado State University greenhouse, Fort Collins (CO, USA), at 18–24 °C with a photoperiod of 15/9 h light/darkness, bottom watered three times per week, and grouped in a randomized complete block design. Photographs of wheat plants were taken at approximately Zadoks growth stage 55 (i.e., heading stage) [37]. For microscopic observations, winter wheat cultivars were grown in the field (New Raymer, CO, USA) under conventional conditions (e.g., precipitation, temperature, photoperiod), and spring wheat cultivars were grown in the greenhouse under the same conditions used for GC-MS analysis.

2.3.2. Leaf Photographs for Glaucousness

Visual determination of variation in glaucousness on leaf adaxial and abaxial, and stem cuticles was done by photographing five individuals from each of the four wheat cultivars at the same age (approximately Zadoks stage 55). All pictures of biological replicates for each cultivar showed similar glaucousness profiles and one replicate per cultivar was picked at random to create Figure 4. All photographs were recorded on the same day using a Canon EOS Rebel T3 camera (Canon Inc., Ōta, Tokyo, Japan) with identical camera setup, background, and light conditions throughout. Pictures were assembled in Figure 4 using Adobe Photoshop v16.0 (Adobe Systems, San Jose, CA, USA) without any technical adjustment such as manipulation of contrast or saturation.

2.3.3. Metabolite Extraction, Detection by GC-MS, Data Processing and Annotation

A total of 80 plants was used for cuticular metabolite extraction, including 21 biological replicates of Hatcher (11 leaf and 10 stem samples), 19 replicates of Denali (10 leaf and nine stem samples), 20 replicates of Conan (10 leaf and 10 stem samples), and 20 replicates of Reeder (10 leaf and 10 stem samples). Equivalent positions were probed in all four cultivars to account for wax variation between the upper and lower parts of the plants. Stems between the third and fourth internodes (starting from the first internode, also termed peduncle), and the fourth leaf of each plant (starting from the flag leaf), were collected. Waxes and non-wax metabolites were extracted as described by Zhang et al. (2005) [22] with the following modifications. Briefly, plain lyophilized leaf pieces (8 mm × 8 mm = area of 64 mm^2 on both sides = 128 mm^2 total) and plain lyophilized stems (1.5 mm radius × 85 mm height = 128 mm^2 total) were dipped into glass vials containing 1 mL of gas chromatography grade hexane (Sigma-Aldrich, Inc., St Louis, MO, USA) [23]. To extract a significant proportion of waxes from the cuticle, samples immersed in

hexane were agitated for 30 s on a rotator at 80 g. Even though samples were gently shaken, this short period was enough for the solvent to locally corrode the cuticle membrane and release intracuticular compounds along with extracuticular waxes [38], notwithstanding the cut-open section of tissue that was immersed in the solvent and potentially released more intracuticular metabolites. Waxes were therefore referred to as "cuticular waxes" in the abstract, results, discussion and materials and methods sections, while the term "epicuticular wax crystals" was employed for microscopy visualization purposes. Solvents were then decanted into new glass vials. Vial containers and tissues were given a further 10-s rinse with the same amount of hexane, and both solutions were combined in a new vial. Hexane-soluble extracts were then evaporated under a continuous gas nitrogen flow. Metabolites were derivatized by adding 60 µL of a pyridine: N-Methyl-N-(trimethylsilyl)trifluoroacetamide (MSTFA) solution (1:1, v:v) and incubating for 30 min at 60 °C. Non-targeted metabolite profiling was performed using gas chromatography-mass spectrometry (GC-MS) as previously described [33]. Briefly, metabolites were detected using a Trace GC Ultra coupled to a Thermo DSQ II mass spectrometer (Thermo Scientific, Waltham, MA, USA). Samples were injected in a 1:10 split ratio twice in discrete randomized blocks. Injection of a pooled quality control was performed every 10 sample injections. High Spearman's rank correlation coefficients ensured the stability of the instrument over time. Separation occurred using a 30 m TG-5MS column with a film thickness of 0.25 µm (Thermo Scientific), and a 1.2 mL per min helium gas flow rate. The program consisted of 80 °C for 30 s, a ramp of 15 °C per min to 330 °C, and an 8-min hold. Other specifications included inlet temperature held at 280 °C and auxiliary line at 300 °C. Masses between 50–650 *m*/*z* (i.e., mass-to-charge ratio) were scanned at five scans per s after electron impact ionization.

Data files from the GC-MS experiment were converted to .cdf format and processed by XCMS in R v3.2.4 (R foundation for Statistical Computing, Vienna, Austria) [39] to create a matrix of molecular features as defined by retention index (RI, Kovats alkane-based index) and mass (*m*/*z*). Upon collection of fatty acid (ranging from C_{18} to C_{36}) retention times using AMDIS v2.71 (NIST, Gaithersburg, MD, USA), the Golm Metabolome Database [40,41] was used to obtain the corresponding RI. Retention indices from other chemical classes were deduced using the Kovats RI for temperature ramped columns in AMDIS. Data was deconvoluted into spectral clusters using the R package RAMClust [42]. Critical RAMClust parameters included minimum module size of 2 (if a feature is clustered in a group with less than two features, it will not be exported as a putative compound); "average" linkage (method used to perform fastcluster-based hierarchical clustering), $h_{max} = 0.9$, st = 4, sr = 5; and features were normalized to total ion current (TIC). The relative quantity of each molecular feature was determined by the mean area of the chromatographic peak among two replicate injections, and spectral clusters were quantified as a weighted abundance of all molecular features in the cluster. Due to TIC normalization and based on the assumption that all extracts have equal metabolite quantities, metabolite abundances were discussed throughout as "content". Identification of metabolites was performed by matching mass spectra and retention indices to in-house and external databases including NIST 14 [43] and the Golm Metabolome Database (gmd20111121_var5_alk). Confidence levels of annotations were designated based on classification of metabolite annotation by Sumner et al. (2007) [44]. In sum, a confidence level of 1 is achieved when two or more forms of data from a given compound match an authentic reference standard, level 2 means a given compound is putatively identified when spectral data or spectra from a database is available but no comparison to a reference

standard, and level 3 is assigned when only the compound class can be identified. All annotated metabolites in this study were assigned a level 2 confidence.

2.3.4. Scanning Electron Microscopy

Wheat cultivars Hatcher and Denali were grown in the field (New Raymer, CO, USA), and Conan and Reeder were grown at the Colorado State University greenhouse due to inconsistent growth of spring wheats in Colorado fields. Leaves and stems from each cultivar were collected at heading stage (approximately Zadoks 55). Tissue samples of 15 cm in length were cut (as in the metabolite extraction protocol, stems between the third and fourth internodes and the fourth leaf of each plant were collected) and placed into 10 mL tubes. Small pieces of tissue (8 mm × 8 mm of leaves, and 8 mm × 8 mm of unrolled stems) were then mounted on stubs and placed in an air-dryer for desiccation to prevent sample shrinkage after exposure to the microscope vacuum chamber. Dried samples were coated with a layer of gold (20 nm) using a Hummer VI sputtering system (Anatech Ltd., Springfield, VA, USA). Cuticles were visualized using a JEOL JSM-6500F scanning electron microscope (JEOL, Peabody, MA, USA) set at a beam accelerating voltage of 15 kV. For each cultivar, three tissue types (adaxial leaf surface, abaxial leaf surface, stem) were observed in two plants (n = 2 biological replicates). For each tissue type, two structures were observed, and each picture was recorded from five different sample areas, for a total of 240 observations.

The qualitative variation observed using SEM was complemented by quantifying epicuticular wax content (percent wax abundance on the cuticle total surface) using image processing software. The software ImageJ v1.51d was used to quantify wax surface content on low magnification pictures (× 140). Briefly, after conversion of images to red-green-blue (RGB) stack, luminosity was manually adjusted to select waxes only (white/greyish pixels). Wax

content was then measured and expressed as percentage of wax coverage across the entire tissue considered.

2.3.5. Statistical Analysis

Metabolite contents were compared using one-way ANOVA for both tissues and cultivars, with a *p* threshold of 0.05. Differences in content among cultivars were further compared using Tukey HSD pairwise comparisons. Benjamini–Hochberg correction was systematically applied across all *t* tests and ANOVA metabolomics results to account for falsely rejected statistical hypotheses when conducting multiple comparisons, termed "false discovery rate" (FDR) [45]. Principal component analysis (PCA) was conducted on the GC-MS data after mean-centering and UV-scaling using SIMCA v14.1 (MKS Data Analytics, Umea, Sweden). Heat maps were prepared in the R environment v3.2.4 using the heatmap.2 function in the R package gplots, and hierarchical clustering was performed using the hclust function in R. Heat map z scores were calculated using the mean and standard deviation of metabolite content: $z = (X - \mu)/\sigma$, where X is the relative content of a metabolite, μ is the mean content for the metabolite across all samples and σ is the standard deviation among all samples.

2.4. Results

2.4.1. Cuticular Waxes Detected on Leaf and Stem Cuticles of Wheat

We focused on four cultivars for their phenotypic variation in: (1) resistance to the Wheat Stem Sawfly (*Cephus cinctus* Norton, WSS) [30,46]; (2) degree of surface glaucousness (Figure 4); and (3) growth habit (spring and winter wheat types) among tissues and cultivars. A total of 263 putative compounds were detected using GC-MS metabolomics. Sixty-nine of the 263 putative compounds were annotated as plant metabolites using retention index RI (derived from retention time as described in the Methodology section) and mass spectral matching, including

58 cuticular waxes (Table 2). Compounds were sorted and numbered in Table 2 based on their chemical class and RI. Bolded numbers in the results and discussion sections correspond to metabolites in Tables 2 and 3. Twenty cuticular wax metabolites were identified as alkanes, ranging from C_{20} (eicosane, **1**, RI = 2000) to C_{42} (dotetracontane, **20**, RI = 4200). Eleven were straight-chain alkanes and nine were methyl-branched at various positions. Fifteen alkanes varied in content between leaf and stem cuticles and 11 varied among the four cultivars (ANOVA, FDR adjusted $p < 0.05$). Twenty-two fatty acids were detected and ranged from C_7 (heptanoic acid, **21**, RI = 1044) to C_{34} (tetratriacontanoic acid, **42**, RI = 3037). Nineteen of the fatty acids were straight chain, including three compounds with one or more double bonds and three fatty acids that were methyl-branched. Fourteen fatty acids varied between tissues and only tetratriacontanoic acid had significant variation in content among cultivars (ANOVA, FDR adjusted $p < 0.05$). Six ketones were detected and ranged from C_9 (nonane-4,6-dione, **43**, RI = 1124) to C_{35} (pentatriacontan-2-one, **48**, RI = 2881), and included two monoketones and four β-diketones. Five ketones significantly varied between leaf and stem cuticles, and tritriacontan-3-one was the only monoketonic structure to vary in content among cultivars (ANOVA, FDR adjusted $p < 0.05$). Ten wax compounds were annotated as primary alcohols and ranged from C_{22} (docosan-1-ol, **49**, RI = 2044) to C_{33} (tritriacontan-1-ol, **58**, RI = 2855). Eight primary alcohols were straight chain metabolites and two were methyl-branched. Out of the ten alcohols, eight showed a statistically significant difference in content between tissues and six differed among cultivars (ANOVA, FDR adjusted $p < 0.05$).

The remaining 11 cuticular compounds out of the 69 annotated metabolites detected in the extract did not represent typical waxes (Table 3). These included three carboxylic acids (**59**–**61**), two carbohydrates (**62**,**63**), one primary amine (**64**), two polycyclic ketones (**65**,**66**), one

ester (**67**), one flavonoid (**68**), and one sterol (**69**). Their carbon structure ranged from C_4 to C_{29} and were characterized by retention indices of 1192 to 2885. Between tissues, six of the non-wax metabolites varied in content and two showed differences among cultivars.

Nine of the 58 annotated wax metabolites were identified in the literature as being involved in plant–insect interactions, and included alkanes, fatty acids, and primary alcohols (Table 2). Further evidence of the biological importance of waxes included antibiotic activity for tetradecanoic acid (**22**) and allelopathic activity for hexacosanoic acid (**33**) [47,48]. Tetracosanoic acid (**32**) has been described as a major wax precursor and hentriacontane-14,16-dione (**46**) is associated with a high degree of glaucousness in wheat [49,50]. Another application of the variation in wax composition is the classification of plants based on biochemical differences (i.e., chemotaxonomy). A total of seven alkanes (e.g., tricosane, **2**; pentacosane, **5**) detected in our study were previously shown to be functional chemotaxonomy markers [24].

2.4.2. Cuticular Wax Composition in Leaves and Stems of Wheat

The general appearance of metabolite profiles between leaf and stem samples of wheat was displayed using example chromatograms in Figure 5. Chromatograms illustrate the distribution in time (retention time) and the total ion current (TIC) intensity of all the putative compounds. Further, the content of the 69 annotated metabolites (including the 58 cuticular waxes) was z-transformed and displayed using a heat map combined with hierarchical clustering (Figure 6). The heat map highlights variation in content for most of the metabolites between tissues. Principal component analysis (PCA) also demonstrated significant variation between tissues (Figure 7A, left; Principal component 1, or PC 1, 25.1% of the variation) due to fatty acids and β-diketones (Figure 7A, right; PC 1 loadings).

As an example, four wax metabolites that contributed to the PCA model were labeled (Figure 7A, right), discussed as they appear from left to right and displayed as box plots to demonstrate variation between tissues (Figure 7B). Fatty acid 23-triacontenoic acid (**38**, FDR adjusted $p = 1.4 \times 10^{-14}$) and β-diketone hentriacontane-14,16-dione (**46**, FDR adjusted $p = 1.3 \times 10^{-15}$) were higher on stems and contributed to the tissue separation for PC 1 (loading scores plot). The primary alcohols octacosan-1-ol (**53**, Student's *t* test, FDR adjusted $p = 3.9 \times 10^{-16}$) and 6-methylheptacosan-1-ol (**54**, Student's *t* test, FDR adjusted $p = 3.3 \times 10^{-19}$) were higher in content on leaf than stem surfaces and highly contributed to the separation of tissues for PC 1 as well.

2.4.3. Wheat Cuticular Wax Composition among Cultivars

A further analysis of the heat map (Figure 6) demonstrates metabolite variation of the four wheat cultivars Conan, Hatcher, Reeder, and Denali. As an example, several alkanes were shown to be lower in content on Reeder stem cuticles compared to other cultivars (tricosane, **2**, FDR adjusted $p = 1.9 \times 10^{-4}$; 4-methyldocosane, **3**, FDR adjusted $p = 2.6 \times 10^{-11}$; 6-methyldocosane, **4**, FDR adjusted $p = 9.1 \times 10^{-6}$). Likewise, Hatcher and Reeder leaf surfaces contained less (9Z,12Z,15Z)-octadeca-9,12,15-trienoic acid (**25**, FDR adjusted $p = 5.2 \times 10^{-3}$), 10-methylheptadecanoic acid (**27**, FDR adjusted $p = 1.6 \times 10^{-10}$), and nonadecanoic acid (**28**, FDR adjusted $p = 5.5 \times 10^{-4}$) compared to Conan and Denali.

The significant variation in wheat cuticular compounds including waxes was further supported by PCA that showed separation among cultivars on leaf and stem cuticles (Figure 8). A total of 11 PCs were generated in the PCA model explaining 77% of the variation. For leaves, the largest separation among cultivars appeared for the combination of PC 2 (that explained 14.7% of the total variation in the sample set) and PC 7 (5.9% of the variation; Figure 8A, upper

left). Twenty (34%) of the annotated waxes were associated with the separation of cultivars within leaves (for all 20 metabolites, ANOVA, FDR-adjusted $p < 0.05$). For stems, the largest separation among cultivars was observed for the combination of PC 5 (6.4% of the total variation) and PC 6 (6% of the variation; Figure 8A, bottom left). Twenty-three of the annotated cuticular waxes (40%) were associated with the separation of cultivars for metabolites within stems (for all 23 wax metabolites, ANOVA, FDR-adjusted $p < 0.05$).

Conan, the glaucous cultivar (Figure 4) with resistance to the Wheat Stem Sawfly [30,46], had no wax metabolites that were unique, among these detected, on its leaf or stem cuticles (i.e., presence/absence). However, several individual metabolites were greater in abundance compared to the other three cultivars, such as the primary alcohols docosan-1-ol (**49**) and 6-methylheptacosan-1-ol (**54**; Figure 8A,B, compounds denoted in the PC loadings plot for leaves, from left to right). An ANOVA followed by Tukey HSD pairwise comparisons revealed variation for docosan-1-ol (**49**; FDR adjusted $p = 2.2 \times 10^{-3}$) and 6-methylheptacosan-1-ol (**54**; FDR adjusted $p = 1.3 \times 10^{-2}$) on Conan leaf surface (Figure 8B).

2.4.4. Association of Epicuticular Wax Content and Crystal Microstructure in Wheat

Scanning electron microscopy (SEM) was performed to characterize wax microstructural variation. This supplementary procedure aimed at complementing the metabolomics data. Leaf and stem cuticle tissue from mature plants was collected, air-dried, and micrographs of the adaxial leaf surface (upper side), abaxial leaf surface (lower side), and stem were obtained for the four cultivars (Figure 9). It is important to note that our study was limited to growing spring wheat cultivars (Conan and Reeder) in a greenhouse and winter wheat cultivars (Denali and Hatcher) were sampled from the field. While the growing location (i.e., controlled versus non-controlled environments) may contribute to variation in wax content and crystal

microstructure, no clear trends were observed between the field- and greenhouse-grown plants.

Based on semi-quantitation of the epicuticular wax content (measure of percent wax abundance on the cuticle total surface using image processing software; Figure 10), microscopy observations revealed specific composition among adaxial and abaxial leaf surfaces and stems. Variation in content among the three tissue types was observed (ANOVA, Tukey HSD post-hoc $p = 2 \times 10^{-16}$; Figure 10). When pooling the four cultivars, the mean wax coverages were 44.4 ± 1.2% for the adaxial leaf surface, 28.8 ± 1.8% for the abaxial leaf surface, and 14.4 ± 0.7% of the whole stem. This distribution of wax crystals (adaxial > abaxial > stem) was consistent for each cultivar except Conan, whose abaxial leaf surface had increased crystal microstructures attributed to platelets. As an example of variation in wax content among tissues, Reeder adaxial leaf surface demonstrated the highest amount of epicuticular wax crystals (55.6 ± 2.2% coverage of leaf surface), compared to Reeder abaxial leaf surface (37.6 ± 1.5%) and stems (12.9 ± 1.7%). This was supported by SEM as Reeder adaxial leaf micrographs displayed more epicuticular wax crystals than Reeder abaxial leaf or stem micrographs (Figure 9A–C). In addition, the adaxial leaf surface of all cultivars was exclusively covered by platelets, whereas stems had only tubules. However, variation among cultivars was observed for the abaxial leaf surface whereby Conan had only platelets (Figure 9D) whereas Reeder (Figure 9E), Hatcher, and Denali had tubules.

2.5. Discussion

2.5.1. Many of the Detected Cuticular Waxes Have Specialized Biological Functions

The work presented herein characterized the chemical composition of cuticular waxes of *Triticum aestivum* on leaf and stem cuticles and among different cultivars. Many of the detected waxes have specialized functions related to important phenotypic traits. Antibiotic (tetradecanoic

acid, **22**) and allelopathic (hexacosanoic acid, **33**) activities have been described for plant waxes [47,48]. Seven alkanes detected in our study, including tricosane (**2**) and pentacosane (**5**), are known as functional chemotaxonomy markers [24]. Further, alkane, fatty acid, and primary alcohol waxes (e.g., eicosane, **1**; hexadecanoic acid; **24**, octacosan-1-ol, **53**) have been shown to stimulate or interfere with insect attachment and oviposition, including the wheat/Hessian Fly interaction [10], and the Seven-Spotted Ladybug (*Coccinella septempunctata*) interaction with bioinspired wax surfaces [51]. Moreover, in common wheat, high β-diketone (e.g., hentriacontane-14,16-dione, **46**) content was associated with glaucousness and drought resistance [3,50]. In [52], hentriacontane-14,16-dione (**46**) was absent in waxless, English Grain Aphid (*Sitobion avenae*) susceptible Triticale (×*Triticosecale*) cultivars, and present in high content in waxy and resistant Triticale cultivars, supporting its role in plant–insect interaction.

The heat map (Figure 6), PCA and univariate analyses (Figures 7 and 8) revealed higher contents of two primary alcohols on leaves of Conan, namely docosan-1-ol (**49**) and 6-methylheptacosan-1-ol (**54**), compared to Reeder, Denali, and Hatcher. Further, increased platelet content on the abaxial leaf surface (Figure 9D) was observed in this cultivar. The glaucous appearance of a plant tissue is mostly due to β-diketones and primary alcohols, and wax matrices with increased primary alcohols can result in the formation of dense crystal platelets that contribute to drought stress resistance [3,12,53]. The genetic regulation of hexaploid wheat wax biosynthesis has been partially elucidated, and studies have identified quantitative trait loci that contribute to wax phenotypes. Specifically, wax synthesis and glaucousness loci (*W1* and *W2*), along with loci coding for their inhibitors (*Iw1* and *Iw2*), were genetically mapped [54]. Another locus of interest is the one that contains the *W3* gene [50]. *W3* facilitates biosynthesis of β-diketones, whereas the *Iw1* gene codes for an inhibitor of β-diketone synthesis, and regulation

of expression of these genes can influence glaucousness and cuticle permeability [14,17,50]. Further, the *TaFAR* gene family (including *TaFAR1* to *TaFAR4*) regulates the accumulation of primary alcohols [55]. Recently, a study of transcription factors involved in the regulation of wax synthesis genes (*TaWXPL1D* and *TaWXPL2B*) demonstrated differential expression in leaves of two wheat cultivars that contrasted in drought resistance and glaucousness, consequently to water deprivation [56]. The allelic diversity in these genes, and their influence on wax composition and glaucousness, is largely unknown and warrants future investigation that will help elucidate the molecular mechanisms underlying resistance to water stress.

2.5.2. Cuticular Waxes Differed between Leaves and Stems

The heat map (Figure 6) and PCA (Figure 7) showed variation for most individual cuticular wax metabolites. The two waxes that were higher in content on stems were the fatty acid 23-triacontenoic acid (**38**) and β-diketone hentriaconane-14,16-dione (**46**; Figure 7B). To our knowledge, fatty acid **38** has not been previously reported as a cuticular wax. Compound **46** is known to be associated with glaucousness in common wheat and pest resistance in Triticale [50,52]. Tubule-shaped crystals were encountered on stems along with high content in β-diketones for all cultivars. The high content in β-diketones results in the formation of tubule-shaped crystals that contribute to both the degree of glaucousness and frost resistance [57-59].

Leaf cuticles were enriched for primary alcohols compared to stems (Figure 7B). High content of typical platelet-shaped crystals involved in both biotic and abiotic stress resistance (e.g., insect and drought resistance) is due to a primary alcohol-rich content on the plant tissue surface [10,12,53,60]. In this study, higher levels in octacosan-1-ol (**53**) and 6-methylheptacosan-1-ol (**54**) were found on leaf cuticles (Figure 7B). Primary alcohol **53** is a potential insect repellent for the Hessian Fly and is thus of importance in plant–insect

interactions [10], and **54** has not been described in the literature. Further, while the role of high fatty acid content on the stem surface of our wheat cultivars remains to be elucidated, the high content of primary alcohols on leaves and β-diketones on stems supports a potential role in protection of these tissues against biotic and abiotic pressure.

2.5.3. Cuticular Waxes Varied in Composition among the Four Cultivars

The contribution of genetic diversity to variation in cuticular wax composition was investigated by comparing four different cultivars, including two spring and two winter wheat types (Figure 6). The analysis revealed a relatively low content of alkanes tricosane (**2**), 4-methyldocosane (**3**) and 6-methyldocosane (**4**) on Reeder stem surface. Reeder is a spring wheat cultivar widely grown in the Northern Great Plains and broadly adapted for rainfed (non-irrigated) production conditions. Drought stress has been shown to increase levels of alkanes on the leaf surface of alfalfa [61]. Thus, it is possible that Reeder modifies its wax composition upon exposure to drought stress, and potentially increases alkane content for its protective effects.

Multivariate analysis allowed for partial cultivar discrimination based on wax metabolite content (Figure 8A). Wax composition has been shown to vary among plant species, and among cultivars within a species. A study showed that foliage wax of onion (*Allium cepa*) varied among four cultivars, resulting in different degrees of resistance to the onion thrips (*Thrips tabaci*) [62]. The growing region of tussock grass species has been shown to correlate with wax content [63]. The two Australian wheat cultivars RAC875 and Kukri display unique wax compositions that result in different types of epicuticular wax crystals on their abaxial leaf surface [3]. While the abaxial leaf surface of RAC875 was made of tubules, the equivalent tissue in Kukri was exclusively made of platelets. Further, changes at higher taxonomy levels are also well

documented, as is the case for two Rocktrumpet species (genus *Mandevilla*) that differ in their wax profiles [19]. Together, these studies support that genetic diversity in wax composition may be common among individual cultivars within a plant species.

Conan leaf cuticles displayed high levels of the primary alcohols 6-methylheptacosan-1-ol (**54**) and docosan-1-ol (**49**; Figure 8B). Although these cuticular waxes have not been described as involved in defense processes, plant leaves that exhibit high content in primary alcohols tend to be covered by epicuticular wax crystals (i.e., platelets) involved in resistance [12,53,60]. The increased production of these two alcohol waxes on Conan leaf cuticles is potentially responsible for reshaping the surface morphology and influencing interactions with the environment and biotic sources.

2.5.4. Cuticular Wax Composition Was Associated with Epicuticular Wax Crystal Microstructure

As previously mentioned, wax chemical composition is associated with wax crystal formation [3]. Scanning electron microscopy analysis revealed the presence of tubule and platelet crystals on the cuticle, and variation among tissues and cultivars was observed (Figure 9). Platelet-shaped structures have been observed in major plant groups including various angiosperms and gymnosperms, where tubules made of a significant proportion of β-diketones, as observed in our wax chemical analysis, are commonly found among the Poaceae [12,15].

The wax content of Conan leaf surface was characterized by a higher proportion in primary alcohols docosan-1-ol (**49**) and 6-methylheptacosan-1-ol (**54**). Waxes made of abundant primary alcohols form platelet-shaped crystals on the plant surface [12]. In addition, the primary alcohol octacosan-1-ol (**53**) is associated with plant–insect interactions and leaf glaucousness

[10]. Wax composition can influence insect attachment to the plant surface [64], and a study on the carnivorous pitcher plant *Nepenthes alata* revealed that a slippery zone on leaves is made of platelet-shaped crystals that detach after the insect touches the tissue, reducing the time of interaction between plant and pest [60]. The cultivar Conan shows a high degree of glaucousness and resistance to the Wheat Stem Sawfly, and our study supports that this may be due to increased wax content, increased content of docosan-1-ol (**49**) and 6-methylheptacosan-1-ol (**54**), and increased platelet-type crystals on leaf cuticles. This hypothesis is supported by the observation of compact layers of platelet-shaped crystals that have been shown to contribute to various means of biotic and abiotic resistance (e.g., insect deterrence, drought stress management, temperature regulation) [10,12,53,60].

It is of importance to note that, due to difficulty in growing spring wheat cultivars in Colorado fields, Conan and Reeder were grown in the greenhouse and this may have had an influence on wax variation when compared to winter cultivars (Denali and Hatcher) grown in the field. Increased wax content in Conan might be due to a genotype by environment (G × E) interaction, however, no clear trend was observed for either wax content (Figure 10) or crystal composition for plants grown in the field or greenhouse.

2.5.5. A GC-MS Metabolomics Workflow Was Applicable to Assess Epicuticular Wax Variation in Wheat

The metabolomics methods applied to this study included uni- and multivariate statistics of quantitative data. Based on these statistics, variation in cuticular wax content between wheat tissues and among cultivars was concluded (Figure 6). Using similar observations described in the literature, we hypothesized that chemical variation in waxes would result in variation of epicuticular wax crystals on the cuticle, and that observing this correlation would help validate

the relevance of our metabolomics model. Data presented in this study support the utility of this method.

The choice of a non-polar solvent for wax extraction shows relevance as hexane yields plant waxes of agronomic interest including alkanes, primary alcohols, fatty acids, ketones, and aldehydes [10,21-23]. In the present work, the use of hexane enabled the detection of 263 putative compounds including 58 cuticular waxes. Twenty alkanes, ten primary alcohols, 22 fatty acids, and six ketones were identified. When comparing acids, alcohols and ketones to alkanes of similar chain length, the former display a relatively higher polarity than the latter. The use of hexane thus allowed for the discrimination of metabolites that belong to a broad range of polarities. Moreover, the relatively short exposure of tissues to hexane (i.e., 30 s) necessary to extract a substantial proportion of waxes makes it an important asset for fast, high-throughput protocols with large sample sizes. Still, careful attention must be given to the duration of tissue exposure due to a potential local disruption of the cuticle membrane and release of internal compounds that are not surface waxes [38]. It is likely that the additional 11 non-wax compounds annotated are intracuticular metabolites that result from either the cut-open section of tissue that was immersed, or a slightly excessive exposure to the solvent. Further, even with a large sample set, little variation was observed among replicates of tissues within cultivars (Figure 6), supporting the reproducibility of our method.

The use of GC-MS instrumentation for low molecular weight, volatile compounds such as cuticular waxes is recommended [11,13,24,28-30]. Gas chromatography apparatuses include a hot evaporation chamber where samples are injected prior to column separation. A split/splitless sample injection mode is selected based on parameters that include peak resolution, column capacity and set up complexity and aims at reducing (split mode) or not (splitless mode) the

sample quantity before transport to the column. While the analytes may suffer from mass discrimination in split mode (high molecular weight compounds do not have enough time to vaporize, and their abundances are consequently less representative), its ease to use and automate, protection from non-volatile compound contamination, less propensity to thermal degradation, and sharper analyte peaks makes it a program of choice for plant wax detection. While splitless mode can result in large peaks with plateaus and tails, split mode generates metabolite profiles that are better suited for quantitative comparisons. Moreover, the GC oven temperature program is critical for separation of wax compounds [24-26]. The relatively short temperature ramp used here allowed for quick discrimination of a complex mixture of waxes from a wide range of mass-to-charge ratio values (i.e., 50–650 *m*/*z*; Tables 2 and 3), and provided quick sample-to-sample run times, thus reducing analytical error and improving quantitative comparisons among samples. However, it is possible that these technical choices prevented the identification of aldehyde, ester or secondary alcohol waxes, given their chemical properties (e.g., polarity, boiling point, molecular weight).

Further, the R packages XCMS and RAMClust were used to create an accurate matrix of molecular features, each representing a putative metabolite [39,42,65]. XCMS data preprocessing includes several common procedures aimed at curating raw data from metabolite profiling experiments, yet few wax studies incorporate this critical tool. Mass spectrometry instruments deliver complex datasets that need thorough preprocessing. XCMS includes consistent filtering, detection and alignment of *m*/*z* peaks, retention time correction, and peak filling that removes zero values from the dataset, as explained by Smith et al. (2006) [39]. Further curation of MS datasets is possible using the R package RAMClust, a deconvolution algorithm [42]. Where XCMS develops a data set by which molecular features are independent,

RAMClust groups features into spectral clusters to represent a single metabolite. The RAMClust method can also improve statistical robustness by reducing the number of data points to analyze (i.e., reducing false discoveries), and by establishing new quantitative values for each metabolite by integrating abundance values from all molecular features within a spectral cluster [42]. However, a potential pitfall that rises from spectral matching is the use of non-exhaustive databases. Further collective efforts must be made to create more reliable and complete directories for GC compounds, including the integration of fragmentation patterns for the most common electron impact configurations.

Studies on wax variation among tissues and cultivars of various plant systems incorporate the use of standardized methods of detection and analysis of metabolites. In wheat, common procedures include the use of polar solvents, splitless injection of samples in the GC column, and importantly, rarely incorporate advanced preprocessing data algorithms (e.g., [10,28,66,67]). Our GC-MS metabolomics methods are well developed and have been applied to a broad range of scientific questions and biological systems [22,23,33,34,42]. The methods used in this study utilized GC-MS detection of waxes and metabolomics pre- and post-processing tools that enabled the detection and relative quantitation of 263 putative metabolites. Future work can apply this workflow to evaluate wax variation important to breeding, genetic mapping, and stress resistance in wheat and other major crops.

2.5.6. Preliminary Conclusions

Our non-targeted GC-MS metabolomics data demonstrate that variation in cuticular wax composition and crystal microstructure exists among tissues and cultivars of common wheat. Leaf surfaces were characterized by high levels of alcohols and stem surfaces showed higher content in β-diketones. While most of the detected compounds were equally distributed among

cultivars, two Conan wax alcohols were higher in content than the other cultivars. Further, SEM imaging provided insights in wheat wax microstructural topography and allowed for the identification of two types of epicuticular wax crystals in wheat: platelets and tubules.

Table 2. Chemical composition of cuticular waxes detected on wheat leaves and stems.[a]

#[b]	IUPAC name (synonym)	Retention index	ANOVA *p* value[c]		Association[d]	Reference
			Tissue	Cultivar		
		Alkanes				
1	Eicosane	2000	‡	0.6	Plant–insect int.	[10]
2	Tricosane	2300	0.13	‡	Chemotaxonomy	[24]
3	4-Methyldocosane	2334	0.33	‡		
4	6-Methyldocosane	2336	‡	‡		
5	Pentacosane	2500	‡	0.77	Chemotaxonomy	[24]
6	Hexacosane	2600	‡	0.17	Chemotaxonomy	[24]
7	5-Methylpentacosane	2641	‡	0.63		
8	7-Methylpentacosane	2645	‡	0.63		
9	Heptacosane	2700	‡	0.56	Chemotaxonomy	[24]
10	4-Methylhexacosane	2727	‡	0.4		
11	12-Methyloctacosane	2912	‡	‡		
12	14-Methyloctacosane	2915	‡	‡		
13	Triacontane	3000	‡	‡	Chemotaxonomy	[24]
14	Hentriacontane	3100	0.12	0.05	Plant–insect int.	[10]
15	7-Methylhentriacontane	3111	‡	‡		
16	13-Methylhentriacontane	3124	‡	‡		
17	Tetratriacontane	3400	0.27	‡	Chemotaxonomy	[24]
18	Pentatriacontane	3500	0.61	0.16	Chemotaxonomy	[24]
19	Tetracontane	4000	‡	‡	Plant–insect int.	[51]
20	Dotetracontane	4200	‡	‡		
		Fatty acids				
21	Heptanoic acid (enanthic acid)	1044	0.25	0.3		
22	Tetradecanoic acid (myristic acid)	1499	‡	0.68	Antibiotic	[47]
23	Hexadecenoic acid	1602	0.51	0.57		
24	Hexadecanoic acid (palmitic acid)	1623	‡	0.9	Plant–insect int.	[10]
25	(9Z,12Z,15Z)-Octadeca-9,12,15-trienoic acid (α-linolenic acid)	1755	‡	0.13	Oil production	[68]
26	Octadecanoic acid (stearic acid)	1765	0.25	0.77	Plant–insect int.	[52]
27	10-Methylheptadecanoic acid	1768	0.12	0.61		
28	Nonadecanoic acid	1825	0.67	0.3	Plant–insect int.	[69]
29	Eicosanoic acid (arachidic acid)	1911	‡	0.52		
30	Docosanoic acid (behenic acid)	2103	‡	0.05	Oil production	[70]
31	Tricosanoic acid	2166	‡	0.77		
32	Tetracosanoic acid (lignoceric acid)	2246	‡	0.09	Major wax precursor	[49]
33	Hexacosanoic acid (cerotic acid)	2404	‡	0.06	Allelopathy	[48]
34	Heptacosanoic acid	2497	0.07	0.17		
35	Octacosanoic acid (montanic acid)	2563	‡	0.46		
36	25-Methylheptacosanoic acid	2569	0.07	0.17		
37	Nonacosanoic acid	2647	0.61	0.25		
38	23-Triacontenoic acid	2728	‡	0.54		
39	12-Methylnonacosanoic acid	2731	‡	0.77		
40	Triacontanoic acid (melissic acid)	2741	‡	0.32		
41	Hentriacontanoic acid	2796	‡	0.32		

42	Tetratriacontanoic acid (geddic acid)	3037	‡	‡	Plant–insect int.	[71]
		Ketones				
43	Nonane-4,6-dione	1124	‡	0.33		
44	Nonacosane-12,14-dione	2689	‡	0.41	Major leaf wax	[50]
45	Triacontane-12,14-dione	2698	‡	0.21		
46	Hentriacontane-14,16-dione	2735	‡	0.39	Glaucousness	[53]
47	Tritriacontan-3-one	2839	0.93	‡		
48	Pentatriacontan-2-one	2881	‡	0.54		
		Primary alcohols				
49	Docosan-1-ol (behenyl alcohol)	2044	‡	‡		
50	Tricosan-1-ol	2112	0.79	‡		
51	Hexacosan-1-ol	2325	‡	‡	Plant–insect int.	[10]
52	Heptacosan-1-ol	2404	0.9	‡		
53	Octacosan-1-ol	2467	‡	0.77	Plant–insect int.	[10]
54	6-Methylheptacosan-1-ol	2498	‡	‡		
55	Triacontan-1-ol (melissyl alcohol)	2668	‡	0.63		
56	Hentriacontan-1-ol	2703	‡	0.25		
57	22-Methylhentriacontan-1-ol	2780	‡	0.41		
58	Tritriacontan-1-ol	2855	‡	‡		

[a]Compounds were classified based on their chemical class and RI. # = compound ID; ‡ = $p <$ 0.05; int. = interaction.
[b]Bold numbers are used to reference compounds in the Results and Discussion sections.
[c]Each p value was calculated using one-way ANOVA (factors of cultivar and tissue) and adjusted by a Benjamini–Hochberg correction.
[d]The Association column refers to biological function with which metabolites are associated.

Table 3. Chemical composition of non-wax cuticular metabolites from wheat leaves and stems.[a]

#[b]	Class	IUPAC name (Synonym)	RI	ANOVA *p* value[c]	
				Tissue	Cultivar
59	Carboxylic acid	2-Hydroxybutanedioic acid (malic acid)	1192	0.19	‡
60		Tetradecanedioic acid	1471	0.14	0.34
61		5-(Dioctadecylamino)-5-oxo-pentanoic acid	2589	‡	0.3
62	Carbohydrate	(3S,4S,5S,6R)-6-(Hydroxymethyl)oxane-2,3,4,5-tetrol (D-mannose)	1602	0.23	‡
63		(2R,3R,4S,5S,6R)-2-[(2S,3S,4S,5R)-3,4-Dihydroxy-2,5-bis(hydroxymethyl)Oxolan-2-yl]oxy-6-(hydroxymethyl)oxane-3,4,5-triol (sucrose)	2140	0.89	0.3
64	Primary amine	Hexadecan-1-amine	854	‡	0.61
65	Polycyclic ketone	1,2-Diphenyl-2-buten-1-one	2184	0.15	0.57
66		3-Acetyl-8-methoxy-2-methyl-1H-naphtho[2,1-b]pyran-1-one	2389	‡	0.14
67	FAME	Methyl-6-(1-hydroxyethyl)phenazine-1-carboxylate(saphenic acid methyl ester)	2885	‡	0.24
68	Flavonoid	3,5-Dihydroxy-4″,7-dimethoxyflavone (pilloin)	2287	‡	0.92
69	Sterol	(3S,8S,9S,10R,13R,14S,17R)-17-[(2R,5R)-5-Ethyl-6-methylheptan-2-yl]-10,13-dimethyl-2,3,4,7,8,9,11,12,14,15,16,17-dodecahydro-1H-cyclopenta[a]phenanthren-3-ol (β-sitosterol)	2801	‡	0.4

[a]Compounds were classified based on their chemical class and RI. # = compound ID; RI = retention index; ‡ = $p < 0.05$; FAME = fatty acid methyl ester.
[b]Bold numbers are used to reference compounds in the Results and Discussion sections.
[c]Each *p* value was calculated using one-way ANOVA (factors of cultivar and tissue) and adjusted by a Benjamini–Hochberg correction.

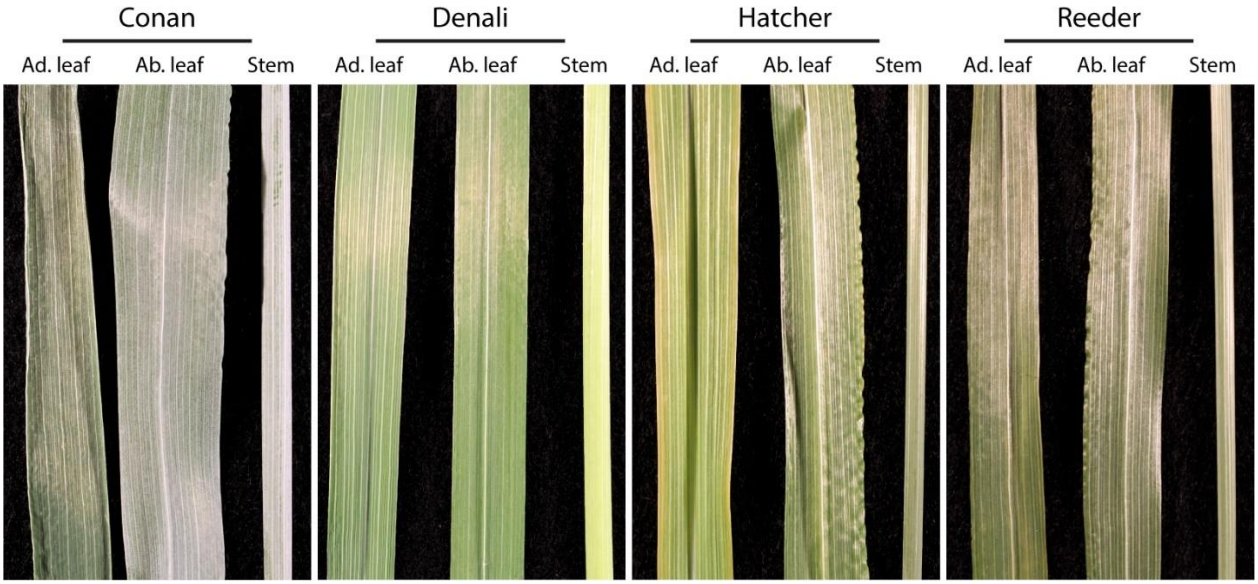

Figure 4. Glaucousness degree on leaf and stem cuticles of four wheat cultivars. Photographs showing a bluish-green appearance (high glaucousness) for the cultivar Conan on both sides of its leaves, and stems. Denali, Hatcher, and Reeder cuticular tissue showed lower levels of glaucousness. All pictures were taken from plants at approximately Zadoks stage 55. Abbreviations: ad. Leaf = adaxial leaf surface; ab. leaf = abaxial leaf surface.

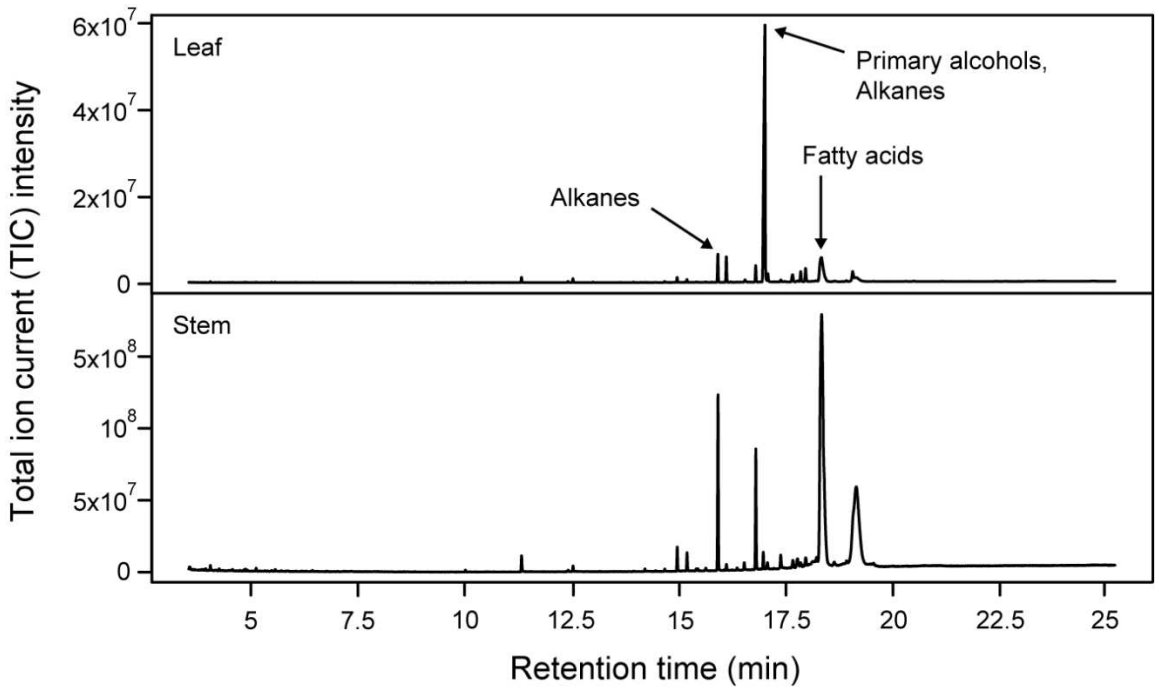

Figure 5. Example GC-MS chromatograms for leaf and stem metabolites in the wheat cultivar Hatcher. Arrows indicate which class of compounds was the most represented at the respective retention times.

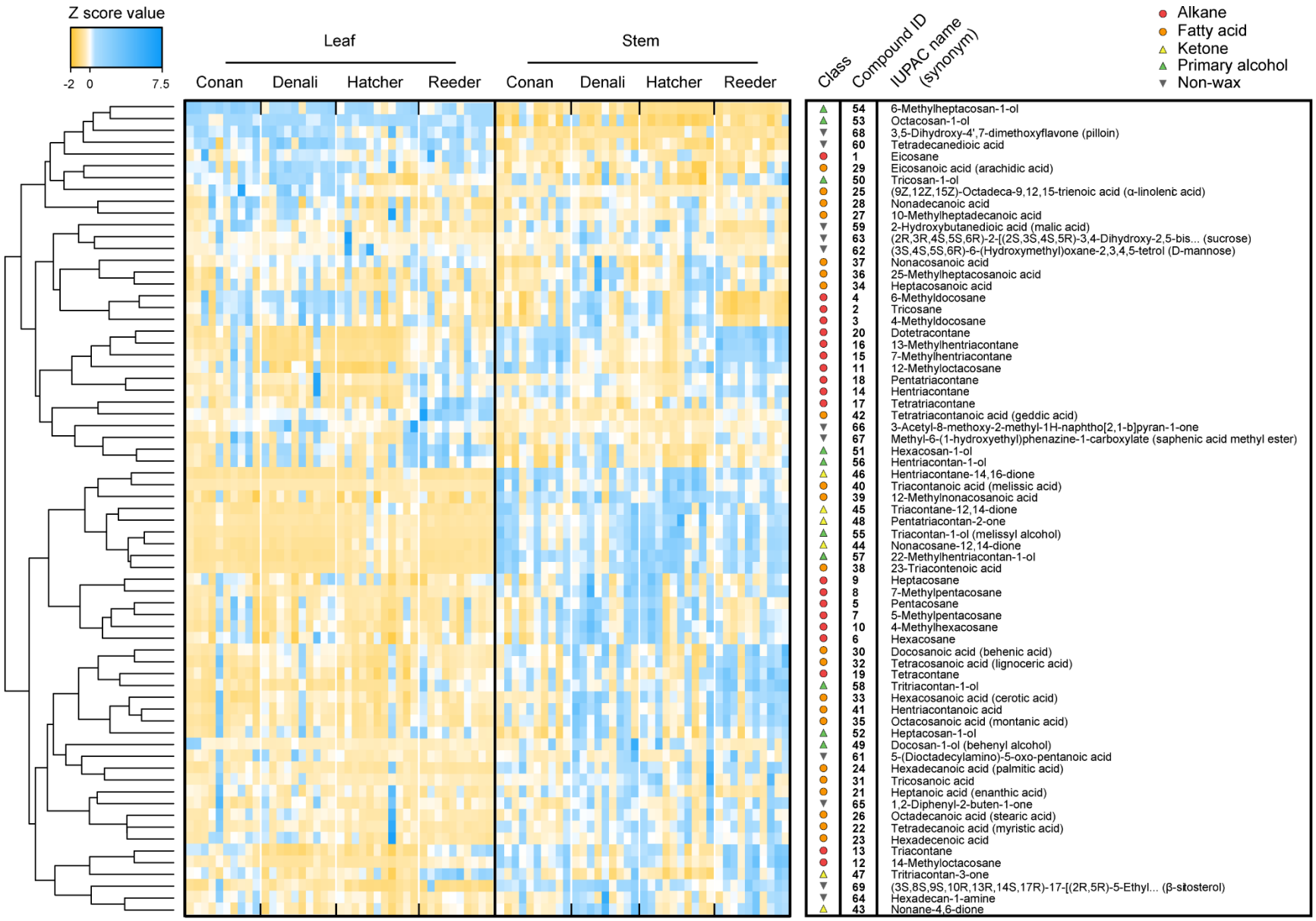
Z score value
-2 0 7.5
Leaf
Stem
Conan Denali Hatcher Reeder Conan Denali Hatcher Reeder
Class
Compound ID
IUPAC name (synonym)
Alkane
Fatty acid
Ketone
Primary alcohol
Non-wax
54 6-Methylheptacosan-1-ol
53 Octacosan-1-ol
68 3,5-Dihydroxy-4',7-dimethoxyflavone (pilloin)
60 Tetradecanedioic acid
1 Eicosane
29 Eicosanoic acid (arachidic acid)
50 Tricosan-1-ol
25 (9Z,12Z,15Z)-Octadeca-9,12,15-trienoic acid (α-linolenic acid)
28 Nonadecanoic acid
27 10-Methylheptadecanoic acid
59 2-Hydroxybutanedioic acid (malic acid)
63 (2R,3R,4S,5S,6R)-2-[(2S,3S,4S,5R)-3,4-Dihydroxy-2,5-bis... (sucrose)
62 (3S,4S,5S,6R)-6-(Hydroxymethyl)oxane-2,3,4,5-tetrol (D-mannose)
37 Nonacosanoic acid
36 25-Methylheptacosanoic acid
34 Heptacosanoic acid
4 6-Methyldocosane
2 Tricosane
3 4-Methyldocosane
20 Dotetracontane
16 13-Methylhentriacontane
15 7-Methylhentriacontane
11 12-Methyloctacosane
18 Pentatriacontane
14 Hentriacontane
17 Tetratriacontane
42 Tetratriacontanoic acid (geddic acid)
66 3-Acetyl-8-methoxy-2-methyl-1H-naphtho[2,1-b]pyran-1-one
67 Methyl-6-(1-hydroxyethyl)phenazine-1-carboxylate (saphenic acid methyl ester)
51 Hexacosan-1-ol
56 Hentriacontan-1-ol
46 Hentriacontane-14,16-dione
40 Triacontanoic acid (melissic acid)
39 12-Methylnonacosanoic acid
45 Triacontane-12,14-dione
48 Pentatriacontan-2-one
55 Triacontan-1-ol (melissyl alcohol)
44 Nonacosane-12,14-dione
57 22-Methylhentriacontan-1-ol
38 23-Triacontenoic acid
9 Heptacosane
8 7-Methylpentacosane
5 Pentacosane
7 5-Methylpentacosane
10 4-Methylhexacosane
6 Hexacosane
30 Docosanoic acid (behenic acid)
32 Tetracosanoic acid (lignoceric acid)
19 Tetracontane
58 Tritriacontan-1-ol
33 Hexacosanoic acid (cerotic acid)
41 Hentriacontanoic acid
35 Octacosanoic acid (montanic acid)
52 Heptacosan-1-ol
49 Docosan-1-ol (behenyl alcohol)
61 5-(Dioctadecylamino)-5-oxo-pentanoic acid
24 Hexadecanoic acid (palmitic acid)
31 Tricosanoic acid
21 Heptanoic acid (enanthic acid)
65 1,2-Diphenyl-2-buten-1-one
26 Octadecanoic acid (stearic acid)
22 Tetradecanoic acid (myristic acid)
23 Hexadecenoic acid
13 Triacontane
12 14-Methyloctacosane
47 Tritriacontan-3-one
69 (3S,8S,9S,10R,13R,14S,17R)-17-[(2R,5R)-5-Ethyl... (β-sitosterol)
64 Hexadecan-1-amine
43 Nonane-4,6-dione

Figure 6. Metabolite levels in wheat. Heat map showing metabolite levels on leaf and stem cuticles of wheat. Composition often was independent of cultivar, and two main clusters were identified: metabolites higher in content on leaf cuticles and lower on stem cuticles (top), and metabolites lower in content on leaf cuticles and higher on stem cuticles (bottom). The 58 wax and 11 non-wax metabolite contents were z-transformed, subjected to hierarchical clustering, and displayed as color (blue = high content, yellow = low content). Each cell represents the z transformed content of a single biological replicate for a total of $n = 9–11$ replicates/cells per cultivar. Z-transformation was based on the mean abundance and standard deviation of the metabolite across all samples.

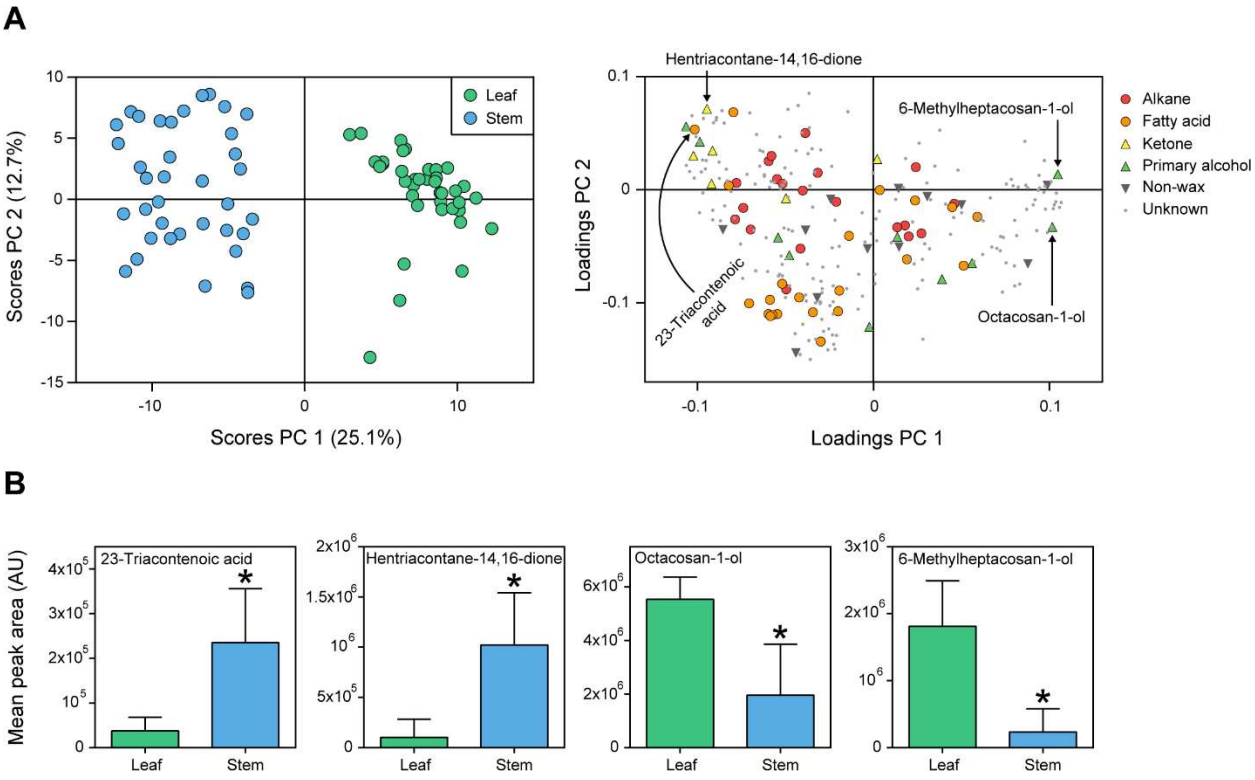

Figure 7. Metabolite distribution in leaf and stem cuticles. Multivariate analysis demonstrating specific composition in cuticular wax chemistry between leaf and stem surfaces of wheat. **(A)** Principal component analysis (PCA) of the four cultivars showed that most metabolite (wax and non-wax) variation was due to differences between leaves and stems (principal component, or PC scores, left). Each PC score point represents the metabolite profile for a single biological replicate (n = 9–11 replicates per cultivar). Loadings were colored by wax type and include primary alcohols, ketones, and fatty acids. Example wax metabolites are indicated by arrows. **(B)** Box plots of example waxes that varied between leaf and stem cuticles. Metabolite values are reported as the mean content across all cultivars ± standard error of the mean (n = 40 biological replicates per tissue). Asterisks indicate variation between tissues (ANOVA, FDR-adjusted p < 0.05). Abbreviations/Notations: PC = principal component; AU = arbitrary unit; unknown = unknown metabolite, no annotation.

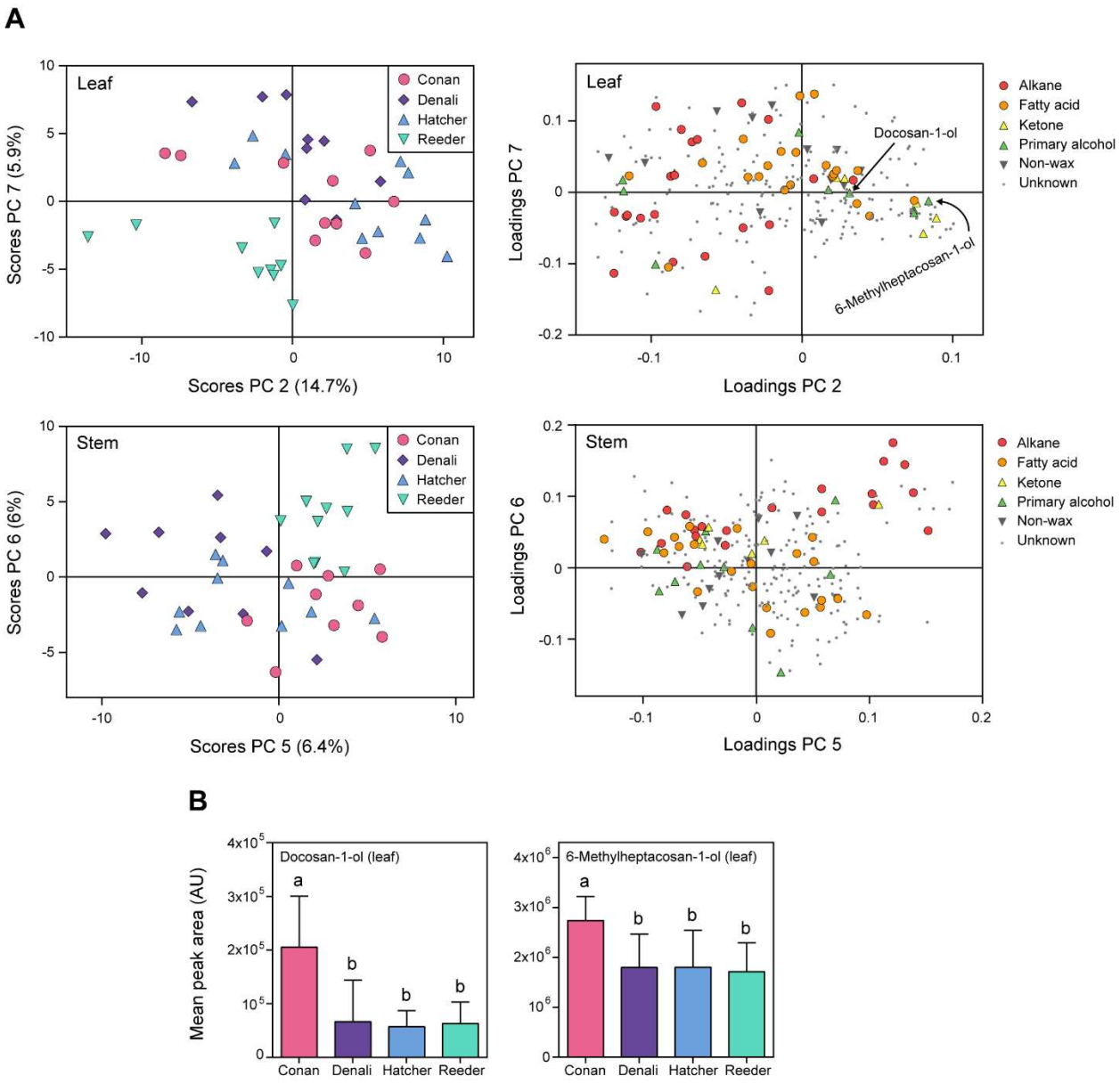

Figure 8. Metabolite levels among cultivars within leaf and stem cuticles. Multivariate analysis showing cuticular wax variation among different cultivars of wheat. **(A)** Principal component analysis showed cultivar variation within leaf (top) and stem (bottom) surfaces. Loadings indicate metabolites involved in the separation of cultivars and are colored based on wax type. Metabolites denoted on the PCA loadings plot exhibited increased content in the cultivar Conan. **(B)** Box plots of two wax metabolites that were higher in content on Conan leaf cuticles. Metabolite values are reported as the mean content of leaf cuticles for each cultivar ± standard error of the mean (n = 9–11 replicates per cultivar). Lowercase letters indicate variation among cultivars (ANOVA, Tukey HSD post-hoc FDR adjusted $p < 0.05$). Abbreviations/Notations: PC = principal component; AU = arbitrary unit; unknown = unknown metabolite, no annotation.

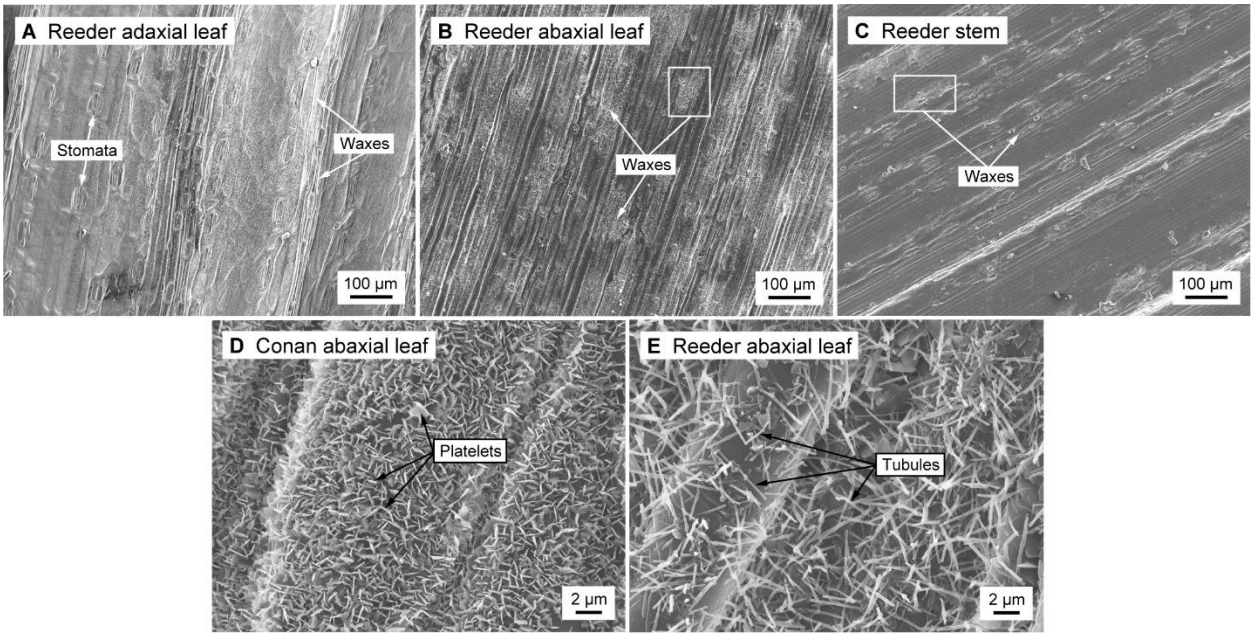

Figure 9. Epicuticular wax crystal variation on the surface of greenhouse-grown wheat. Scanning electron micrographs of wheat epicuticular wax crystals showed that: **(A)** Reeder adaxial leaf surface had the highest content in wax crystals; **(B)** Reeder abaxial leaf surface displayed intermediate wax crystal content; **(C)** Reeder stem had low wax crystal content; **(D)** Conan abaxial leaf surface was exclusively made of platelet crystals; and **(E)** Reeder abaxial leaf surface consisted of tubules.

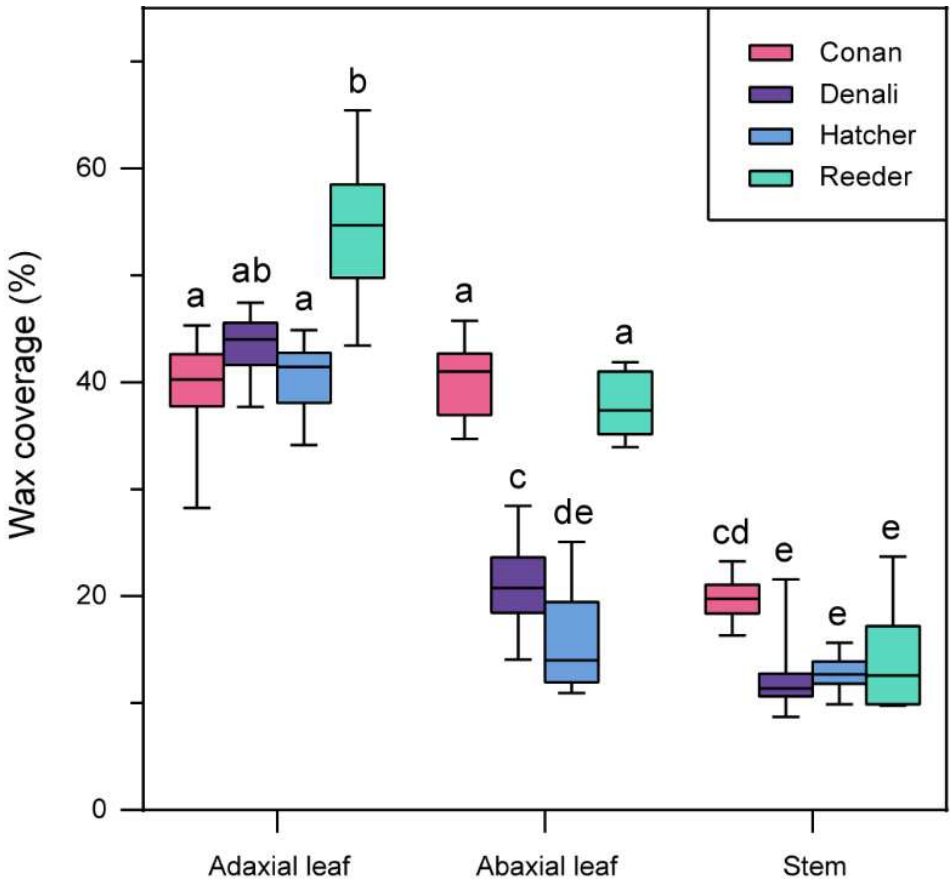

Figure 10. Epicuticular wax content among cultivars and tissue types. Wax contents are expressed as the percentage of the total surface covered and reported as the mean content for each cultivar within each tissue ($n = 2$ biological replicates and $n = 5$ technical replicates per cultivar per tissue). Lower case letters indicate Tukey HSD post-hoc groupings (ANOVA, Tukey HSD post-hoc $p < 0.05$).

REFERENCES

1. Pandey, P.; Irulappan, V.; Bagavathiannan, M.V.; Senthil-Kumar, M. Impact of combined abiotic and biotic stresses on plant growth and avenues for crop improvement by exploiting physio-morphological traits. *Front. Plant Sci.* **2017**, *8*, 537.

2. Riederer, M.; Schreiber, L. Protecting against water loss: analysis of the barrier properties of plant cuticles. *J. Exp. Bot.* **2001**, *52*, 2023–2032.

3. Bi, H.; Luang, S.; Li, Y.; Bazanova, N.; Morran, S.; Song, Z.; Perera, M.A.; Hrmova, M.; Borisjuk, N.; Lopato, S. Identification and characterization of wheat drought-responsive MYB transcription factors involved in the regulation of cuticle biosynthesis. *J. Exp. Bot.* **2016**, *67*, 5363–5380.

4. Baur, P.; Buchholz, A.; Schönherr, J. Diffusion in plant cuticles as affected by temperature and size of organic solutes: similarity and diversity among species. *Plant Cell Environ.* **1997**, *20*, 982–994.

5. Yeats, T.H.; Rose, J.K. The formation and function of plant cuticles. *Plant Physiol.* **2013**, *163*, 5–20.

6. Kunst, L.; Samuels, L. Plant cuticles shine: advances in wax biosynthesis and export. *Curr. Opin. Plant Biol.* **2009**, *12*, 721–727.

7. Serrano, M.; Coluccia, F.; Torres, M.; L'Haridon, F.; Metraux, J.P. The cuticle and plant defense to pathogens. *Front. Plant Sci.* **2014**, *5*, 274.

8. Eigenbrode, S.D.; Espelie, K.E.; Shelton, A.M. Behavior of neonate Diamondback moth larvae [*Plutella xylostella* (L.)] on leaves and on extracted leaf waxes of resistant and susceptible cabbages. *J. Chem. Ecol.* **1991**, *17*, 1691–1704.

9. Krauss, P.; Markstadter, C.; Riederer, M. Attenuation of UV radiation by plant cuticles from woody species. *Plant Cell Environ.* **1997**, *20*, 1079–1085.

10. Cervantes, D.E.; Eigenbrode, S.D.; Ding, H.-J.; Bosque-Pérez, N.A. Oviposition responses by Hessian fly, *Mayetiola destructor*, to wheats varying in surfaces waxes. *J. Chem. Ecol.* **2002**, *28*, 193–210.

11. Jenks, M.A.; Gaston, C.H.; Goodwin, M.S.; Keith, J.A.; Teusink, R.S. Seasonal variation in cuticular waxes on *Hosta* genotypes differing in leaf surface glaucousness. *HortScience* **2002**, *37*, 673–677.

12. von Wettstein-Knowles, P. *Plant waxes*. Publisher: John Wiley & Sons, Ltd., Chichester, UK, 2012.

13. Wang, Y.; Wang, J.; Chai, G.; Li, C.; Hu, Y.; Chen, X.; Wang, Z. Developmental changes in composition and morphology of cuticular waxes on leaves and spikes of glossy and glaucous wheat (*Triticum aestivum* L.). *PLoS One* **2015**, *10*, e0141239.

14. Hen-Avivi, S.; Savin, O.; Racovita, R.C.; Lee, W.S.; Adamski, N.M.; Malitsky, S.; Almekias-Siegl, E.; Levy, M.; Vautrin, S.; Berges, H.; Friedlander, G.; Kartvelishvily, E.; Ben-Zvi, G.; Alkan, N.; Uauy, C.; Kanyuka, K.; Jetter, R.; Distelfeld, A.; Aharoni, A. A metabolic gene cluster in the wheat

W1 and the barley *Cer-cqu* loci determines β-diketone biosynthesis and glaucousness. *Plant Cell* **2016**, *28*, 1440–1460.

15. Barthlott, W.; Neinhuis, C.; Cutler, D.; Ditsch, F.; Meusel, I.; Theisen, I.; Wilhelmi, H. Classification and terminology of plant epicuticular waxes. *Bot. J. Linn. Soc.* **1998**, *126*, 237–260.

16. Chambers, T.C.; Ritchie, I.M.; Booth, M.A. Chemical models for plant wax morphogenesis. *New Phytol.* **1976**, *77*, 43–49.

17. Adamski, N.M.; Bush, M.S.; Simmonds, J.; Turner, A.S.; Mugford, S.G.; Jones, A.; Findlay, K.; Pedentchouk, N.; von Wettstein-Knowles, P.; Uauy, C. The *Inhibitor of wax 1* (*Iw1*) prevents formation of β- and OH-β-diketones in wheat cuticular waxes and maps to a sub-cM interval on chromosome arm 2BS. *Plant J.* **2013**, *74*, 989–1002.

18. Blenn, B.; Bandoly, M.; Küffne, A.; Otte, T.; Geiselhardt, S.; Fatouros, N.E.; Hilker, M. Insect egg deposition induces indirect defense and epicuticular wax changes in *Arabidopsis thaliana*. *J. Chem. Ecol.* **2012**, *38*, 882–892.

19. Cordeiro, S.Z.; Simas, N.K.; Arruda, R.C.O.; Sato, A. Composition of epicuticular wax layer of two species of *Mandevilla* (Apocynoideae, Apocynaceae) from Rio de Janeiro, Brazil. *Biochem. Syst. Ecol.* **2011**, *39*, 198–202.

20. Still, G.G.; Davis, D.G.; Zander, G.L. Plant epicuticular lipids: alteration by herbicidal carbamates. *Plant Physiol.* **1970**, *46*, 307–314.

21. Athukorala, Y.; Mazza, G. Supercritical carbon dioxide and hexane extraction of wax from triticale straw: content, composition and thermal properties. *Ind. Crop. Prod.* **2010**, *31*, 550–556.

22. Zhang, J.Y.; Broeckling, C.D.; Blancaflor, E.B.; Sledge, M.K.; Sumner, L.W.; Wang, Z.Y. Overexpression of *WXP1*, a putative *Medicago truncatula* AP2 domain-containing transcription factor gene, increases cuticular wax accumulation and enhances drought tolerance in transgenic alfalfa (*Medicago sativa*). *Plant J.* **2005**, *42*, 689–707.

23. Zhang, J.Y.; Broeckling, C.D.; Sumner, L.W.; Wang, Z.Y. Heterologous expression of two *Medicago truncatula* putative ERF transcription factor genes, *WXP1* and *WXP1*, in *Arabidopsis* led to increased leaf wax accumulation and improved drought tolerance, but differential response in freezing tolerance. *Plant Mol. Biol.* **2007**, *64*, 265–278.

24. Bush, R.T.; McInerney, F.A. Leaf wax *n*-alkane distributions in and across modern plants: implications for paleoecology and chemotaxonomy. *Geochim. Cosmochim. Acta* **2013**, *117*, 161–179.

25. Loneman, D.M.; Peddicord, L.; Al-Rashid, A.; Nikolau, B.J.; Lauter, N.; Yandeau-Nelson, M.D. A robust and efficient method for the extraction of plant extracellular surface lipids as applied to the analysis of silks and seedling leaves of maize. *PLoS One* **2017**, *12*, e0180850.

26. Yang, Y.; Zhou, B.; Zhang, J.; Wang, C.; Liu, C.; Liu, Y.; Zhu, X.; Ren, X. Relationships between cuticular waxes and skin greasiness of apples during storage. *Postharvest Biol. Technol.* **2017**, *131*, 55–67.

27. Osorio, S.; Thi Do, P.; Fernie, A.R. Profiling primary metabolites of tomato fruit with gas chromatography/mass spectrometry. In *Plant metabolomics: methods and protocols*; Hardy, N.W.,

Hall R.D., Eds.; Publisher: Springer/Humana Press, New York City, NY, USA, 2012; pp. 101–109; 9761617795947.

28. Racovita, R.C.; Hen-Avivi, S.; Fernandez-Moreno, J.P.; Granell, A.; Aharoni, A.; Jetter, R. Composition of cuticular waxes coating flag leaf blades and peduncles of *Triticum aestivum* cv. Bethlehem. *Phytochemistry* **2016**, *130*, 182–192.

29. Steinbauer, M.J.; Davies, N.W.; Gaertner, C.; Derridj, S. Epicuticular waxes and plant primary metabolites on the surfaces of juvenile *Eucalyptus globulus* and *E. nitens* (Myrtaceae) leaves. *Aust. J. Bot.* **2009**, *57*, 474–485.

30. Weaver, D.K.; Buteler, M.; Hofland, M.L.; Runyon, J.B.; Nansen, C.; Talbert, L.E.; Lamb, P.; Carlson, G.R. Cultivar preferences of ovipositing wheat stem sawflies as influenced by the amount of volatile attractant. *J. Econ. Entomol.* **2009**, *102*, 1009–1017.

31. Aretz, I.; Meierhofer, D. Advantages and pitfalls of mass spectrometry based metabolome profiling in systems biology. *Int. J. Mol. Sci.* **2016**, *17*, 632.

32. Heuberger, A.L.; Robison, F.M.; Lyons, S.M.A.; Broeckling, C.D.; Prenni, J.E. Evaluating plant immunity using mass spectrometry-based metabolomics workflows. *Front. Plant Sci.* **2014**, *5*, 291.

33. Santangelo, M.P.; Heuberger, A.L.; Blanco, F.; Forrellad, M.; Taibo, C.; Klepp, L.; Sabio García, J.; Nikel, P.I.; Jackson, M.; Bigi, F. Metabolic profile of *Mycobacterium smegmatis* reveals Mce4 proteins are relevant for cell wall lipid homeostasis. *Metabolomics* **2016**, *12*.

34. Abdel-Ghany, S.E.; Day, I.; Heuberger, A.L.; Broeckling, C.D.; Reddy, A.S.N. Metabolic engineering of Arabidopsis for butanetriol production using bacterial genes. *Metab. Eng.* **2013**, *20*, 109–120.

35. Haley, S.D.; Quick, J.S.; Johnson, J.J.; Peairs, F.B.; Stromberger, A.; Clayshulte, S.R.; Clifford, B.L.; Rudolf, J.B.; Seabourn, B.W.; Chung, O.K.; Jin, Y.; Kolmer, J. Registration of 'Hatcher' wheat. *Crop Sci.* **2005**, *45*, 2654–2656.

36. Haley, S.D.; Johnson, J.J.; Peairs, F.B.; Stromberger, J.A.; Hudson, E.E.; Seifert, S.A.; Kottke, R.A.; Valdez, V.A.; Rudolph, J.B.; Martin, T.J.; Bai, G.; Chen, X.; Bowden, R.L.; Jin, Y.; Kolmer, J.A.; Chen, M.-S.; Seabourn, B.W. Registration of 'Denali' wheat. *J. Plant Regist.* **2012**, *6*, 311–314.

37. Zadoks, J.C.; Chang, T.T.; Konzak, C.F. A decimal code for the growth stages of cereals. *Weed Res.* **1974**, *14*, 415–421.

38. Holloway, P.J.; Jeffree, C.E. Epicuticular waxes. In *Encyclopedia of applied plant sciences*; 2nd ed.; Thomas, B., Murphy, D.J., Murray, B.G., Eds.; Publisher: Academic press, Cambridge, Massachusetts, MA, USA, 2017; Volume 2, pp. 374–386; 9780123948083.

39. Smith, C.A.; Want, E.J.; O'Maille, G.; Abagyan, R.; Siuzdak, G. XCMS: processing mass spectrometry data for metabolite profiling using nonlinear peak alignment, matching, and identification. *Anal. Chem.* **2006**, *78*, 779–787.

40. Kopka, J.; Schauer, N.; Krueger, S.; Birkemeyer, C.; Usadel, B.; Bergmuller, E.; Dormann, P.; Weckwerth, W.; Gibon, Y.; Stitt, M.; Willmitzer, L.; Fernie, A.R.; Steinhauser, D. GMD@CSB.DB: the Golm Metabolome Database. *Bioinformatics* **2005**, *21*, 1635–1638.

41. Golm Metabolome Database. Available online: http://gmd.mpimp-golm.mpg.de/.

42. Broeckling, C.D.; Afsar, F.A.; Neumann, S.; Ben-Hur, A.; Prenni, J.E. RAMClust: a novel feature clustering method enables spectral-matching-based annotation for metabolomics data. *Anal. Chem.* **2014**, *86*, 6812–6817.

43. National Institute of Standards and Technology. Available online: http://www.nist.gov/.

44. Sumner, L.W.; Amberg, A.; Barrett, D.; Beale, M.H.; Beger, R.; Daykin, C.A.; Fan, T.W.; Fiehn, O.; Goodacre, R.; Griffin, J.L.; Hankemeier, T.; Hardy, N.; Harnly, J.; Higashi, R.; Kopka, J.; Lane, A.N.; Lindon, J.C.; Marriott, P.; Nicholls, A.W.; Reily, M.D.; Thaden, J.J.; Viant, M.R. Proposed minimum reporting standards for chemical analysis. *Metabolomics* **2007**, *3*, 211–221.

45. Benjamini, Y.; Hochberg, Y. Controlling the false discovery rate: a practical and powerful approach to multiple testing. *J. R. Stat. Soc.* **1995**, *57*, 289–300.

46. Heo, H.Y.; Blake, N.; Stougaard, R.N.; Kephart, K.D.; Wichman, D.M.; Carr, P.; Briar, S.; Miller, J.; Reddy, G.V.P.; Lamb, P.; Eckhoff, J.; Chen, C.; Nash, D.; Talbert, L.E. Performance evaluation and recommendations for spring wheat. Unpublished work.

47. Agoramoorthy, G.; Chandrasekaran, M.; Venkatesalu, V.; Hsu, M.J. Antibacterial and antifungal activities of fatty acid methyl esters of the blind-your-eye mangrove from India. *Braz. J. Microbiol.* **2007**, *38*, 739–742.

48. Broz, A.K.; Broeckling, C.D.; De-la-Peña, C.; Lewis, M.R.; Greene, E.; Callaway, R.M.; Sumner, L.W.; Vivanco, J.M. Plant neighbor identity influences plant biochemistry and physiology related to defense. *BMC Plant Biol.* **2010**, *10*.

49. Kim, J.; Jung, J.H.; Lee, S.B.; Go, Y.S.; Kim, H.J.; Cahoon, R.; Markham, J.E.; Cahoon, E.B.; Suh, M.C. Arabidopsis 3-ketoacyl-coenzyme A synthase9 is involved in the synthesis of tetracosanoic acids as precursors of cuticular waxes, suberins, sphingolipids, and phospholipids. *Plant Physiol.* **2013**, *162*, 567–580.

50. Zhang, Z.; Wei, W.; Zhu, H.; Challa, G.S.; Bi, C.; Trick, H.N.; Li, W. *W3* is a new wax locus that is essential for biosynthesis of β-diketone, development of glaucousness, and reduction of cuticle permeability in common wheat. *PLoS One* **2015**, *10*, e0140524.

51. Gorb, E.; Bohm, S.; Jacky, N.; Maier, L.P.; Dening, K.; Pechook, S.; Pokroy, B.; Gorb, S. Insect attachment on crystalline bioinspired wax surfaces formed by alkanes of varying chain lengths. *Beilstein J. Nanotechnol.* **2014**, *5*, 1031–1041.

52. Leszczynski, B.; Goławska, S.; Matok, H. Allelopathic action of Triticale allochemicals towards grain aphid. In *Allelopathy: new concepts and methodology*; Fujii, Y., Hiradate., S., Eds.; Publisher: CRC Press, Boca Raton, Florida, FL, USA, 2007; pp. 353–364; 9781578084463.

53. Johnson, D.A.; Richards, R.A.; Turner, N.C. Yield, water relations, gas exchange, and surface reflectances of near-isogenic wheat lines differing in glaucousness. *Crop Sci.* **1983**, *23*, 318–325.

54. Wu, H.; Qin, J.; Han, J.; Zhao, X.; Ouyang, S.; Liang, Y.; Zhang, D.; Wang, Z.; Wu, Q.; Xie, J.; Cui, Y.; Peng, H.; Sun, Q.; Liu, Z. Comparative high-resolution mapping of the wax inhibitors *Iw1* and *Iw2* in hexaploid wheat. *PLoS One* **2013**, *8*, e84691.

55. Wang, M.; Wang, Y.; Wu, H.; Xu, J.; Li, T.; Hegebarth, D.; Jetter, R.; Chen, L.; Wang, Z. Three *TaFAR* genes function in the biosynthesis of primary alcohols and the response to abiotic stresses in *Triticum aestivum*. *Sci. Rep.* **2016**, *6*, 25008.

56. Bi, H.; Luang, S.; Li, Y.; Bazanova, N.; Borisjuk, N.; Hrmova, M.; Lopato, S. Wheat drought-responsive WXPL transcription factors regulate cuticle biosynthesis genes. *Plant Mol. Biol.* **2017**, *doi: 10.1007/s11103-017-0585-9*.

57. Tulloch, A.P.; Hoffman, L.L. Epicuticular waxes of *Secale cereale* and *Triticale hexaploide* leaves. *Phytochemistry* **1974**, *13*, 2535–2540.

58. Richards, R.A.; Rawson, H.M.; Johnson, D.A. Glaucousness in wheat: its development and effect on water-use efficiency, gas exchange and photosynthetic tissue temperatures. *Aust. J. Plant Physiol.* **1986**, *13*, 465–473.

59. Barber, H.N.; Jackson, W.D. Natural selection in action in *Eucalyptus*. *Nature* **1957**, *179*, 1267–1269.

60. Gorb, E.; Haas, K.; Henrich, A.; Enders, S.; Barbakadze, N.; Gorb, S. Composite structure of the crystalline epicuticular wax layer of the slippery zone in the pitchers of the carnivorous plant *Nepenthes alata* and its effect on insect attachment. *J. Exp. Biol.* **2005**, *208*, 4651–4662.

61. Ni, Y.; Guo, Y.J.; Guo, Y.J.; Han, L.; Tang, H.; Conyers, M. Leaf cuticular waxes and physiological parameters in alfalfa leaves as influenced by drought. *Photosynthetica* **2012**, *50*, 458–466.

62. Damon, S.J.; Groves, R.L.; Havey, M.J. Variation for epicuticular waxes on onion foliage and impacts on numbers of onion thrips. *J. Amer. Soc. Hort. Sci.* **2014**, *139*, 495–501.

63. Cowlishaw, M.G.; Bickerstaffe, R.; Connor, H.E. Intraspecific variation in the epicuticular wax composition of four species of *Chionochloa*. *Biochem. Syst. Ecol.* **1983**, *11*, 247–259.

64. Eigenbrode, S.D.; Jetter, R. Attachment to plant surface waxes by an insect predator. *Integr. Comp. Biol.* **2002**, *42*, 1091–1099.

65. Mahieu, N.G.; Genenbacher, J.L.; Patti, G.J. A roadmap for the XCMS family of software solutions in metabolomics. *Curr. Opin. Chem. Biol.* **2016**, *30*, 87–93.

66. Kosma, D.K.; Nemacheck, J.A.; Jenks, M.A.; Williams, C.E. Changes in properties of wheat leaf cuticle during interactions with Hessian fly. *Plant J.* **2010**, *63*, 31–43.

67. Koch, K.; Barthlott, W.; Koch, S.; Hommes, A.; Wandelt, K.; Mamdouh, W.; De-Feyter, S.; Broekmann, P. Structural analysis of wheat wax (*Triticum aestivum*, *c.v.* 'Naturastar' L.): from the molecular level to three dimensional crystals. *Planta* **2006**, *223*, 258–270.

68. Vanhercke, T.; Wood, C.C.; Stymne, S.; Singh, S.P.; Green, A.G. Metabolic engineering of plant oils and waxes for use as industrial feedstocks. *Plant Biotechnol. J.* **2013**, *11*, 197–210.

69. Karmakar, A.; Barik, A. *Solena aplexicaulis* (Cucurbitaceae) flower surface wax influencing attraction of a generalist insect herbivore, *Aulacophora foveicollis* (Coleoptera: Chrysomelidae). *Int. J. Trop. Insect Sci.* **2016**, *36*, 70–81.

70. Dyer, J.M.; Stymne, S.; Green, A.G.; Carlsson, A.S. High-value oils from plants. *Plant J.* **2008**, *54*, 640–655.

71. Evans, D.; Knights, B.A.; Math, V.B.; Ritchie, A.L. β-diketones in *Rhododendron* waxes. *Phytochemistry* **1975**, *14*, 2447–2451.

CHAPTER 3 – WHEAT PROTEOMIC AND METABOLOMIC RESPONSES ASSOCIATED WITH RESISTANCE TO THE WHEAT STEM SAWFLY PEST[a,b]

3.1. Summary

Bread wheat (*Triticum aestivum* L.) is a global staple crop and wheat insect pests can significantly impact grain yield. The Wheat Stem Sawfly (*Cephus cinctus*, WSS) is a major wheat pest and partial resistance has been developed by breeding for solid-stem traits that interfere with the WSS life cycle. Here, we evaluated a selection of wheat cultivars in a WSS-infested field and found some with increased yield and reduced WSS infestation values. The molecular basis of this resistance was evaluated in a greenhouse study that characterized proteomic and metabolomic signatures of wheat stems associated with WSS infestation. WSS herbivory was induced in stems of four wheat cultivars: Hatcher (hollow-stem resistant), Conan (semi-solid-stem resistant), and Denali and Reeder (hollow-stem susceptible). Stem proteins (1832) and metabolites (1823) were detected using liquid chromatography-mass spectrometry methods. The proteome contained proteins involved in five major biological processes including metabolic processes and response to stimuli, and the metabolome was comprised of eight main chemical classes that included alkaloids, benzenoids, and lipids. During infestation with WSS, 62 proteins and 29 metabolites were differentially regulated in the hollow-stem resistant cultivar. Metabolic processes that were associated with resistance included enzymatic detoxification,

---

[a]This chapter is adapted from a research article that is being prepared for publication in the Journal of Proteome Research, with minor modifications.
[b]Authors: Florent D. Lavergne, Corey D. Broeckling, Kitty Brown, Darren M. Cockrell, Scott D. Haley, Frank B. Peairs, Stephen Pearce, Lisa M. Wolfe, Courtney E. Jahn, Adam L. Heuberger.

proteinase inhibition, and anti-herbivory compound production, specifically via benzoxazinoids, neolignans, and phenolics. Compared to the semi-solid cultivar Conan, hollow-stem and resistant Hatcher had increased abundance of proteins and metabolites with known roles in plant defense against insects. Taken together, the combined proteomics and metabolomics approach enabled the characterization of metabolism in wheat stems that is associated with WSS infestation and resistance. These results provide the first evidence of a metabolic basis of resistance to WSS in hollow-stem wheat.

3.2. Introduction

Bread wheat (*Triticum aestivum* L., Poaceae) is a global staple crop and grain yield can be greatly reduced by biotic stresses. A major pest of wheat is the Wheat Stem Sawfly (*Cephus cinctus* Norton, WSS hereafter), and infestation outbreaks can cause up to US $350 million annual losses in North America [1]. Sawfly infestations were first described in 1872 from specimens of native grass in Colorado [2]. A host jump to spring wheat, more than a century ago, resulted in dramatic expansion of WSS distribution across the Northern Great Plains and South Canada [1,3]. Spring wheat is extensively grown in North America but remains difficult to produce in dryland areas such as Colorado, where farmers typically grow winter varieties. The grass feeding insect exclusively infested spring varieties until the early 1980s and another episode of host jump to winter wheat. Research on the genetic diversity of WSS in North America indicates the existence of distinct haplotypes, and phenotypic variation is an important driving factor of host adaptation [4]. Recent field studies conducted on winter wheat in Colorado indicate rapid WSS adaptation to this new host and support that *C. cinctus* can colonize wheat at an alarming pace [5].

Most of the WSS life cycle is spent in larval stages, and larval feeding causes major tissue damage to plant stems. After the larvae pupate, they emerge from stems, mate in the spring and females oviposit (i.e., deposit eggs) into wheat stems within approximately ten days [6]. Over the course of a season, hatched WSS larvae chew through inner stem tissue downwards to reach soil level, cut a V-shaped notch inside the stem and prepare for overwintering [7]. Larvae pupate in early spring and adults leave the stem stubs to start a new cycle. Sawfly infestation reduces grain yield through two mechanisms: (1) "cutting", that is larval chewing within the stem that causes plants to lodge and affects harvesting efficiency and (2) larval feeding within stem vascular tissue that reduces photosynthetic capacity and therefore grain yield per plant [8-10].

No single control measure has been broadly adopted to combat WSS. Chemical and biological control is difficult because most of the WSS life cycle resides inside the stem. Partial control through plant genetics can be attained by breeding plants to contain a solid stem (i.e., degree of pith expression inside the stem), as most wheat stems are hollow [11,12]. The major quantitative trait locus (QTL) for stem solidness, *Qss.msub-3BL*, has been characterized and controls most of the variation in stem pith formation [13]. The semi-solid-stem cultivar (i.e., cultivated variety) Conan is resistant to WSS, and this is achieved by having a solid stem in early development – which corresponds to the period of WSS peak emergence – and becoming hollow only later into maturity [14]. However, the solid-stem trait has low levels of adoption due to a fitness penalty (i.e., reduced grain yields when no infestation is present) [1]. Further, wheat plants that carry the major stem solidness QTL show relative inconsistency in pith expression and the effectiveness of that trait can be influenced by weather conditions [7].

In addition to mechanical protection against pests (e.g. solid stems, trichomes, hairs), plants can achieve resistance through changes in plant metabolism that modify the composition of proteins and metabolites. One type of defense against insects is the "direct" defense, whereby the plant changes the morphology and chemistry of its tissues in response to physical contact by the pest. The recognition is attained through release of damage- and herbivore-associated molecular patterns (DAMPs and HAMPs), which bind to plant cell receptors and begin signaling cascades that include increased calcium fluxes, oxidative burst and detoxification activities, and up-regulation of wound-induced protein kinases (WIPK), products of specialized metabolism (e.g., phytoalexins), and proteinase inhibitors [15-17]. Further, protein regulation (anabolism/catabolism) via tRNA synthetases and ubiquitin-proteasome complexes changes during plant pest infestations [18,19]. Infestation can increase the synthesis of proteinase inhibitors, detoxification enzymes (e.g., peroxidases, glutathiones), and toxic proteins (e.g., lectins, remorins) [15,20-22]. This plant metabolic response to a pest can be integrated with a basal molecular resistance, which can include pre-formed toxins ("phytoanticipins") such as alkaloids, phenolics, and benzoxazinoids (the latter common in the Poaceae plant family, including wheat) [23]. Insect manipulation of host defenses has been described in many plant/pest systems and the role of small non-coding RNA (snRNA) sequences in suppressing wheat defense responses to WSS larval feeding is currently being investigated [24].

Several studies have characterized metabolic changes that occur during plant–pest interactions, specifically in areas of central and toxin metabolism. Changes to photosynthesis (decrease), gluconeogenesis (decrease), and phenylpropanoid synthesis (increase) commonly occur during an herbivore infestation, allowing the plant to shift metabolism to protect against oxidative damage, increase specialized metabolite pathways, and fortify tissues. Research on

maize (*Zea mays*) plants infested with caterpillars of *Spodoptera exigua* revealed decreased expression of gluconeogenesis genes that co-occurred with a temporal readjustment of photosynthetic capacity, as well as overexpression of phenylpropanoid-related genes [25]. Biosynthesis of lignin through the phenylpropanoid pathway promotes structural fortification of cell walls, and wound-induced overexpression of lignin biosynthesis-related genes has been described in maize [26]. Likewise, increased levels of detoxification enzymes in bread wheat exposed to aphids (*Sitobion* spp.) support the importance of an oxidative burst during response to herbivory [27]. Importantly, a recent study on the molecular response of wheat to WSS feeding described protein and metabolite variation in the phenylpropanoid and pentose phosphate pathways, in wheat cultivars with different levels of resistance to the insect [28]. However, it is unclear whether the reallocation of proteins and metabolites is the downstream result of intense damage in susceptible plants or an active response that aims at strengthening tissues.

In the present study, we compare the proteomic and metabolic response of wheat during WSS infestation. A selection of wheat cultivars was evaluated in a field trial, and a subset of two cultivars, as well as two other cultivars that were not represented in the trial, were further interrogated using omics analysis to associate metabolism with resistance to WSS. The four cultivars were selected and compared based on phenotypic variation for (1) degree of resistance to WSS, (2) yield performance in the field (reported herein), and (3) growth habit (spring or winter type). Two previously characterized cultivars include Conan and Reeder (not represented in the field trial), which are both spring wheat cultivars that vary for stem solidness and resistance to WSS [29,30]. Particular interest is pointed towards Hatcher, a cultivar with hollow stems that shows consistent resistance and high yields under WSS pressure (field trial results). We hypothesize that critical metabolic and protein variation occurs in Hatcher in response to

WSS pressure and that it does not rely on the solid-stem trait. A unique proteomic and/or metabolomic profile of Hatcher (in response to WSS) would support a molecular basis of resistance to WSS in wheat, providing the foundation to breed for novel resistance phenotypes that do not depend on stem solidness.

3.3. Methodology

3.3.1. Plant Material for the Omics Study

Protein and metabolite profiles were obtained from hard red winter wheat (*Triticum aestivum* L., Poaceae) cultivars "Hatcher" (PI 638512) [31] and "Denali" (PI 664256) [32], and hard red spring wheat cultivars "Conan" (PI 607549) and "Reeder" (PI 613586). For proteomics and metabolomics, Hatcher and Denali were vernalized for 8 weeks at 3 °C ± 2 °C. Spring wheat cultivars were vernalized for 10 d at 3 °C ± 2 °C to facilitate synchronous development with the winter wheat cultivars. Wheat seedlings were planted in 5-inch circular pots in the following mix: 7 parts Fafard professional metro mix (45–55% Canadian Sphagnum peat moss, vermiculite, bark, dolomite lime, and wetting agent; Sun Gro Horticulture, Agawam, MA, USA), 2 parts coarse perlite, 1 part Fort Collins, CO, USA loam soil supplemented with aged manure and Osmocote slow release fertilizer (Greenhouse Products Pty Ltd., Princess, South Africa) as per the manufacturer's instructions. Plants were fertilized weekly with Peters Professional Fertilizer (J. R. Peters Inc., Allentown, PA, USA) to promote tillering. The Colorado State University insectary facility, Fort Collins (CO, USA), was used to grow all plants. Controlled growth conditions included temperature held at 18–24 °C with a photoperiod of 15/9 h light/darkness, and bottom watering 3 times per week. Plants were grouped in a randomized complete block design.

3.3.2. Insect Collection, Handling, and Plant Infestation

The site for insect collection was located approximately one mile West of New Raymer, CO, USA where 2014 infestation levels were found to be > 96%. Wheat stubble from the previous year's crop (from the cultivar 'Byrd') was removed and placed in 3.785 L size plastic bags. The bags were stored at 3 °C ± 2 °C for 30–90 d (depending on collection date) for the insects to complete their mandatory cold diapause period [33]. The stubble was misted weekly to prevent the larvae from desiccating. After completion of larval diapause, stubs were stored in a greenhouse at 18–24 °C with a photoperiod of 15/9 h light/darkness. Adult WSS emerged within 4–6 weeks after removal from the refrigerator, and bioassays were conducted within 24 h of adult emergence.

Plants were exposed to female WSS only and were considered infested when WSS successfully deposited eggs inside the stem. Wheat stems were enclosed with a WSS container to control the location of WSS oviposition (Figure 11). Insect containers were made from a 5 cm long × 1.5 cm diameter plastic tube (cut off from a 15 mL Falcon tube) with organza netting on either opening to allow airflow. Containers were slipped over stems of interest between the third and fourth internodes (starting from the first internode) and held in place using bamboo stakes. Clothes pins were used to close either end of the containers by clamping the organza tight, without disrupting plant tissue. Female WSS were allowed to oviposit on stems within the containers area for 10 d. Control plants had containers clipped in place but were WSS absent. Plants were infested with WSS females at approximately Zadoks growth stage 55 [34].

3.3.3. Protein Extraction, Detection, Data Processing, and Annotation

Protein extractions were performed on 24 wheat plants (6 infestation replicates per each of the 4 cultivars). Three biological replicates per cultivar were infested with WSS and 3 other replicates were left non-infested as controls. Stems between internodes 3 and 4 were cut, flash frozen in liquid nitrogen and lyophilized for 72 h. Dried, frozen stems were then placed in 5 mL conical centrifuge tubes and ground to a fine powder using a mix of 3.2 mm and 11 mm diameter stainless steel beads and a Buller Blender Storm 5 tissue homogenizer (Next Advance, Troy, NY, USA). For each sample, 50 mg of stem powder were transferred to a 2 mL glass vial and immersed in a 1 mL tricholoroacetic acid (TCA):acetone solution (TCA 10% w/v, acetone 90%, dithiothreitol to 10 mM; Sigma-Aldrich, Inc., St Louis, MO, USA). The solution was vortexed for 30 s (4 °C, 2500 g) and centrifuged for 5 min (4 °C, 2850 g), supernatant was discarded, and the pellet was reconstituted in 500 μL TCA:acetone. Centrifugation and discarding of supernatant were repeated until pellets were white or lightly colored. Clean pellets were further resuspended in 750 μL cold acetone:water (1:1, v/v, dithiothreitol to 10 mM), centrifuged for 5 min (4 °C, 2850 g), and dried under gas nitrogen flow.

The total protein content of all samples was further quantified twice via Pierce bicinchoninic acid (BCA) Protein Assay Kit (Thermo Fisher Scientific, Waltham, MA, USA). Solid matter from dried protein pellets was loosened by pipette tip and transferred to microcentrifuge tubes. A total of 500 μL 8 M urea was added to each tube, and vortexed to resuspend the protein pellet, followed by sonication at room temperature for 10 min. Samples were then centrifuged at 2850 g for 5 min at 4 °C. A small aliquot of supernatant was diluted (1:20) in 2 M urea before being subjected to BCA following manufacturer's recommendations. Fifty μg of total protein content were aliquoted from each sample and processed for in-solution

trypsin digestion as previously described [35]. To generate a mixed quality control (QC) sample, 2 μg of total protein were pooled from each sample for digestion. Briefly, proteins were resolubilized in 8 M urea and 0.2% ProteaseMAXtm surfactant trypsin enhancer (Promega, Madison, WI, USA). Samples were reduced and alkylated with 5 mM dithiothreitol and 5 mM iodoacetamide. Trypsin (Pierce MS-Grade, Thermo Fisher Scientific) was added at an enzyme to substrate ratio of 1:50 and incubated at 37 °C for 3 h. Trypsin was deactivated with the addition of 5% trifluoroacetic acid and desalted using Pierce C18 spin columns (Thermo Fisher Scientific) using manufacturer's instructions. Peptide eluate was dried in a vacuum evaporator and resuspended in 5% acetonitrile/0.1% formic acid. Once resolubilized, absorbance at 205 nm was measured on a NanoDrop (Thermo Fisher Scientific) and total peptide concentration was subsequently calculated using an extinction coefficient of 31 [36].

Mass spectrometry analyses were performed using nano high performance liquid chromatography-tandem mass spectrometry (nHPLC-MS/MS). A total of 0.5 μg of peptides was purified from each sample and concentrated using an online enrichment column (5 μm, 100 μm ID x 2 cm C18 column; Thermo Fisher Scientific). Subsequent chromatographic separation was performed on a reverse phase nanospray column (EASYnano-LC, 3 μm, 75 μm ID x 100 mm C18 column; Thermo Fisher Scientific) using a 90 min linear gradient from 5% to 30% buffer B (100% ACN, 0.1% formic acid) at a flow rate of 400 nL/min. Peptides were eluted directly into the mass spectrometer (Orbitrap Velos, Thermo Fisher Scientific) equipped with a Nanospray Flex ion source (Thermo Fisher Scientific) and spectra were collected over a *m*/*z* range of 400–2000 in positive mode ionization, with charge states +2 and +3 selected for MS^2. Dynamic exclusion enforced a limit of 2 MS/MS spectra of a given *m*/*z* value for 30 s (exclusion duration of 90 s). The instrument was operated in Fourier transform (FT) mode for MS detection

(resolution of 60,000) and ion trap mode for MS/MS detection with a normalized collision energy set to 35%. Instrument suitability was monitored through analysis of commercially purchased BSA standard digest and automated monitoring using Panorama QC v15.0 (LabKey, San Diego, CA, USA) [37]. Metrics (e.g., mass accuracy, peak area, retention time) were monitored and flagged as outliers should results be outside ± 3 standard deviations of the guide set (i.e., optimal operation). Values for all metrics were within normal limits throughout the duration of the experiment, indicating instrument stability and data robustness. Quality control samples were injected between every 5 samples throughout the course of the experiment.

Compound lists of the resulting spectra were generated using Xcalibur v3.0 software (Thermo Fisher Scientific) with a signal-to-noise (s/n) threshold of 1.5 and one scan per group. Tandem mass spectra were extracted, charge state deconvoluted and deisotoped by ProteoWizard MsConvert v3.0. Spectra from all samples were searched using Mascot v2.3.01 (Matrix Science, London, UK) against the wheat_peptides_rev062716 in-house database (200688 entries) assuming the digestion enzyme trypsin. Mascot was searched with a fragment ion mass tolerance of 0.8 Da and a parent ion tolerance of 20 ppm. Oxidation of methionine and carboxymethylation of cysteine were specified in Mascot as variable modifications. Search results from all samples were imported and combined using the probabilistic protein identification algorithms [38] implemented in the Scaffold software v4.8.4 (Proteome Software Inc., Portland, OR, USA) [39]. Peptide thresholds were set (95%) such that a peptide FDR of 1% was achieved based on hits to the reverse database [40]. Protein identifications were accepted if they could be established at greater than 99% probability and contained at least two identified peptides. Protein probabilities were assigned by the Protein Prophet algorithm [41]. Proteins that contained similar peptides and could not be differentiated based on MS/MS analysis alone were grouped to satisfy the principles

of parsimony. Proteins sharing significant peptide evidence were grouped into clusters. Protein accession numbers obtained from the in-house database were further annotated using the Wheat Protein Database [42]. A match with a database wheat accession was confirmed for peptide sequences with > 80% homology to a *T. aestivum* peptide sequence and > 90% homology to a protein sequence from another model species. Gene ontology (GO) data was retrieved from the UniProt database [43].

3.3.4. Metabolite Extraction, Detection, Data Processing, and Annotation

A total of 40 plants were used for metabolite extraction and included 10 biological replicates per cultivar. Five biological replicates of each cultivar were infested with WSS as described above for proteomics, and 5 replicates were not infested and used as controls. After infestation, stems between the third and fourth internodes were excised, flash frozen in liquid nitrogen and lyophilized for 72 h. Stems were then placed in 5 mL conical centrifuge tubes and ground to a powder as described for protein extraction. Non-volatile metabolites were extracted as performed by Broeckling and Prenni (2018) [44] with modifications. Briefly, 50 mg of powdered stems were transferred to 2 mL glass vials and immersed in 500 μL of a cold methanol:methyl tert-butyl ether (MTBE) solution (2:1, 75% methanol:MTBE; Sigma-Aldrich). Samples were vortexed for 1 h at 4 °C and 125 μL of cold liquid chromatography grade water (Sigma-Aldrich) were then added to the mixture. Samples were centrifuged for 15 min (4 °C, 2850 g), and the isolated aqueous layer was transferred to a new glass vial. Water-soluble extracts were then evaporated under a continuous gas nitrogen flow and reconstituted in 120 μL of methanol:water (1:1, v/v).

Non-targeted metabolite profiling was performed using UPLC-MS/MS as previously described [44]. Briefly, 2 μL of extracts were injected onto an Acquity UPLC system (Waters

Corporation, Milford, MA, USA) in discrete, randomized blocks with a pooled QC injection after every 10 sample injections, and the coefficient of variance was used to ensure instrument stability over the course of the experiment. Compounds were separated using a Waters Acquity UPLC CSH phenyl hexyl column (1.7 μm, 1.0 × 100 mm; Waters Corporation), using a gradient from solvent A (2 mM ammonium hydroxide, 0.1% formic acid) to solvent B (acetonitrile, 0.1% formic acid). Injections were made in 100% A, held for 1 min, ramped to 98% B over 12 min, held at 98% B for 3 min, and then returned to starting conditions over 0.05 min and allowed to re-equilibrate for 3.95 min, with a 200 μL/min constant flow rate. The column and samples were held at 65 °C and 6 °C, respectively. The column eluent was infused into a Xevo G2 Q-TOF mass spectrometer (Waters Corporation) with an electrospray source in positive ion mode, scanning 50-2000 *m/z* at a rate of 5 scans per sec, alternating between MS (6 V collision energy) and MS^E mode (15–30 V ramp). Calibration was performed prior to sample analysis using sodium iodide with 1 ppm mass accuracy. The capillary voltage was held at 2200 V, the source temperature at 150 °C, and nitrogen desolvation temperature at 350 °C with a gas flow rate of 800 L/h.

A matrix of molecular features as defined by retention time and mass (*m*/*z*) was created from LC-MS data files after conversion to .cdf format and processing by XCMS [45] in R software v3.3.1 [46]. The R package RAMClust was used to deconvolute data into spectral clusters [47]. Molecular features were normalized to total ion current (TIC), the relative quantity of each feature was determined by the mean area of the chromatographic peak among two replicate injections ($n = 2$), and spectral clusters were quantified as a weighted abundance of all molecular features in the cluster. Identification of metabolites was performed manually by matching mass spectra and retention times to in-house and external databases including METLIN

[48,49], the Human Metabolome Database (HMDB) [50], and through the following workflow: the R package InterpretMSSpectrum and the MS-FINDER program v2.40 [51,52] were used to determine molecular weights, and chemical formulas and structures, respectively. Next, the Chemical Translation Service web application program interface (API) was used to retrieve chemical names of compounds with available International Chemical Identifiers (InChIKey), and the ClassyFire web API was used to assign full chemical ontology [53]. Confidence levels were all assigned based upon classification of metabolite annotation as described by Sumner et al. (2007) [54]. All annotated metabolites in this study were assigned a level 1 or 2 confidence.

3.3.5. Plant Material and Measurements for the Field Study

Wheat varieties (a mixture of both cultivars, including Hatcher and Denali, and advanced breeding lines) were planted in New Raymer fields on Sep. 30, 2013; Sep. 18, 2014; and Sep. 18, 2015, and harvested on Jul. 23, 2014; Jul. 30, 2015; and Jul. 14, 2016, for 2014, 2015, and 2016 measurements, respectively. Soil fertility amendments were applied by the cooperating farmer based on soil fertility recommendations appropriate for the area. For each variety, plots were 5 feet wide by 12 feet long and seeded at an approximate density of 700,000 seeds per acre, in 6 rows per plot with 9-inch spacing between rows. Plots were harvested using a Wintersteiger Elite combine with a Grainguage weighing system. An area of 60 square feet was used for yield calculations and adjusted to 12% moisture basis according to the moisture value provided by the combine. Field infestation levels by WSS were determined by collecting wheat stubble after harvest from the middle of plots using a shovel. One hundred tillers were randomly selected for each cultivar and bisected in the lab using a scalpel to determine presence/absence of WSS larvae. Infestation percentages were calculated as such: % = (infested tillers/total number of tillers) × 100.

3.3.6. Statistical Analysis

Metabolite content and total spectral counts of proteins (TSC) were compared using Student's *t* tests for treatments only (No WSS = Controls vs. WSS = infested plants) and treatments within cultivars, and one-way ANOVA was used for comparisons of cultivars, with a *p* threshold of 0.05. Benjamini–Hochberg correction was systematically applied across all *t* tests and ANOVA *p* values to account for multiple comparisons [55]. For proteomics analyses, fold changes were calculated as such: (mean WSS)/(mean No WSS) treatments and centered around zero using $\log_2$ transformation. "Presence" of detected proteins was determined when at least two out of three replicates had non-null TSC values, and "absence" was determined otherwise. A residual value of 10^{-6} was assigned to null TSCs to calculate fold change. For metabolomics analyses, fold change was calculated as (mean WSS)/(mean No WSS) treatments. Orthogonal projection to latent structures discriminant analyses (OPLS-DA) were conducted on the metabolomics data after mean-centering and unit variance (UV)-scaling using SIMCA v14.1 (MKS Data Analytics, Umea, Sweden) with infested and non-infested as the two classes in the model. Variable importance on OPLS projection (VIP) scores were calculated for each variable by summing the squares of the OPLS loading weights, weighted by the amount of sum of squares explained in each model component.

3.4. Results

3.4.1. WSS Resistance Was Identified in Hollow-Stem Wheat

Here, a field study was performed to identify hollow-stem cultivars with resistance to WSS. Plants were grown in three consecutive years and two cultivars were identified with consistent, contrasting trends for both percent WSS infestation and yield: Hatcher and Denali (Figure 12). For the years 2014, 2015, and 2016, the mean for WSS infestation across varieties

was 41%, 51%, and 76%, Hatcher mean infestation was 35.5%, 53.5%, and 70.5%, and Denali had 59.5%, 70.5%, and 78% of stubs infested (Figure 12A). Grain yield mean across the wheat selection reached 66 bu/ac, 87 bu/ac, and 64 bu/ac, where Hatcher yielded 71 bu/ac, 81.7 bu/ac, and 68.1 bu/ac, and Denali yielded 62 bu/ac, 75 bu/ac, and 70.6 bu/ac in the years 2014, 2015, and 2016 respectively (Figure 12B). Given the present data and previous reports of cultivar performance, we hereafter refer to Hatcher and Conan as resistant cultivars and refer to Denali and Reeder as susceptible.

3.4.2. Variation Was Observed in the Proteome among the Four Wheat Cultivars

Liquid chromatography-mass spectrometry analysis on the four selected cultivars yielded a total of 255,401 spectra that were condensed to 1832 peptides. Gene ontology data were used to classify peptides based on biological processes. A table that reports information on each detected protein (e.g., molecular function, molecular weight, statistical results) is provided in the supplementary files (Table S1). Peptides were associated with 1039 low-level (i.e., lower-level child entry in the ancestor chart) [56] biological processes (Figure 13A). These low-level processes were then grouped under five major biological processes. The total number of major process occurrences is higher than the number of processes due to overlap across proteins (e.g., glutathione-S-transferases play roles in response to stimuli but are also involved in metabolic and cellular processes). Thereby, 498 proteins were associated with metabolic processes, 651 with cellular processes, 186 with biological regulation, 105 with localization, 182 with response to stimuli, and 215 with other types of processes. Data indicated a relatively steady amount of biological processes related to significant proteins between treatments of resistant cultivars (Hatcher and Conan), with a noticeable exception for response to stimuli (Figure 13A). Hatcher showed differential normalized total spectral counts (TSC) for 60 peptides (Student's *t* test FDR

adjusted $p < 0.05$) associated with 185 biological process occurrences. Hatcher plants had 16 and 25 occurrences of response to stimulus-associated proteins, down and up-regulated after infestation with WSS, respectively. Likewise, Hatcher had 22 and 26 occurrences of metabolic process, 23 and 25 occurrences of cellular process, eight and 12 occurrences of biological regulation, five and five occurrences of localization, and ten and eight occurrences of other processes, respectively down and up-regulated after infestation (Figure 13A). Conan, Denali, and Reeder had significant TSC between treatments for, respectively, 80 (235 biological processes total), 60 (201 biological processes total), and 38 proteins (associated with 107 process occurrences; FDR adjusted $p < 0.05$ for significant TSC; Figure 13A).

Among the 1039 low-level biological processes associated with detected proteins, 143 were further explored and grouped within 17 processes known for their importance in the plant response to stress (Figure 13B). These represented approximately 18% of the complete set of detected GO biological processes (associated with both significant and non-significant proteins) and included defense response to biotic stress (3.36% of all detected processes), photosynthesis (2.43%), sugar/H_2O_2 metabolism (1.76%), and hypersensitive response (0.27%).

3.4.3. Differentially Regulated Proteins among Wheat Cultivars Due to Infestation

Further analysis of the proteomics data demonstrated variation among the four wheat cultivars due to WSS infestation. Of the 1832 proteins detected among cultivars, 224 had total spectral counts (TSC) that differed between infested stems and non-infested control stems (for all, Student's *t* test FDR adjusted $p < 0.05$). As described in Figure 13, the 224 proteins were classified in five major processes: metabolic process, cellular process, biological regulation, localization, response to stimulus, and an additional miscellaneous category. Results are displayed as volcano plots using the $\log_2$ fold change and $-\log_{10} p$ value proteins for comparisons

within a cultivar (Figures 14 and 15). Hatcher had a total of 62 proteins that varied including ten down- and 11 up-regulated proteins with molecular process activities (for all, Student's *t* test FDR adjusted $p < 0.05$; Figure 14). A detailed description of each protein entry for Hatcher is provided in Table 4A. Down-regulated proteins included a cinnamoyl CoA reductase (FDR adjusted $p = 2.2 \times 10^{-2}$), and up-regulated proteins included the gluconeogenesis-related enzyme fructose-1,6-bisphosphatase (FDR adjusted $p = 5 \times 10^{-4}$). The analysis also revealed five down- and 11 up-regulated proteins described as key regulators of response to stimuli. Down-regulated response regulators included a heat shock-related peptide, a mannose-binding lectin as well as a catalase, where up-regulated proteins included two glutathione-S-transferases, a calmodulin, and a thioredoxin (for all, FDR adjusted $p < 0.05$; Table 4A). Detailed information on differentially regulated proteins detected in Conan, Denali, and Reeder is available in Figure 15 and Table 4B–D.

Several proteins were conjointly down- or up-regulated or showed opposite patterns among cultivars, after infestation (Table 4). These included a ubiquitin-activating enzyme and an alanyl-tRNA synthase that were down-regulated in Hatcher and up-regulated in Conan (for all, FDR adjusted $p < 0.05$). Interestingly, three enzymes were conjointly up-regulated in Hatcher and Denali infested plants (i.e., vacuolar ATP synthase subunit, aspartate aminotransferase, bifunctional enolase; for all, FDR adjusted $p < 0.05$), and a cinnamoyl CoA reductase was down-regulated in both cultivars (for both, FDR adjusted $p < 0.05$). Conversely, no proteins displayed identical or opposite expression patterns between Hatcher and Reeder.

3.4.4. Overview of Detected Metabolites in Stems of Wheat

Metabolite profiles were collected using LC-MS metabolomics (Figure 16), and a total of 1823 putative compounds were detected. Of these 1823 compounds, 1639 (90%) were assigned a chemical formula based on hydrogen rearrangement rules using MS-FINDER v2.40 [51,52], and 607 (33% of total) compounds were tentatively annotated as a distinct metabolite [54]. A detailed description of all detected metabolites is provided in the supplementary files (Table S1).

Classification of annotated metabolites based on chemical structures yielded ontology trees for 489 compounds (Figure 17). Metabolites were sorted within eight chemical superclasses (i.e., alkaloids, benzenoids, lignans, lipids, organic acids, organic nitrogen/oxygen compounds, phenylpropanoids) and an additional "other" class that contained minor superclasses (e.g., organoheterocyclic compounds, nucleosides). For clarification, lignans share, with lignin, common biosynthesis via the phenylpropanoid pathway, but have anti-insect activities rather than structural roles. Nine ontology levels were used in the classification, from chemical kingdom (highest chemical hierarchy, i.e., organic compounds) to parent level 5 (lowest hierarchy, e.g., α amino acids). In our metabolomics dataset, the classification analysis revealed the presence of eight alkaloids and derivatives, 40 benzenoids (e.g., 12 phenolics), 11 lignans (e.g., five lignan glycosides), 112 lipids, 74 organic acids and derivatives including 61 carboxylic acids, 16 organic nitrogen compounds including 11 amines, 51 organic oxygen compounds (e.g., 38 carbohydrates and conjugates, and six alcohols and polyols), 57 phenylpropanoids and polyketides including 19 flavonoids and seven coumarins, and 120 compounds classified in the "other" category (e.g., 104 organoheterocyclic compounds and 13 nucleosides).

3.4.5. Differentially Regulated Metabolites among Wheat Cultivars Due to Infestation

Variation in metabolite abundance between treatments and among cultivars was demonstrated using both univariate and multivariate statistics. Of the 607 annotated metabolites, 44 varied between treatments (infested and non-infested plants) regardless of cultivars (for all comparisons, Student's *t* test FDR adjusted $p < 0.05$), including two phenolics and two flavonoids (Figure 17). Regardless of treatment, 308 metabolites were found significant when comparing the four cultivars (for all comparisons, ANOVA FDR adjusted $p < 0.05$). These included five phenolics, four lignan glycosides, 25 terpenoids, 15 flavonoids, and four coumarins. When comparing treatments within cultivars (interaction of factors), 62 annotated metabolites were found significant within Hatcher plants. Down-regulated metabolites included the benzoxazinoid glycoside DIBOA-glucoside (FDR adjusted $p = 7.5 \times 10^{-3}$), and up-regulated compounds included a neolignan, a flavonoid glycoside structure, a butanolide, and two carbohydrates (for all, FDR adjusted $p < 0.05$). Other cultivars yielded fewer significant compounds: 14 within Conan plants, 11 in Denali, and 11 in Reeder (for all, FDR adjusted $p < 0.05$). Conan and Denali (both spring wheat cultivars) shared three down- or up-regulations of metabolites, that is the phenylpropanoid integerrimine (down-regulated), the flavonoid beilschmieflavonoid B and a non-classified compound (both up-regulated; for all, FDR adjusted $p < 0.05$). The only other metabolite that showed a common pattern between cultivars was a pyrimidine ribonucleoside monophosphate structure that was up-regulated in both Hatcher and Denali (for both, FDR adjusted $p < 0.05$).

The metabolite content of each sample was further analyzed using orthogonal projection to latent structures discriminant analyses (OPLS-DA) to identify compounds that highly contribute to the multivariate models, within each cultivar. Hatcher is a semi-solid-stem cultivar

that is relatively resistant to WSS and has consistent high yields in the field. The proteomics data indicate a unique response of Hatcher to WSS, and metabolomics revealed a much higher degree of metabolite changes for this cultivar compared to others. An OPLS-DA model on Hatcher revealed separation of infested and non-infested plants based on metabolite distribution (Figure 18A). The model consisted of one predictive and five orthogonal components with $R^2Y = 95.1\%$ of sample class variance explained by the model and $Q^2 = 71.3\%$ to indicate a good predictive power of the model. Twenty-nine of the annotated metabolites contributed to the separation of treatments within Hatcher samples (for all, FDR adjusted $p < 0.05$). All selected variables had a high variable importance for the projection (VIP) score (for all, VIP ≥ 1.45). Areas that contained only high VIP scored metabolites were highlighted in light red (down-regulated in the WSS treatment) and blue (up-regulated) in the OPLS biplots (Figure 18A). Eight annotated metabolites were lower and 21 were greater in abundance after infestation (Figure 18A, red and blue areas, respectively). These compounds that contributed to the OPLS-DA model were labeled (Figure 18A) and displayed in variable line plots (VLP) to emphasize high content variation between treatments and low variation within treatments (Figure 18B). The 29 metabolites that highly contributed to the OPLS-DA model in Hatcher were further analyzed for changes in abundance relative to treatments and compared to other cultivars (Figure 18C). Detailed information for important metabolites detected in all cultivars is provided in Tables 5 and 6. Highly down-regulated metabolites included an organic oxygen compound and the benzoxazinoid glycoside DIBOA-glucoside (for both, fold change of WSS/No WSS < 0.5) and a highly up-regulated metabolite was the nucleoside pyrimidine ribonucleoside monophosphate (fold change > 4).

Multivariate statistics applied to other cultivars revealed interesting changes in several key plant–insect interaction metabolites. The OPLS-DA model for Conan was driven by a down-regulation of the phenylpropanoid integerrimine and an up-regulation of a lipid-like structure (for all, FDR adjusted $p < 0.05$; Figure 18B and Table 5). Denali displayed eight metabolites with high model contribution, including down-regulation of the same phenylpropanoid integerrimine as in Conan, and up-regulation of two other phenylpropanoid structures (for all, FDR adjusted $p < 0.05$; Figure 18B and Table 5). Multivariate analysis in Reeder yielded four major contributors that were all down-regulated (for all, FDR adjusted $p < 0.05$; Figure 18B and Table 5). Fold change analysis of important metabolites in Hatcher revealed two down-regulated metabolites in Hatcher that were highly up-regulated in Denali (i.e., indolizidine structure and DIBOA-glucoside; for both, fold change of WSS/No WSS > 2), and these two cultivars shared higher contents in pyrimidine ribonucleoside monophosphate after infestation with WSS (fold change > 4; Figure 18C).

3.5. Discussion

3.5.1. Field Data Supports Wheat Genetic Resistance to WSS That Does Not Rely on the Solid-Stem Trait

Previous work on hard red spring wheat cultivars Conan and Reeder has established a relationship between degree of stem solidness and pest resistance capacity [14,29,30]. Conan and Reeder carry different alleles at the *Qss.msub-3BL* locus, described as the major solid-stem quantitative trait locus (QTL) [11,12]. While hollow-stem Reeder plants show high levels of infestation, semi-solid stems from Conan appear to provide relatively good tolerance to WSS attacks. Rapid temporal expression of stem pith allows Conan individuals to resist sawfly infestations at periods of peak emergence. Increased stem density results in reduced host

preference and higher rates of larval mortality, also termed antibiosis [14,30]. Conversely to Conan, Reeder has poor stem pith expression throughout the growing season and higher host suitability.

Neither hard red spring wheat cultivars Hatcher and Denali have been assessed for correlation between stem solidness and resistance to WSS. Hatcher was released in Colorado in 2004, is now widely grown in the state and shows susceptibility to important wheat pathogens (i.e., bacterial and viral pathogens such as stem rust caused by *Puccinia graminis*, and streak mosaic virus) but resistance to major pests such as the Hessian Fly (*M. destructor*) and the Russian Wheat Aphid (*Diuraphis noxia*) [57]. Denali was released in Colorado in 2011 and shows varying degrees of resistance to pathogens: moderate resistance to stem rust, resistance to stripe rust (*Puccinia striiformis*), and susceptibility to the wheat streak mosaic virus. Denali is also resistant to *M. destructor* but susceptible to *D. noxia* [57]. Recent reports from Cockrell et al. (2017) [5] define Hatcher as a hollow-stem cultivar that is susceptible to *C. cinctus*. Our 3-year field data suggests otherwise as it revealed overall high performance of Hatcher for WSS infestation and yield (Figure 12). Denali also has low pith expression but conversely showed poor field performance for both infestation rates and yield (Figure 12). These data support genetic resistance to WSS that relies on plant pathology-based molecular mechanisms that have only been explored very recently [24,28,58]. Hatcher has a hollow stem that does not provide consistent protection during periods of WSS outbreaks, yet shows high performance in the field in the context of high sawfly pressure. Advantageous allelic variants at the solid-stem locus provide a certain degree of resistance but are known for inconsistent expression of stem pith under varying weather conditions [7]. Molecular studies to understand key actors of WSS resistance in wheat cultivars that do not have solid stems are thus warranted.

3.5.2. Proteome Analysis Provides Evidence of Unique Response to WSS at the Cultivar Level

Investigation of the protein content of four wheat cultivars that vary for (1) resistance to WSS infestation, (2) field yield performance, and (3) growth habit (spring/winter) indicated unique response profiles to WSS exposure (Figures 12 and 13). A total of 1832 proteins were identified among samples and a high proportion were involved in metabolic (27%) and cellular processes (36%), 10% in biological regulation, 6% in localization, 10% in response to stimuli, and 11% in other processes (Figures 13A and S1). Further analysis revealed that the four most encountered processes included defense responses to biotic stress (3.36%), photosynthesis (2.43%), translation (2.24%), and response to oxidative stress (1.97%). A closer look at the 62 significant proteins detected in Hatcher showed noticeable down-regulation patterns after WSS infestation for three carbohydrate anabolism-related enzymes, including a UDP-glucose dehydrogenase that converts UDP-glucose into UDP-glucuronate, a precursor of major cell wall polysaccharides (Figure 14 and Table 4A) [59]. Interestingly, a cinnamoyl CoA reductase was also down-regulated. Cinnamoyl CoA reductases are key enzymes of the lignin biosynthetic pathway and facilitate the fortification of plant cell walls [60]. A calreticulin and a catalase (Ca^{2+} and H_2O_2 homeostasis) that are known for their importance in the molecular signal cascade that leads to the stress response also had low expression levels. Other down-regulated stress-related proteins included a heat shock protein and a lectin. Where heat shock proteins are often overexpressed to limit plant stress, mannose-binding lectins can recognize specific foreign elicitors [61,62]. Lastly, four protein biosynthesis-related enzymes were down-regulated after infestation with WSS (i.e., three ribosomal components and an alanyl-tRNA synthetase), as well as two photosynthesis-related compounds (i.e., transketolase and ferredoxin:NADP(H) oxidoreductase; Figure 14 and Table 4A) and a serine carboxypeptidase-like enzyme involved in

proteolysis. On the other hand, WSS exposure led to up-regulation of four detoxification enzymes (i.e., NADPH-dependent alkenal/one oxidoreductase, thioredoxin M-type, two glutathione S-transferases). Alkenal/one oxidoreductases have been described for their activity in reactive carbonyl detoxification [63]. Amino acid biosynthesis was promoted through up-regulation of two cysteine synthases and an aspartate aminotransferase. Up-regulation of primary metabolites such as cysteine increases defenses to biotic stress. Cysteine and other amino acids are the building blocks for the biosynthesis of numerous antioxidants and toxic compounds [64]. One starch biosynthesis and one glycolysis-related enzymes were also overexpressed (i.e., pfkB-like carbohydrate kinase and glyceraldehyde-3-phosphate dehydrogenase). Four enzymes involved in photosynthesis (including a fructose-1,6-bisphosphatase), six in protein biosynthesis (i.e., ribosomal components) and one in proteolysis had increased total spectral counts (TSCs, i.e., total number of spectra identified for a protein). The riboflavin synthase 6,7-dimethyl-8-ribityllumazine synthase also had increased levels yet has mostly been described as priming the defense of plants against microbial pathogens [65]. Likewise, up-regulation of a proteinase inhibitor, remorin, and calmodulin were observed in all infested plants. Calmodulins are known calcium sensor proteins that initiate signaling cascades and promote the defense response [66].

Low levels of tissue damage inflicted by sawfly larvae allow plants to keep relatively steady levels of enzymes involved in energy production and protein synthesis. Down-regulation of enzymes that influence cell wall strengthening is in agreement with a potential anti-herbivory compound-based model of defense rather than expression of stem pith that promotes larval death. In Hatcher, allocation of energy is redirected to primary and specialized metabolism to increase levels of anti-herbivory compounds, and less energy is devoted to fortifying the interior of the stem through synthesis of structural carbohydrates and lignins. Low levels of defense-related

compounds such as calreticulins, catalases, heat shock proteins and lectins potentially indicate a tentative manipulation of host defenses by the insect. In the case of a compatible interaction with wheat, the Russian Wheat Aphid (*D. noxia*) takes advantage of host defenses to increase its fitness [67]. Likewise, small non-coding RNA (snRNA) exchanges between wheat and WSS larvae have been characterized and suspected to suppress the immune response [24]. A successful defense response to stress requires ion fluxes for signal transduction, and the up-regulation of a calmodulin enzyme supports the ability of Hatcher tissue to propagate Ca^{2+}-based signals to trigger defense cascades [18,66]. One consequence of pest recognition by the host plant is the establishment of an oxidative burst response. High levels of detoxification enzymes were found in Hatcher and demonstrate an effective defense response through active scavenging of reactive oxygen species to mitigate oxidative damage [15]. Proteinase inhibitors contribute to pest protection through inhibition of digestive proteinases, and consequently increased larval mortality through starvation [17]. High levels of the PR-6 proteinase inhibitor in Hatcher wheat plants potentially participate in reduction of larval feeding. Likewise, two cysteine synthases had increased levels in Hatcher infested plants. Up-regulation of cysteine leads to the synthesis of additional antioxidants and anti-herbivory metabolites [64]. A riboflavin synthase with increased TSCs after infestation also indicates signal transduction and allocation of energy to priming of non-infested tissues through systemic acquired resistance (SAR) [18,65,68].

Wheat cultivar Conan has a semi-solid-stem and pith is expressed at its maximum during WSS flight periods [14]. An allelic variant at the *Qss.msub-3BL* confers solidity and increased resistance to insect attacks [11,12]. The molecular response of Conan to WSS was characterized by down-regulation of a plethora of detoxification enzymes (seven total, e.g., peroxiredoxin, peroxidase) and nine proteins related to photosynthesis (Figure 15). Eleven key enzymes of

protein biosynthesis and proteolysis had higher levels, along with a couple enzymes involved in carbohydrate biosynthesis (e.g., sucrose synthase). No activity related to the pentose phosphate pathway was detected in Conan although other studies suggest up-regulation of energy synthesis enzymes and compounds involved in mechanical support in cultivars with higher degree of stem solidness [28]. The higher carbohydrate synthesis activity observed in Conan nonetheless suggests use of energy to activate defenses upon larval damage, however, the pith is already thick at times of WSS infestation and the plant might rely on passive resistance rather than activating energy-consuming defense pathways. The major down-regulation in detoxification activity is in agreement with a model where the solid stem provides mechanical defense, the plant thus does not require additional molecular defenses and larval manipulation of host response is efficient enough to shut down reactive species scavenging [24]. Reduced photosynthesis in Conan infested stems indicates active measures to starve larvae from energy and nutrients. Susceptible cultivars Denali and Reeder showed typical reactions of plant that undergo massive stress, as both had increases in numerous energy-related proteins such as glycolysis and the tricarboxylic acid cycle (Figures 13 and 15, and Table 5). Hollow stems increase larval survival and fitness, damage inflicted upon chewing is not manageable and reallocation of energy to primary and specialized metabolism (e.g., putrescine and spermine biosynthesis in Denali, lignin biosynthesis in Reeder) is rendered inefficient. The balance between energy synthesis and usage eventually breaks and grain yield is impacted [69]. In all, the protein response was unique to each cultivar and supports that Hatcher relies on alternative strategies than stem solidness to resist sawfly damage.

A recent study on the molecular response of wheat to WSS feeding described protein and metabolite variation in the phenylpropanoid and pentose phosphate pathways in wheat cultivars

with different levels of resistance to the insect [28]. Reallocation of carbohydrates may, however, be the downstream result of intense damage in susceptible plants rather than an active response that aims at strengthening tissues. This omics study relied upon molecular techniques such as 2D-PAGE proteomics and GC-MS targeted metabolomics that did not allow for detection of a large set of molecules, especially anti-herbivory compounds. We rather used LC-MS proteomics and non-targeted metabolomics to maximize the detection of important proteins and compounds in response to WSS infestation.

Another promising line of research on plant–insect interactions is the study of non-coding RNAs such as lncRNAs (long non-coding RNAs) and miRNAs (micro RNAs) using transcriptomics methods. Recent literature describes ncRNAs as key actors of mRNA regulation with implications in plant–pest communication and the response to herbivory [24]. Thousands of lnc/miRNAs from WSS larvae were characterized by Cagirici et al. (2017) and included miR-277, a short RNA sequence that targets several loci on chromosome 3B (region that contains the major stem-solidness QTL *Qss.msub-3BL*). Predicted targets of miR-277 in wheat showed significant similarity to ankyrin-like proteins with known functions in biotic resistance [70]. It is hypothesized that sawfly larvae actively express ncRNAs to suppress the defense response in wheat. Given the great diversity in small non-coding RNA sequences, their involvement in plant direct defenses is also expected. In our study, two ankyrin repeat domain-containing proteins were identified among the differentially regulated peptides: one that was down-regulated in Hatcher infested plants and an up-regulated ankyrin-like protein in Conan. Although preliminary conclusions remain speculative, future work on the response of wheat to WSS infestations warrants the integration of transcriptomics tools to elucidate the role of ncRNA cross-talk between plants and insects and provide novel targets for wheat breeding.

3.5.3. Hatcher Metabolism Was Heavily Impacted in Response to Pest Infestation

Non-targeted LC-MS analysis resulted in the detection of 1823 putative metabolites, and 607 metabolites were annotated and included several major plant defense-related structures (e.g., lignans, terpenoids, alkaloids; Figures 17 and S1) [15,18]. To clarify, lignans and lignin are biosynthesized via the phenylpropanoid pathway, but where the lignans are usually described as toxic compounds, lignin rather imparts support and rigidity to the cell wall. Uni- and multivariate analyses were conducted on the four cultivars to identify compounds that contributed to variation between non-infested and infested plants (Figure 18). Strikingly, *t* tests revealed that resistant and hollow-stem cultivar Hatcher yielded 62 significant shifts in annotated metabolite abundances between treatments, compared to 14 in semi-solid-stem and resistant Conan, and 11 in both hollow-stem and susceptible Denali and Reeder. Further multivariate statistics (i.e., OPLS-DA) on all detected metabolites indicated that 29 (that were significant based on *t* test results as well) were high contributors for the separation of samples based on treatment in Hatcher, four highly contributed to the Conan multivariate model, and eight and four highly contributed to the Denali and Reeder models, respectively. These data indicate important changes in enzymatic activity in Hatcher, and up-regulation of a cysteine synthase observed in Hatcher infested plants may participate to de novo synthesis of specialized metabolites with demonstrated effects on pest fitness reduction [64].

Detailed analysis on the 29 high contributors to the Hatcher OPLS-DA model revealed down-regulation of metabolites that included one alkaloid (**1**), one lipid (**2**), an organic oxygen compound (**3**), three organoheterocyclic structures (**4**-**6**), and a benzoxazinoid (**8**), in infested plants (Figure 18, Table 6). None of these structures have been described in wheat except for the benzoxazinoid structure. Lower abundance of DIBOA-glucoside (**8**) suggests active use of this

phytochemical in Hatcher. Benzoxazinoid structures act as antifeedant and insecticidal metabolites, are largely represented in the Poaceae, and affect both chewing and piercing-sucking pests [23]. Inactive benzoxazinone glucosides are stored in the plant vacuole, released upon insect damage and cleaved to their active and toxic form by β-glucosidases [71]. These compounds are therefore classified as phytoanticipins and down-regulation of their glycoside form leads to up-regulation of the toxic variant [23]. As opposed to phytoanticipins, the below mentioned compounds are rather synthesized de novo and belong to the phytoalexin class. Increased abundance in structures including benzenoids, lignans, and organoheterocyclic compounds was observed in Hatcher individuals exposed to *C. cinctus* (Figure 18, Table 6). Methoxyphenol benzenoids (**9**) are known volatile attractants for natural enemies of pests, as shown in the interaction of soybean looper (*Pseudoplusia includes*) with parasitoid *Microplitis demolitor* [72]. Neolignan structures (**10**) have toxic and deterrent effects on insect herbivores and these properties have been demonstrated in *Magnolia virginiana* resistant plants to the Swallowtail Butterfly (*Troilus* spp.) [73]. The anti-herbivory effect of coumaric acids (**17**) was described in groundnuts (*Arachis hypogea*) is response to various feeding lepidopterans [74]. Several other metabolite structures that were overexpressed in Hatcher infested tissue and with demonstrated activities in defense included a pyranocoumarin (**19**), a butanolide (**22**), an azaphilone (**23**), and a benzopyran [75-78]. In addition, a > 4-fold increase in pyrimidine nucleoside in infested Hatcher and Denali indicated large use of this metabolic precursor to produce toxic specialized metabolites [79].

The three metabolites with highest abundance compared to controls in Conan included two unclassified structures and a lipid-like structure (Table 5). Metabolites that highly contributed to the Denali OPLS-DA model for their increased abundance in infested plants

included the same pyrimidine nucleoside found in > 4-fold increase in Hatcher. More evidence of phytotoxic activity in Denali was illustrated by increase in abundance for a flavonoid-7-O-glycoside and a 7-O-methylated flavonoid. No metabolites were found higher in abundance in Reeder infested plants. In sum, various compounds with described biocidal activities were found in high abundance in Hatcher infested plants and corroborate the high content in cysteine synthase that is a central precursor of anti-herbivory metabolites [64]. Two metabolites with anti-herbivory potential were identified in Denali, however, high susceptibility of this cultivar to WSS indicates insufficient defense resources to increase larval mortality once established inside the stem. Conan also showed very little phytotoxic activity, and this is consistent with its ability to express high levels of stem pith and impede larval fitness without the need for additional layers of defense that include the biosynthesis of toxic molecules. Reeder plants that were exposed to WSS had four metabolites with decrease in abundance, and none that increased. As in Denali, Reeder hollow stems undergo rapid and massive tissue damage from larval feeding because of a weak defense response upon recognition of insects.

3.5.4. Proposed Model for Molecular-Based Defense of Wheat Cultivar Hatcher to C. cinctus

Sawflies respond to emissions of semiochemical compounds from wheat, and detection of these chemical cues by females determine the choice of host plant for oviposition [80,81]. Once landed on the plant cuticle, oviposition behavior of female WSS mainly relies upon direct contact cues [82]. Egg deposition often involves the secretion of oviposition fluids by females and this can constitute a first instance of pest recognition by the plant [83]. Recognition of foreign tissue and activity through release of damage- and herbivore-associated molecular patterns (DAMPs and HAMPs) also triggers plant defense mechanisms (Figure 19) [84,85]. While receptors of insect elicitors (e.g., NBS-LRR protein receptors) have not been detected in

the proteomics data, it is likely that these are constitutively expressed in Hatcher plants and recognize DAMPs and HAMPs such as volicitin-like structures. The fatty-acid–amino-acid conjugate volicitin is an example of chemical released through saliva that elicits host responses [86]. Volicitin has been described in several interactions including infestations of maize (*Z. mays*) by the Beet Armyworm (*S. exigua*) and promotes indirect responses through the release of volatile organic compounds (VOCs) that attract natural enemies of the pest (i.e., parasitoids; Figure 19). A similar response in Hatcher is potentially triggered and volatile methoxyphenol benzenoids are then released to attract WSS parasitoids (e.g., *Bracon cephi* and *Bracon lissogaster*). Upon recognition, triggered immunity involves the establishment of early events, including changes in transmembrane potential and intracellular Ca^{2+} concentrations, kinase cascades (e.g., WIPK), jasmonic acid signaling, and the oxidative burst [15-17]. Non-coding RNAs are exchanged and participate to the regulation of plant molecular responses [24]. No hypersensitive response at the site of oviposition is visible in Hatcher plants, nonetheless, evidence of calmodulin-based Ca^{2+} fluxes and reactive oxygen species scavenging was shown in infested plants [18,66]. Gene expression is then modified and Hatcher defense cascades involve up-regulation of proteinase inhibitors that reduce larval fitness [17]. Although there was no evidence of phytohormone signaling in Hatcher, up-regulation of a riboflavin synthase indicates a capacity to prime intact tissue through SAR [65,68]. Production and activation of phenylpropanoid pathway-related benzoxazinoids is promoted in infested Hatcher through cleavage of the inactive glycoside form and release of the toxic variant. Increased levels of two cysteine synthases and pyrimidine nucleoside enhance anti-herbivory compound and antioxidant biosynthesis [64,79]. Several defense metabolites are synthesized de novo upon infestation, and include neolignan compounds, coumaric acids, and benzopyrans. Hatcher is resistant to other

major pests of wheat such as *M. destructor* and *D. noxia*. Although insect elicitors are specific to pests down to the biotype level, generalist mechanisms of defense are triggered upon infestation by all types of phytophagous insects [16]. A general yet efficient wounding response occurs in Hatcher plants and contributes to high yield performance.

3.5.5. Preliminary Conclusions

Mass spectrometry-based proteomics and metabolomics data demonstrate a unique molecular response to insect infestation in the hollow-stem and WSS resistant cultivar Hatcher. Hatcher up-regulated proteins upon WSS feeding included detoxification, Ca^{2+} flux, proteinase inhibitor, and systemic signaling activities. Increased metabolites upon infestation included anti-herbivory structures and associated precursors. Semi-solid-stem and resistant Conan displayed a different set of protein and metabolic changes after exposure to WSS, suggesting that pith expression is the major means of resistance in this cultivar and Hatcher resistance relies upon alternative molecular mechanisms that have been unexplored until then. Recent advances in wheat functional genomics, genome editing, and breeding techniques open new avenues for rapid identification and introgression of desirable traits [87]. Our data will be invaluable for wheat geneticists and breeders that seek to discover alternative candidate genes for resistance to *C. cinctus*.

Table 4. Differentially regulated proteins between control and infested plants.[a]
(A) Hatcher proteins

Biological process[b] MPCPBR L RS O[c]	Predicted ID[d]	FC[e]	*p* value[f]	Accession number[g]	Other cultivar[h]
Down-regulated in the WSS treatment					
● ○ ○ ○ ○	Cinnamoyl CoA reductase	‡[i]	2.2×10^{-2}	Traes_5DL_D93D4EE55.1	d
● ○	Dihydrolipoamide S-acetyltransferase	‡	6.5×10^{-3}	Traes_5BL_BA19E1CE3.1	
● ○ ○ ○	Embryo defective 1473	‡	1.6×10^{-3}	Traes_3B_62C323792.1	
● ○	S-adenosyl-L-homocysteine hydrolase	0.72	1.9×10^{-2}	Traes_2DL_488816050.2	
● ○ ○ ○ ○	Serine hydroxymethyltransferase	‡	8.1×10^{-4}	Traes_1AL_8EF2B803D.1	
● ○ ○	Transketolase	‡	1.1×10^{-4}	Traes_7AS_CB60FA3AE.1	
● ○ ○	Ubiquitin-activating enzyme E1 2	0.27	1.6×10^{-2}	Traes_5DL_0BE2B1D42.2	C
● ○ ○	UDP-glucose dehydrogenase	0.45	2.9×10^{-2}	Traes_5DL_0A7630D1E.1	
● ○ ○ ○ ○ ○	UDP-glucose pyrophosphorylase 2	‡	5.3×10^{-4}	Traes_4AL_7CC1A63D3.1	
● ○	UDP-XYL synthase 6	0.56	1.9×10^{-2}	Traes_4AS_C839DCF3A.1	
○ ● ○	Alanyl-tRNA synthetase	0.11	3×10^{-3}	Traes_4AL_4CF27F6B1.1	C
○ ● ○ ○	ATP synthase β-subunit	0.52	4.9×10^{-3}	Traes_3AL_964D4D4CF.1	
○ ● ○ ○	Ferredoxin:NADP(H) oxidoreductase	‡	3.7×10^{-3}	Traes_7AS_7BF04E4E6.1	
○ ●	pfkB-like carbohydrate kinase	0.37	2.6×10^{-2}	Traes_7DL_1A847FDCC.1	
○ ●	Ribosomal L18p/L5e family protein	‡	1.9×10^{-2}	Traes_5BL_FA3E0DB03.1	
○ ● ○	Ribosomal protein L35Ae	0.66	5.4×10^{-4}	Traes_7BS_20CBEEF3C.1	
○ ● ○	Ribosomal protein S3Ae	‡	8.1×10^{-4}	Traes_4BL_66E76E6B0.1	
○ ●	Serine carboxypeptidase-like 49	‡	2.7×10^{-4}	Traes_6DS_972C7F490.1	
○ ○ ○ ● ○ ○	H^+ translocating inorganic pyrophosphatase	‡	5.4×10^{-4}	Traes_7BS_55CB27B54.1	
●	H^+-ATPase subunit E isoform 3	0.67	7.1×10^{-3}	TRAES3BF081200010CFD_t1	
○ ○ ○ ● ○ ○	Sterol carrier protein 2	0.17	9.7×10^{-3}	Traes_6DL_5C12D3124.1	
●	Ankyrin repeat domain-containing protein 2A	0.85	2.9×10^{-2}	Traes_5BL_B66B801E5.1	
○ ●	Calreticulin-1	0.66	2.5×10^{-2}	Traes_2AL_070A611F6.2	
○ ○ ● ○	Catalase-1	0.79	4.7×10^{-2}	Traes_4DL_4FC0D4B27.1	
○ ○ ○ ● ○	Heat shock protein 70	‡	9×10^{-4}	Traes_4BS_15014415A.1	
●	Mannose-binding lectin superfamily protein	‡	1.1×10^{-3}	Traes_2BS_A1F541056.1	
Up-regulated in the WSS treatment					
● ○	6,7-dimethyl-8-ribityllumazine synthase	‡	8.1×10^{-3}	Traes_2DL_868EFCEB6.2	
●	α/β-hydrolase	4.03	6.2×10^{-3}	Traes_5BL_885C2757D.2	
● ○	Aspartate aminotransferase 3	1.31	1.1×10^{-2}	Traes_3DL_870617108.1	D
● ○ ○ ○	Cysteine synthase	1.51	2.1×10^{-3}	Traes_5BS_1AC8D3009.2	
● ○ ○	Cysteine synthase 1	1.85	1.2×10^{-3}	Traes_5DS_581AB88F8.2	
● ○ ○	Embryo defective 2171	1.89	4.6×10^{-2}	Traes_1AL_D20D648FD.1	
● ○ ○	Fructose-1,6-bisphosphatase	‡	5×10^{-4}	Traes_1AL_DA0EE1337.2	
● ○ ○	Glyceraldehyde-3-phosphate dehydrogenase	1.5	3.1×10^{-2}	Traes_4DL_F394FF94A.1	
● ○	NADPH-dependent alkenal/one oxidoreductase	1.39	5×10^{-2}	Traes_6AS_0D08DEFD0.1	
● ○	pfkB-like carbohydrate kinase	1.53	3.6×10^{-2}	TRAES3BF078000040CFD_t1	
● ○ ○	UBC35/UBC13A	2.61	2.1×10^{-2}	TRAES3BF050900020CFD_t1	
○ ● ○ ○ ○	40S ribosomal protein S6-2	1.86	1.3×10^{-2}	Traes_2AS_C7813CD47.1	
○ ● ○	50S ribosomal protein L16	‡	2.1×10^{-3}	EPlTAEP00000010050	
○ ● ○ ○ ○ ○	Acidic protein associated with 40S ribosomal subunit	1.3	3.9×10^{-2}	Traes_2AS_3F458D2CF.1	

◦	●	◦		◦	Ferredoxin:NADP(H) oxidoreductase	1.47	4.3×10^{-2}	Traes_4AL_B9FA07247.2	
◦	●			◦	Photosystem I light harvesting complex	1.51	7.7×10^{-3}	Traes_2AS_B86EFFF66.1	
◦	●			◦	Photosystem I reaction center subunit VI-2	1.44	1.8×10^{-2}	Traes_1AL_C42DE440F.1	
◦	●	◦		◦	Ribosomal L28e protein family	2.68	3.4×10^{-2}	Traes_1DL_115A0324A.1	
◦	●	◦			◦ Ribosomal protein L10	1.5	4.2×10^{-2}	Traes_4BL_C336491A71.1	
◦	●	◦			Ribosomal protein S5	‡	10^{-3}	Traes_5BL_E948DCA4A.2	
	◦	●	◦		◦ Profilin 5	1.4	4.7×10^{-2}	Traes_7AS_DA1089F6B.2	
			●	◦	Plasma membrane intrinsic protein 2;8	1.96	3×10^{-2}	Traes_2BS_D8EC76A3B.2	
◦	◦		●	◦	◦ Vacuolar ATP synthase subunit	1.19	3.6×10^{-2}	Traes_7DL_D4B6FF473.1	D
				●	Adenylate kinase	1.22	3×10^{-3}	Traes_7AL_B7810831E.1	
◦	◦	◦		●	Bifunctional enolase 2	1.22	4.2×10^{-2}	Traes_5AS_116663495.1	D
				●	Calmodulin	1.93	1.7×10^{-2}	Traes_4AS_E2D1D9E5D.1	
◦	◦			●	Glutathione S-transferase	‡	6.8×10^{-4}	Traes_5AL_72929F651.1	
◦	◦			●	Glutathione S-transferase Z1	‡	6.4×10^{-3}	Traes_5DL_9F421ABDC.1	
◦	◦			●	Hydroxypyruvate reductase	1.31	2.4×10^{-2}	Traes_6AS_27483C00F.1	
					KH domain-containing protein	‡	1.7×10^{-2}	Traes_6AS_8C9DF7D23.1	
	◦	◦	◦	●	◦ Plasma-membrane associated cation-binding protein 1	1.52	3×10^{-2}	TRAES3BF114000090CFD_t1	
				●	PR-6 proteinase inhibitor	5.18	2.1×10^{-2}	TRAES3BF070600020CFD_t1	
				●	Remorin	3.85	5×10^{-2}	Traes_2AL_47B1A5BF2.1	
				●	Stress response component	4.99	1.9×10^{-2}	Traes_5DL_DC720C4C0.2	
◦		◦		●	Thioredoxin M-type	1.64	2.2×10^{-2}	Traes_5BS_B72CD04F2.1	
					● Plastid transcriptionally active 16	1.2	4.5×10^{-2}	Traes_3DL_43F4381AA.1	

[a]Proteins were arranged based on their regulation after WSS infestation, major biological process, then alphabetical order.
[b]The five major biological processes were selected based on gene ontology data.
[c]MP = metabolic process; CP = cellular process; BR = biological regulation; L = localization; RS = response to stimulus; O = other biological process; ● = most important GO biological process hit; ◦ = GO biological process hit.
[d]Predicted IDs correspond to the best found hit using the Wheat Protein Database [42].
[e]Fold changes were calculated as (mean WSS)/(mean No WSS) treatments, where WSS corresponds to the infested plants, No WSS represents controls.
[f]*p* values were calculated from *t* tests (factors of treatment) and adjusted by a Benjamini–Hochberg correction.
[g]Spectra were searched and accession numbers obtained using Mascot v2.3.01 against the in-house wheat peptide database.
[h]Important Hatcher proteins that were also differentially regulated in another cultivar. C = up-regulated in Conan; d = down-regulated in Denali; D = up-regulated in Denali.
[i]‡ = protein detected in only one treatment.

(B) Conan proteins

Biological process						Predicted ID	FC	*p* value	Accession number
M	P	C	P	B	R	L R S O			
Down-regulated in the WSS treatment									
●	◦			◦		D-ribulose-5-phosphate-3-epimerase	0.5	1.6×10^{-2}	Traes_4AS_13C312D8E.1
●	◦			◦		Fructose-1,6-bisphosphatase	0.12	8.8×10^{-3}	Traes_3AL_392D17B3C.2
●	◦	◦		◦	◦	Gamma-aminobutyrate transaminase POP3	0.19	1.7×10^{-2}	Traes_2AL_0BD6646BA.1
●	◦			◦	◦	Glutamine synthetase 2	0.65	9.6×10^{-3}	Traes_2BL_342BDEA35.2
●	◦	◦				Glycine cleavage T-protein	0.64	1.8×10^{-2}	Traes_2BL_2768AE3B1.1
●	◦					Glycolate oxidase	0.74	1.1×10^{-2}	Traes_5BL_D70B77649.3
●	◦			◦		Glyoxalase/Bleomycin resistance protein	‡	1×10^{-3}	Traes_5BL_1D07AA86C.2
●	◦					NAD-dependent malate dehydrogenase	0.57	1×10^{-2}	Traes_5BL_8A99D83A5.1
●	◦					NDH-dependent cyclic electron flow 1	0.62	3.7×10^{-2}	Traes_4AS_DE6DD58CC.1
●	◦					Ribulose bisphosphate carboxylase	0.73	7.3×10^{-3}	EPlTAEP00000010047
●	◦	◦		◦	◦	Serine transhydroxymethyltransferase 1	0.81	2.4×10^{-2}	Traes_4BS_A435E6D76.2
●	◦			◦		Triosephosphate isomerase	0.78	4.8×10^{-2}	Traes_3DS_9C173AB38.1
◦	●			◦	◦	Chlorophyll a/b binding protein CP26	0.69	1.8×10^{-2}	Traes_4DS_CC9F9317E.2
	●					Cyclophilin CYP20-3	‡	8.3×10^{-4}	TRAES3BF160500010CFD_t1
◦	●	◦		◦		Cytochrome b6-f complex iron-sulfur subunit	0.8	3.6×10^{-2}	Traes_2AS_1475F8BDB.1
◦	●			◦		Ferredoxin:NADP(H) oxidoreductase	0.76	1.7×10^{-2}	Traes_6DS_7A1EB4B66.1
◦	●					Photosystem I P700 chlorophyll a apoprotein A1	0.52	4.5×10^{-2}	EPlTAEP00000010026
◦	●					Photosystem II CP47 reaction center protein	0.67	5.5×10^{-3}	EPlTAEP00000010015
◦	●				◦	Photosystem II reaction center PsbP family	0.11	1.5×10^{-3}	Traes_5BS_69F251543.2
◦	●					PsbP-like protein 1	0.44	5.3×10^{-3}	Traes_4DS_80C6168FE.1
◦	●			◦	◦	ZKT	‡	2.7×10^{-2}	Traes_2BS_90255A78E.2
		●		◦		Lipoamide dehydrogenase	0.72	2.7×10^{-2}	Traes_1BS_15C828137.2
◦	◦		●	◦		ATP synthase subunit beta	0.79	4×10^{-2}	Traes_2BS_68A7179D8.2
◦	◦		●	◦		ATP synthase subunit beta	0.79	2.9×10^{-2}	Traes_1AS_45DF41500.1
			●			GTP-binding protein-related	0.18	2.2×10^{-2}	Traes_5DL_64C6A2250.1
		◦		●		2-Cys peroxiredoxin	‡	3×10^{-5}	Traes_2BL_E6F86DAFA.1
		◦		●	◦	Beta carbonic anhydrase	0.74	4.4×10^{-3}	TRAES3BF026200060CFD_t1
◦	◦	◦		●		Calmodulin-binding protein	0.67	3.3×10^{-2}	TRAES3BF153400060CFD_t1
◦	◦	◦		●	◦	Chloroplast RNA binding	0.64	1.6×10^{-3}	Traes_5BS_4D44AE9D6.2
◦	◦			●	◦	Chloroplast stem-loop binding protein	0.41	3.8×10^{-3}	Traes_6AS_606F61E8B.1
		◦		●	◦	Cystathionine beta-synthase domain-containing protein	0.57	8.4×10^{-3}	Traes_4DS_4D761086B.1
◦	◦			●		Glycine-rich RNA-binding protein 8	0.8	1.1×10^{-2}	Traes_5BS_8ECE54AC4.1
				●		Glyoxylate reductase 2	‡	5×10^{-5}	TRAES3BF042100010CFD_t1
◦	◦	◦		●		Heat shock protein 70	0.78	2.8×10^{-2}	Traes_1AL_51CED3DBF.1
◦	◦			●		Microsomal ascorbate peroxidase APX3	0.59	4.5×10^{-2}	Traes_7AS_81327ECA0.1
◦	◦	◦		●		Oxygen-evolving enhancer protein 2	0.81	3.1×10^{-2}	Traes_2AL_0A039E562.1
◦	◦			●		Peroxidase	‡	1×10^{-2}	Traes_6AS_D49C93E84.1
◦	◦	◦		●		Thylakoid ascorbate peroxidase	0.6	1.3×10^{-2}	Traes_6BL_83DE6DC09.1
						?	0.06	1×10^{-2}	Traes_2DL_9E58CB2D5.1
					●	Thiosulfate:cyanide sulfurtransferase	0.56	3.3×10^{-2}	Traes_5BS_F8604D316.2
Up-regulated in the WSS treatment									
●	◦			◦		AICARFT/IMPCHase bienzyme family	1.78	2.6×10^{-2}	Traes_1AL_3336F1DFB.1
●	◦					Alpha-l-arabinofuranosidase/beta-d-xylosidase	5.73	9.8×10^{-3}	Traes_4AL_351DA9BAE.1
●	◦					Biotin synthetase	‡	6.8×10^{-3}	Traes_3AL_45EF63187.1
●	◦					GDP-D-mannose 3',5'-epimerase	‡	3.5×10^{-3}	Traes_1BL_1CCF44ECE.1

●	◦				Glutamate decarboxylase 5	1.81	6.7×10^{-3}	TRAES3BF050800360CFD_t1
●	◦			◦	◦ Glycyl-tRNA synthetase	‡	1.5×10^{-2}	Traes_7DS_817122161.1
●	◦			◦	◦ NADP-ME2	‡	2×10^{-5}	Traes_1AS_A53D11A37.1
●	◦			◦	◦ Phosphoenolpyruvate carboxylase	1.88	3.8×10^{-2}	Traes_5BL_6642E2A8B.1
●	◦	◦		◦	Sucrose synthase activity	10.53	3.5×10^{-2}	Traes_4AL_2BC235062.1
●	◦			◦	Ubiquitin-activating enzyme E1 2	7.37	4.1×10^{-2}	Traes_5DL_0BE2B1D42.2
●	◦	◦			Ubiquitin-like modifier (SUMO) polypeptide	6.71	5.1×10^{-3}	TRAES3BF091100230CFD_t1
◦	●				20S proteasome beta subunit	1.51	4.5×10^{-2}	Traes_4DS_8EF070D72.1
◦	●			◦	20S proteasome beta subunit	1.48	1.2×10^{-2}	Traes_4DS_058D6EF22.1
◦	●			◦	Alanyl-tRNA synthetase	3.53	3.1×10^{-2}	Traes_4AL_4CF27F6B1.1
◦	●				Cytochrome b559 subunit alpha	1.45	4×10^{-2}	EPlTAEP00000010041
◦	●				NADH-ubiquinone oxidoreductase-related	‡	3.4×10^{-3}	Traes_4BL_3EFFEDE44.1
◦	●			◦	Photosystem II type I chlorophyll a/b-binding protein	4.72	3.8×10^{-2}	Traes_1AL_0F39673AF1.3
◦	●				◦ Ribosomal protein L1p/L10e family	2.28	7.2×10^{-3}	Traes_4BS_4DB5737A6.1
◦	●				◦ Ribosomal protein L7Ae/L30e/S12e/Gadd45 family	16.38	2.3×10^{-4}	Traes_5DL_1299E23A4.1
◦	●	◦		◦	Ribosomal protein large subunit 27	2.94	3.6×10^{-2}	TRAES3BF146000050CFD_t1
◦	●	◦	◦		Ribosomal protein S4	4.55	2.5×10^{-2}	Traes_5AS_9F681D8F1.1
	●	◦			◦ Sec14p-like phosphatidylinositol transfer family	5.14	1.9×10^{-2}	TRAES3BF043700170CFD_t1
	●				TCP-1/cpn60 chaperonin family	5.96	3.2×10^{-2}	Traes_7AL_F3ED3303D.1
	●			◦	TCP-1/cpn60 chaperonin family protein	2.52	3.7×10^{-3}	Traes_6DL_30AD166CD.1
			●		ARM repeat superfamily	‡	8.2×10^{-3}	Traes_5AS_33A86266A.1
	◦		●		◦ Clathrin heavy chain 1	‡	3.8×10^{-3}	Traes_4DS_EB7A5C35C.2
			●		Coatomer	‡	2.9×10^{-3}	Traes_5AL_E153CEC65.1
	◦	◦	●	◦	GDP dissociation inhibitor	‡	5×10^{-3}	Traes_1DL_401D433BE.1
◦	◦		●		Vacuolar ATP synthase subunit B1	1.22	3.4×10^{-2}	Traes_7AL_B89A5FB9A.1
◦	◦	◦		●	◦ 26S proteasome subunit	2.27	3.2×10^{-2}	Traes_2AS_DFDA79E58.1
◦	◦	◦	◦	●	Ankyrin repeat domain-containing protein 2B	1.61	3×10^{-2}	Traes_7AS_860ACFB35.1
		◦		●	Elongation factor 1-beta	1.46	3.8×10^{-2}	Traes_2DS_C6B631387.1
◦	◦	◦		●	General regulatory factor	1.61	4.1×10^{-2}	Traes_4BS_342A62CE6.1
◦	◦	◦		●	General regulatory factor	1.29	1.9×10^{-2}	Traes_4AL_6B5C89E7C.1
◦	◦			●	Phi glutathione transferase	1.99	5.7×10^{-3}	Traes_4BL_689C6389A.1
	◦	◦		●	◦ Thioredoxin family	1.2	1.8×10^{-2}	Traes_1AS_C0D4CD39A.2
	◦	◦		◦	● Actin	1.1	1.5×10^{-2}	Traes_1AS_A8AD3BE99.2
	◦	◦		◦	● DC1 domain-containing protein	3.55	4.7×10^{-2}	Traes_2DL_28DFAC79D.2
◦	◦				● Nucleolin like 1	‡	3.5×10^{-3}	Traes_7BS_1F4C5C328.1
					Aluminum induced protein	1.46	4×10^{-2}	Traes_5BL_17F1F28B6.1

(**C**) Denali proteins

Biological process						Predicted ID	FC	*p* value	Accession number
M	P	C	P	B	R	L R S O			
						Down-regulated in the WSS treatment			
●	○			○	○	Cinnamoyl CoA reductase	0.65	3.5×10^{-2}	Traes_5DL_D93D4EE55.1
●	○				○	Geranylgeranyl reductase	‡	3.4×10^{-2}	Traes_6DL_0FF72D765.1
●	○				○	Glutamate-1-semialdehyde 2,1-aminomutase	0.62	1.9×10^{-2}	Traes_7AS_9C283FE66.1
●	○	○		○		Glycolate oxidase	0.72	4.4×10^{-2}	Traes_2AL_C51BB91CC.3
●	○			○	○	NADPH:protochlorophyllide oxidoreductase B	0.37	4.3×10^{-2}	Traes_1AL_BB3D071F8.1
○	●			○	○	26S proteasome subunit RPN8a	0.58	9.2×10^{-3}	Traes_2AL_AA6937D6B.1
○	●					Cytochrome b559 subunit alpha	0.4	4.4×10^{-2}	EPlTAEP00000010041
○	●					Ribosomal protein L3 family	0.4	4×10^{-3}	Traes_6AS_478618F75.1
○	●					Ribosomal protein L4	0.57	2.6×10^{-2}	Traes_4DL_31D6228F5.1
○	●	○	○	○	○	Thylakoid formation 1	0.57	1.7×10^{-2}	Traes_2DS_D106620BE.1
	○		○	●	○	Chaperone protein htpG family	0.51	4.2×10^{-2}	Traes_5AL_1DA3B4631.1
	○	○		●	○	Chloroplast chaperonin 60	0.65	4.9×10^{-2}	Traes_7AS_3247D97E8.2
○	○			●	○	Chloroplast RNA binding protein	0.26	1.4×10^{-2}	Traes_2DS_01D518748.1
○		○		●	○	Chloroplastic drought-induced stress protein	0.24	4.3×10^{-2}	Traes_6DL_C6E63ED1C.1
○	○			●		Glyoxylate aminotransferase	0.65	4.8×10^{-2}	Traes_2AL_85FCE950B.1
		○		●	○	Rubisco activase	0.61	1.3×10^{-2}	Traes_4DS_5C2095EE7.2
						Up-regulated in the WSS treatment			
●	○	○		○	○	26S proteasome AAA-ATPase subunit RPT4a	2.38	3.2×10^{-2}	Traes_7AL_EA1DE71E6.1
●	○					3-keto-acyl-CoA thiolase 2 precursor	1.8	1.9×10^{-2}	Traes_6DL_7960654CF.2
●	○			○	○	Aconitase	1.29	1.5×10^{-2}	Traes_6AL_28CCA7F5D.1
●	○			○	○	Aconitase	1.25	3.9×10^{-2}	Traes_6BL_4704FF2B4.1
●	○			○		Aconitase 1	1.81	1.5×10^{-2}	Traes_4DL_3D374FF4C.1
●	○					Aldolase	1.16	1.8×10^{-2}	Traes_3AL_441C0AE1B.1
●	○	○		○		Aldolase-type TIM barrel family protein	1.3	4.6×10^{-2}	TRAES3BF142600080CFD_t1
●	○					Aspartate aminotransferase 3	2.03	1.3×10^{-3}	Traes_3DL_870617108.1
●	○	○				Betaine aldehyde dehydrogenase	1.46	4.9×10^{-2}	Traes_6AL_42AEB5299.1
●	○				○	Dehydroquinate-shikimate dehydrogenase	7.48	6.1×10^{-3}	Traes_5AS_908BF5D38.1
●	○	○		○		Enolase	1.31	2×10^{-2}	Traes_5AS_116663495.1
●	○	○		○	○	Glycosyltransferase	‡	2.5×10^{-3}	Traes_7BL_0E93FBCFF.2
●	○	○		○		Hydroxycinnamoyl-Coenzyme A shikimate/quinate hydroxycinnamoyltransferase	4.69	2.5×10^{-2}	Traes_6AL_D8A91F983.1
●	○			○		Lactate/malate dehydrogenase	‡	4×10^{-5}	Traes_6DS_5DBF48560.1
●	○			○		Mitochrondrion targeted citrate synthase	1.68	4.1×10^{-2}	Traes_6BS_682497935.1
●						NAD(P)-linked oxidoreductase	1.43	1.1×10^{-2}	Traes_2BL_2FD539228.2
●	○	○		○		NADP+-isocitrate dehydrogenase	1.61	4.4×10^{-2}	Traes_3AL_3D5C860FD.1
●	○					N-carbamoylputrescine amidase	‡	4.8×10^{-4}	Traes_5DS_01D241425.1
●	○					Nitrilase/cyanide hydratase	5.62	4.7×10^{-2}	Traes_4AS_CDEB9D532.2
●	○			○		Orotate phosphoribosyltransferase/orotidine-5'-phosphate decarboxylase	6.56	2.2×10^{-2}	TRAES3BF139100030CFD_t1
●	○			○	○	Phosphoenolpyruvate carboxylase	1.71	4.6×10^{-2}	Traes_5BL_6642E2A8B.1
●	○					Pyrophosphorylase 2	1.45	3.3×10^{-2}	Traes_6AL_7E70268F1.2
●	○	○		○		Spermine synthase	‡	1.7×10^{-2}	Traes_1DL_43FED2619.1
●	○	○				Ubiquitin-like modifier (SUMO) polypeptide	5	3.7×10^{-2}	TRAES3BF091100230CFD_t1
○	●					20S proteasome beta subunit PBB2	1.28	2.5×10^{-2}	Traes_1BS_548536A26.2
○	●	○		○	○	26S proteasome AAA-ATPase subunit RPT3	9.05	3.2×10^{-2}	Traes_2AL_80D15B4FB.1
○	●			○		60S acidic ribosomal protein P2	‡	4.7×10^{-4}	Traes_6AS_D49C93E84.1
○	●			○		Cysteine proteinase	1.8	1.7×10^{-2}	Traes_5DL_AC7C885A0.1

		●				F1F0-ATPase inhibitor protein	‡	8×10^{-5}	Traes_7DS_427AD6E51.1
	◦	◦	●	◦		GDP dissociation inhibitor	8.91	2.1×10^{-2}	Traes_1DL_401D433BE.1
◦	◦	◦	●		◦	Pleckstrin homology (PH) domain superfamily	2.17	2.8×10^{-2}	Traes_1AL_06BC2ED91.1
			●	◦		Rab1 GTPase	1.42	4.5×10^{-2}	Traes_3DL_4B8AB34A9.1
◦	◦		●	◦	◦	Vacuolar ATP synthase subunit	1.4	1.3×10^{-2}	Traes_7DL_D4B6FF473.1
			◦	●		Annexin	1.54	4.7×10^{-2}	Traes_7AS_FFB7CAFC3.1
◦	◦			●	◦	Chitinase	‡	9.8×10^{-4}	Traes_6DS_AA77F7548.1
	◦			●	◦	heat shock protein 90	1.23	2.5×10^{-2}	Traes_7DS_CB359539B.1
				●		Mitochondrial aldehyde dehydrogenase	1.45	1.3×10^{-2}	Traes_7AS_DE1248005.1
◦	◦			●		Peroxidase	‡	1.3×10^{-2}	Traes_2DL_1CB540BCC.3
◦	◦			●		Phi glutathione transferase	1.37	7.5×10^{-3}	Traes_1AL_1B8FDA3D4.1
◦	◦	◦	◦	●	◦	Phytochelatin synthase	4.23	4.6×10^{-2}	Traes_4DL_A6F0CFF85.1
	◦	◦		●	◦	Protein disulfide-isomerase	1.73	2.9×10^{-2}	Traes_4DS_26272902A.1
◦	◦	◦		●	◦	Sulfite reductase	1.92	2×10^{-2}	Traes_1AL_5A7E85C4E.1
	◦	◦		◦	●	DC1 domain-containing protein	1.94	3.8×10^{-2}	Traes_2DL_28DFAC79D.2
	◦	◦		◦	●	Receptor for activated C kinase 1C	1.81	3.3×10^{-2}	TRAES3BF007900030CFD_t1

(D) Reeder proteins

Biological process						Predicted ID	FC	*p* value	Accession number
M	P	C	P	B	R				
L			R	S	O				
Down-regulated in the WSS treatment									
●		◦	◦	◦		Chalcone synthase	‡	5×10^{-5}	Traes_2BS_9E10D26DB.1
●	◦			◦		Glutamate dehydrogenase	0.15	1.8×10^{-2}	Traes_5AL_1DD952467.1
●	◦			◦		Phosphofructokinase	0.2	2×10^{-2}	Traes_7BS_0BE381F61.1
●	◦		◦			Sucrose-phosphate synthase	‡	4.7×10^{-3}	Traes_3AS_6505083E0.1
●	◦			◦		Triosephosphate isomerase	0.87	1.9×10^{-4}	Traes_3AS_AE3D5013D.1
◦	●				◦	CDC48-interacting UBX-domain protein	‡	1.6×10^{-3}	Traes_2DL_8D23EB0D7.1
				●		GTP binding elongation factor Tu family	0.19	1.5×10^{-2}	Traes_4AL_766B299B1.1
	◦	◦		●	◦	Homologous to co-chaperon DNAJ	0.13	1.4×10^{-2}	Traes_5BL_CF5A8348D.2
◦	◦			●		Lambda glutathione transferase	‡	1.1×10^{-3}	Traes_4AS_2197EE051.1
				●		Late embryogenesis abundant protein	0.61	3.6×10^{-2}	Traes_5BL_CE7069050.1
◦	◦		◦	●	◦	Phytochelatin synthase	‡	2.9×10^{-3}	Traes_4DL_A6F0CFF85.1
Up-regulated in the WSS treatment									
●	◦			◦	◦	Alpha-1,4-glucan-protein synthase family	‡	2×10^{-2}	Traes_2AL_41B176D01.2
●	◦	◦		◦		Aspartate aminotransferase 5	1.47	4.4×10^{-2}	Traes_6DL_961B6AFC5.1
●	◦			◦		Dehydroascorbate reductase 1	‡	4×10^{-5}	Traes_7AS_0BB13DD79.1
●	◦			◦		D-ribulose-5-phosphate-3-epimerase	1.8	2.6×10^{-2}	Traes_4AS_13C312D8E.1
●	◦			◦		Fructose-bisphosphate aldolase 1	1.27	9.3×10^{-3}	Traes_4BS_D12DBE6D3.1
●	◦			◦		Fructose-bisphosphate aldolase 2	1.35	1.2×10^{-2}	Traes_5DS_D693664F7.4
●	◦					Glyceraldehyde 3-phosphate dehydrogenase A subunit 2	1.15	4×10^{-2}	Traes_2BL_5D64E8C87.1
●	◦			◦		Glyceraldehyde-3-phosphate dehydrogenase	1.52	2.1×10^{-2}	Traes_4DL_F394FF94A.1
●	◦					Pinoresinol reductase	‡	2.2×10^{-2}	Traes_2BS_23E0AC565.2
●	◦				◦	Triosephosphate isomerase	1.45	2.9×10^{-2}	Traes_5BL_D5F2A5070.1
◦	●	◦		◦		50S ribosomal protein L12-C	2.14	4.9×10^{-2}	TRAES3BF028000060CFD_t1
◦	●			◦		Cysteine proteinase	1.54	3×10^{-2}	Traes_5DL_AC7C885A0.1
◦	●			◦		Light harvesting complex of photosystem II	1.35	1.8×10^{-2}	Traes_2BS_4AE914BE2.1
◦	●			◦		Ribulose bisphosphate carboxylase	1.38	3.5×10^{-2}	Traes_5AL_AD0034878.1
◦	●			◦		Rubisco small subunit (RBCS)	1.31	4.6×10^{-2}	Traes_2AS_3953901E4.1
◦	●					Thylakoid photosystem I subunit	2.47	4.8×10^{-2}	Traes_2AS_D26D32A7C.1
◦	●	◦		◦		U2 small nuclear ribonucleoprotein A	‡	1.1×10^{-2}	Traes_4AL_8C7636C36.1
		●		◦	◦	RNA-binding family	5.88	1.5×10^{-2}	Traes_5DL_63AB65800.2
			●			Vacuolar ATP synthase subunit D	1.58	4.3×10^{-2}	Traes_2AL_2B01693491.2
			●			Vacuolar membrane ATPase complex	3.03	3.3×10^{-2}	Traes_2AL_152FE9E5F.1
◦	◦			●		Beta-d-xylosidase	1.65	2×10^{-2}	Traes_2AL_3E4F9254A.1
				●		Disease resistance-responsive family	1.96	3.8×10^{-2}	Traes_4DS_234713A1E.1
				●		Early endosome antigen	3.33	2.8×10^{-2}	Traes_2DL_8A52AFA08.2
◦	◦			●	◦	Fumarate hydratase 1	1.75	8.9×10^{-3}	Traes_4AS_2DCA42965.1
				●	◦	Methionine sulfoxide reductase	1.7	2.5×10^{-2}	Traes_4DS_AFAF2A29E.1
◦	◦			●		Nucleoside diphosphate kinase type 1	1.34	2.3×10^{-2}	Traes_1AL_6F2E87864.2
◦	◦			●		Phi glutathione transferase	2.83	3.3×10^{-2}	Traes_3DL_B1E3D279A.1

Table 5. Differentially regulated metabolites between control and WSS infested wheat.[a]

Superclass[b]	Subclass[c]	Chemical name (abbr…)[d]	RT[e]	*m/z*[f]	*p* value[g]	
Down-regulated in the WSS treatment - Hatcher						
Alkaloid/der.	Harmala alkaloid	1-(9H-β-Carbolin-1…	204	422.1744	7.7×10^{-3}	●[h]
Lipid/lipid-like cmp.	Taxane/der.	(2aR,4S,4aS,5R,6R,8S,9aS…	309	650.294	2.7×10^{-2}	
	Saccharolipid	2-[4-({[(2R*,3E,4R*)-3-ethyl…	225	910.3106	4.2×10^{-2}	
	Diterpenoid	4-[Formyl(methyl)amino]…	340	468.3094	2.7×10^{-2}	
	1-acyl-sn-glycero-3-phosphocholine	LPC(18:3)	452	517.3178	2.4×10^{-2}	
	Trihydroxy acid	-	331	586.2915	3×10^{-2}	
	Hydroxysteroid	-	313	806.3362	1.3×10^{-2}	●
Organic acid/der.	Tetracarboxylic acid	(1R,3S,4S,5S,6R,7R)-4,7…	267	666.2885	4×10^{-2}	
	Tetracarboxylic acid	Decipinin A	290	600.2207	3.4×10^{-2}	
	Oligopeptide	-	260	372.2118	3.2×10^{-2}	
	Keto acid/der.	-	354	248.1073	4.8×10^{-2}	
Organic oxygen cmp.	Aminocyclitol glycoside	(1R,2S,3S,4S,5S,6R)-2,3,4…	28	355.1485	5.1×10^{-3}	●
	Glucuronic acid der.	2,3,5-trihydroxy-4-methoxy…	335	224.0531	3.5×10^{-2}	
	Monosaccharide phosphate	2-Deoxy-6-O-phosphono…	46	246.0511	3.5×10^{-2}	
Organoheterocyclic cmp.	Indolizidine	-	300	434.1245	1.3×10^{-3}	●
	6-aminopurine	9-(β-D-Erythro-pentofuran…	300	265.081	5.9×10^{-3}	●
	Isoindolone	(2R,2'R,4'aS,6'R,8'aS)-7-Aceton…	264	441.2505	2.1×10^{-2}	●
Phenylpropanoid/ polyketide	Cinnamic acid ester	{2-[4-(Hydroxymethyl)-2…	288	396.1574	4.8×10^{-2}	
	Coumarin/der.	Scoparon	379	206.0588	4.6×10^{-2}	
	Flavonoid-7-O-glycoside	Veno-V	222	608.1732	3.9×10^{-2}	
-	Benzoxazinoid glycoside	DIBOA-glucoside	106	343.0913	7.5×10^{-3}	●
	Benzodioxole	Fagaramide	61	247.1213	4×10^{-2}	
	-	4-{[(3R,4R)-4-(4-Hydroxy-3…	225	520.1936	7.9×10^{-3}	●
	-	(1S,3aS,4R,6aR)-1,4-Bis…	246	536.1899	1.4×10^{-2}	
	-	Propanamide, N…	248	555.2224	4.3×10^{-2}	
Up-regulated in the WSS treatment - Hatcher						
Benzenoid	Tyrosol/der.	Propanoic acid 4-hydroxy…	240	194.0946	1.4×10^{-2}	●
	Benzenesulfonyl cmp.	4-(4-isopropoxyphenyl)…	221	292.0779	3×10^{-2}	
	Benzene	4,4-dimethyl-2-phenyl…	32	175.1005	3.1×10^{-2}	
	Methoxyphenol	-	383	208.0743	8.6×10^{-3}	●
Lignan	Neolignan	Methyl (2E)-3-(4-{[(1R,2R)-1,3…	285	404.1488	1.6×10^{-3}	●
	Furanoid lignan	(1S,2S,1'S,2'S)-2,2'-{(1R,3aS…	359	810.3093	3.1×10^{-2}	
		Huazhongilexin	286		6.2×10^{-3}	
Lipid/lipid-like cmp.	Fatty alcohol ester	[(2Z,8Z)-10-hydroxydeca-2,8…	337	204.0789	2.1×10^{-2}	●
	Methionine/der.	(2S)-2-amino-4-dimethyl…	224	163.0673	4×10^{-2}	
	Triterpenoid	Microtropioside B	370	502.3147	4×10^{-2}	
	Guaianolide/der.	-	277	376.1521	1.9×10^{-2}	●
	Colensane/clerodane diterpenoid	-	322	806.3351	3.8×10^{-2}	
	Xanthophyll	-	417	738.3807	4.8×10^{-2}	
Nucleoside	1-ribosyl-imidazole carboxamide	-	23	380.073	9.9×10^{-5}	●

	Pyrimidine ribonucleoside monophosphate	-	23	542.1261	1.2×10^{-2}	●
Organic acid/der.	Tricarboxylic acid/der.	8-O-Acetyl-pumilin	343	416.1479	6×10^{-3}	●
Organic nitrogen cmp.	Nitroguanidine	Confidor	237	255.0532	2.7×10^{-2}	
Organic oxygen cmp.	O-glycosyl cmp.	β-D-Glucopyranose, 6-O-D…	312	372.1274	5.2×10^{-3}	●
	Thioglycoside	Isopropyl 4-O-(β-D…	349	400.1404	1.6×10^{-2}	●
Organoheterocyclic cmp.	Butenolide	-	333	208.0744	2×10^{-5}	●
	Azaphilone	-	335	416.1479	4.8×10^{-3}	●
	Phenylimidazole	3-Nitroso-2-phenylimidazo…	311	224.0703	6.2×10^{-3}	●
	2-benzopyran	8-Hydroxy-5-(hydroxymethyl…	299	208.0745	7.4×10^{-3}	●
	Bi/oligopyridine	Coretec	245	250.0854	4.2×10^{-2}	
	Indole	Didemethylasterriquinone D	632	370.096	2.9×10^{-2}	
	Pyranone/der.	4-Methoxy-5-methyl-6-oxo…	318	208.0745	1.3×10^{-2}	●
Phenylpropanoid/ polyketide	Coumaric acid/der.	Methyl (2E)-3-(4-hydroxy…	293	208.0745	1.1×10^{-2}	●
	2-arylbenzofuran flavonoid	Egonol acetate	336	368.125	4.7×10^{-2}	
	Flavonoid O-glycoside	[(2S,4S,5R)-2-[(2S)-2-(3,4…	387	568.1588	1.4×10^{-2}	●
	Angular pyranocoumarin	-	322	388.1522	1.8×10^{-2}	●
-	Hydropyrimidine	-	522	270.1479	3.8×10^{-2}	
	-	(2Z)-4-{2,6-Dihydroxy-3-[(2E)...	337	546.1894	2.6×10^{-3}	●
	-	2-Acetyl-5-methoxyphenyl…	339	622.2111	1.3×10^{-2}	●
	-	(4aR,6S,7R,7aR)-4-Formyl-1…	239	522.1747	1.9×10^{-2}	●
	-	4,4'-{(2R,2'S,5R,5'S,6S,6'R)…	353	810.3092	4.9×10^{-2}	
	-	Cicerin 7-(6-malonylglucoside)…	302	578.1276	1.9×10^{-2}	
	-	(2R)-3-Hydroxy-3-methyl…	355	386.1371	3.1×10^{-2}	
Down-regulated in the WSS treatment - Conan						
Lignan	Lignan glycoside	Obtusifoside B	255	892.3011	2.9×10^{-2}	
Organoheterocyclic cmp.	Naphthopyranone	3-(9,10-Dihydroxy-7-methoxy…	163	476.1106	4.7×10^{-2}	
Phenylpropanoid/ polyketide	7-O-methylated flavonoid	Beilschmieflavonoid B	157	600.2352	3.8×10^{-2}	
	Macrolide	Integerrimine	277	335.1733	1.9×10^{-2}	●
Up-regulated in the WSS treatment - Conan						
Lipid/lipid-like cmp.	Xanthophyll	-	425	738.3865	4.5×10^{-3}	●
	Terpene glycoside	-	251	583.2268	3.5×10^{-2}	
Organic acid/der.	Oligopeptide	-	539	480.1098	2.9×10^{-2}	
Organoheterocyclic cmp.	8-prenylated xanthone	3,4,8-trihydroxy-2-methoxy…	279	342.1111	1.2×10^{-2}	
	Dihydropyridinecarboxylic acid	Adalate	232	346.1156	1.6×10^{-2}	
-	-	(1S,3aS,4Z,6S,7R,8S,8aS,11R…	247	598.2256	3.1×10^{-2}	
	-	2-(6a-Hydroxy-8,9-dimethoxy…	253	588.1851	1.3×10^{-2}	●
	-	3-[(5-Acetyl-4,6-dihydroxy…	208	400.1528	5.6×10^{-4}	●
	-	3-Hydroxy-2-{[(2E)-3-(4…	279	252.0642	4.6×10^{-2}	
	-	Alanyl-N-(6-amino-2-pyridinyl)…	264		3.6×10^{-2}	
Down-regulated in the WSS treatment - Denali						
Organic acid/der.	α amino acid/der.	Fosfocreatinine	18	193.026	4.2×10^{-2}	●
Phenylpropanoid/ polyketide	Macrolide	Integerrimine	277	335.1733	1.9×10^{-2}	●
Up-regulated in the WSS treatment - Denali						
Benzenoid	Benzylether	6-[(1S,2R)-1-Hydroxy-2-methoxy…	281	248.1053	4.9×10^{-2}	●

Lipid/lipid-like cmp.	Medium-chain fatty acid	-	280	310.1188	2.9×10^{-2}	
Nucleoside	Pyrimidine ribonucleoside monophosphate	-	23	542.1261	2.7×10^{-3}	●
Organoheterocyclic cmp.	Carbazole	(2'S,3'S,4R)-2,2"-Diimino-2'…	418	508.2338	1.8×10^{-2}	
	Dioxolopyran	(2,2,7,7-Tetramethyltetrahydro…	209	353.1146	1.1×10^{-2}	●
Phenylpropanoid/ polyketide	Flavonoid-7-O-glycoside	[(2R,3S,4R,5R,6S)-6-[(2S,3R,4S…	236	708.1907	10^{-4}	●
	7-O-methylated flavonoid	Beilschmieflavonoid B	157	600.2352	1.2×10^{-3}	●
-	-	3-[(5-Acetyl-4,6-dihydroxy…	208	400.1528	5.6×10^{-4}	
	-	Isopropyl 2-methoxyethyl…	269	418.1733	2.4×10^{-3}	●
Down-regulated in the WSS treatment - Reeder						
Benzenoid	Benzenesulfonamide	4-(3-amino-1H-indazol-5-yl)-N…	206	344.1302	2.6×10^{-2}	
Organic acid/der.	α amino acid/der.	(3R,6S)-3-Hydroxy-3-(3-hydroxy…	266	424.1388	2.1×10^{-2}	●
	α amino acid amide	Tert-butyl (2S)-2-carbamoyl…	66	228.1476	2.7×10^{-2}	
Organoheterocyclic cmp.	Porphyrin	-	280	648.2717	2.4×10^{-2}	●
	Phtalide	Salvianduline C	224	400.1531	3.7×10^{-2}	
	Hydroxypyrimidine	Thymine 5-methyluracil	63	126.0434	4×10^{-2}	
Phenylpropanoid/ polyketide	Coumaric acid/der.	Prenyl caffeate	256	248.1045	2.3×10^{-2}	●
-	-	Methyl {(1R,2R)-2-[(2Z)-5…	339	402.189	4.8×10^{-3}	●
Up-regulated in the WSS treatment - Reeder						
Organic oxygen cmp.	Monosaccharide phosphate	-	259	344.1343	4.1×10^{-2}	
-	-	(1aR,3aS,5aR,6S,9S,10aS,10bR)…	150	494.2884	4.1×10^{-2}	
	-	Athrombin K	242	308.1043	4.4×10^{-2}	

[a]Compounds were classified based on their regulation in the WSS treatment and superclass. Abbr… = abbreviated name, full names are available in Table S1; RT = retention time; *m*/*z* = mass-to-charge ratio; VIP = variable importance for the projection; der. = derivative; cmp. = compound.
[b]Superclasses correspond to the second highest level of ontology based on the ClassyFire algorithm.
[c]Subclasses correspond to the lowest level of ontology based on the ClassyFire algorithm.
[d]Compounds were assigned chemical names using the International Union of Pure and Applied Chemistry (IUPAC) nomenclature.
[e]Compound retention times were measured based on the time of elution from the chromatography column.
[f]mass-to-charge ratios were obtained from mass spectrometry output.
[g]*p* values were calculated from *t* tests (factors of treatment) and adjusted by a Benjamini–Hochberg correction.
[h]Metabolite with high variable importance of the projection (VIP) score in the OPLS model.

Table 6. Metabolites with high contribution to the Hatcher OPLS-DA model.[a]

#[b]	Superclass[c]	Sucblass[d]	Chemical name (abbr…)[e]	RT[f]	*m/z*[g]	*p* value[h]	VIP score[i]
			Down-regulated in the WSS treatment				
1	Alkaloid/der.	Harmala alkaloid	1-(9H-β-Carbolin-1…	204	422.1744	7.7×10^{-3}	1.58
2	Lipid/lipid-like cmp.	Hydroxysteroid	-	313	806.3362	1.3×10^{-2}	1.55
3	Organic oxygen cmp.	Aminocyclitol glycoside	(1R,2S,3S,4S,5S,6R)-2,3,4…	28	355.1485	5.1×10^{-3}	1.64
4	Organoheterocyclic cmp.	Indolizidine	-	300	434.1245	1.3×10^{-3}	1.74
5		6-aminopurine	9-(β-D-Erythro-pentofuran…	300	265.081	5.9×10^{-3}	1.62
6		Isoindolone	(2R,2'R,4'aS,6'R,8'aS)-7-Aceton…	264	441.2505	2.1×10^{-2}	1.5
7	-	-	4-{[(3R,4R)-4-(4-Hydroxy-3…	225	520.1936	7.9×10^{-3}	1.6
8		Benzoxazinoid glycoside	DIBOA-glucoside	106	343.0913	7.5×10^{-3}	1.58
			Up-regulated in the WSS treatment				
9	Benzenoid	Methoxyphenol	-	383	208.0743	8.6×10^{-3}	1.58
10		Tyrosol/der.	Propanoic acid 4-hydroxy…	240	194.0946	1.4×10^{-2}	1.55
11	Lignan	Neolignan	Methyl (2E)-3-(4-{[(1R,2R)-1,3…	285	404.1488	1.6×10^{-3}	1.72
12	Lipid/lipid-like cmp.	Guaianolide/der.	-	277	376.1521	1.9×10^{-2}	1.5
13		Fatty alcohol ester	[(2Z,8Z)-10-hydroxydeca-2,8…	337	204.0789	2.1×10^{-2}	1.49
14	Organic acid/der.	Tricarboxylic acid/der.	8-O-Acetyl-pumilin	343	416.1479	6×10^{-3}	1.64
15	Organic oxygen cmp.	O-glycosyl cmp.	β-D-Glucopyranose, 6-O-D…	312	372.1274	5.2×10^{-3}	1.63
16		Thioglycoside	Isopropyl 4-O-(β-D…	349	400.1404	1.6×10^{-2}	1.5
17	Phenylpropanoid/ polyketide	Coumaric acid/der.	Methyl (2E)-3-(4-hydroxy…	293	208.0745	1.1×10^{-2}	1.57
18		Flavonoid O-glycoside	[(2S,4S,5R)-2-[(2S)-2-(3,4…	387	568.1588	1.4×10^{-2}	1.53
19		Angular pyranocoumarin	-	322	388.1522	1.8×10^{-2}	1.51
20	Nucleoside	1-ribosyl-imidazole carboxamide	-	23	380.073	9.9×10^{-5}	1.86
21		Pyrimidine ribonucleoside monophosphate	-	23	542.1261	1.2×10^{-2}	1.54
22	Organoheterocyclic cmp.	Butenolide	-	333	208.0744	2×10^{-5}	1.89
23		Azaphilone	-	335	416.1479	4.8×10^{-3}	1.64
24		Phenylimidazole	3-Nitroso-2-phenylimidazo…	311	224.0703	6.2×10^{-3}	1.63
25		2-benzopyran	8-Hydroxy-5-(hydroxymethyl…	299	208.0745	7.4×10^{-3}	1.62
26		Pyranone/der.	4-Methoxy-5-methyl-6-oxo…	318	208.0745	1.3×10^{-2}	1.55
27	-	-	(2Z)-4-{2,6-Dihydroxy-3-[(2E)...	337	546.1894	2.6×10^{-3}	1.69
28		-	2-Acetyl-5-methoxyphenyl…	339	622.2111	1.3×10^{-2}	1.56
29		-	(4aR,6S,7R,7aR)-4-Formyl-1…	239	522.1747	1.9×10^{-2}	1.47

[a]Compounds were classified based on their regulation in the WSS treatment and superclass. Abbr… = abbreviated name, full names are available in Table S1; RT = retention time; *m/z* = mass-to-charge ratio; VIP = variable importance for the projection; der. = derivative; cmp. = compound.
[b]Bold numbers are used to reference compounds in the Results and Discussion sections.
[c]Superclasses correspond to the second highest level of ontology based on the ClassyFire algorithm.
[d]Subclasses correspond to the lowest level of ontology based on the ClassyFire algorithm.

[e]Compounds were assigned chemical names using the International Union of Pure and Applied Chemistry (IUPAC) nomenclature.
[f]Compound retention times were measured based on the time of elution from the chromatography column.
[g]mass-to-charge ratios were obtained from mass spectrometry output.
[h]*p* values were calculated from *t* tests (factors of treatment) and adjusted by a Benjamini–Hochberg correction.
[i]Variable importance of the projection (VIP) scores were calculated by summing the squares of the OPLS loading weights and weighted by the amount of sum of squares explained in each model component.

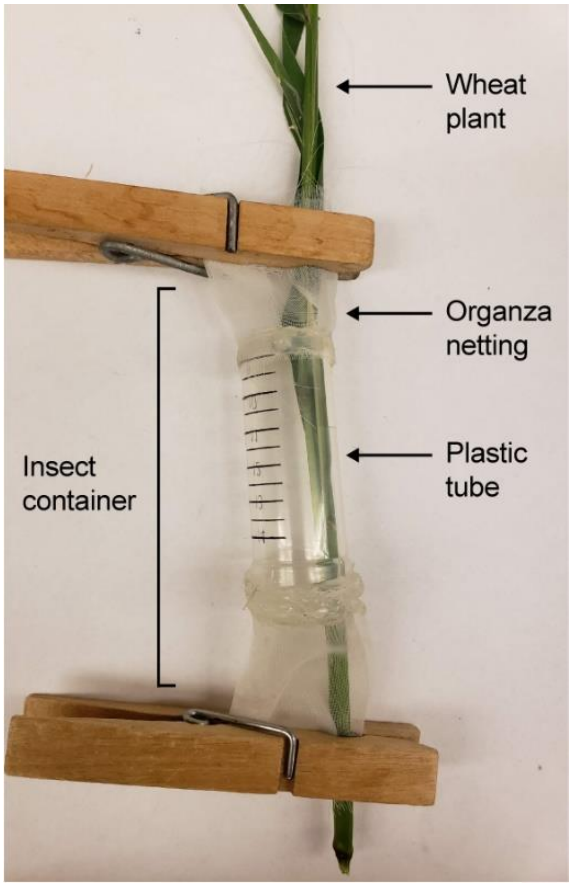

Figure 11. Insect container setup for the WSS infestation experiment. A 5 cm long × 1.5 cm diameter plastic tube with organza netting on both openings was placed around wheat stems to contain female WSS and control for oviposition location. Insects were left for egg deposition within the container area for ten days.

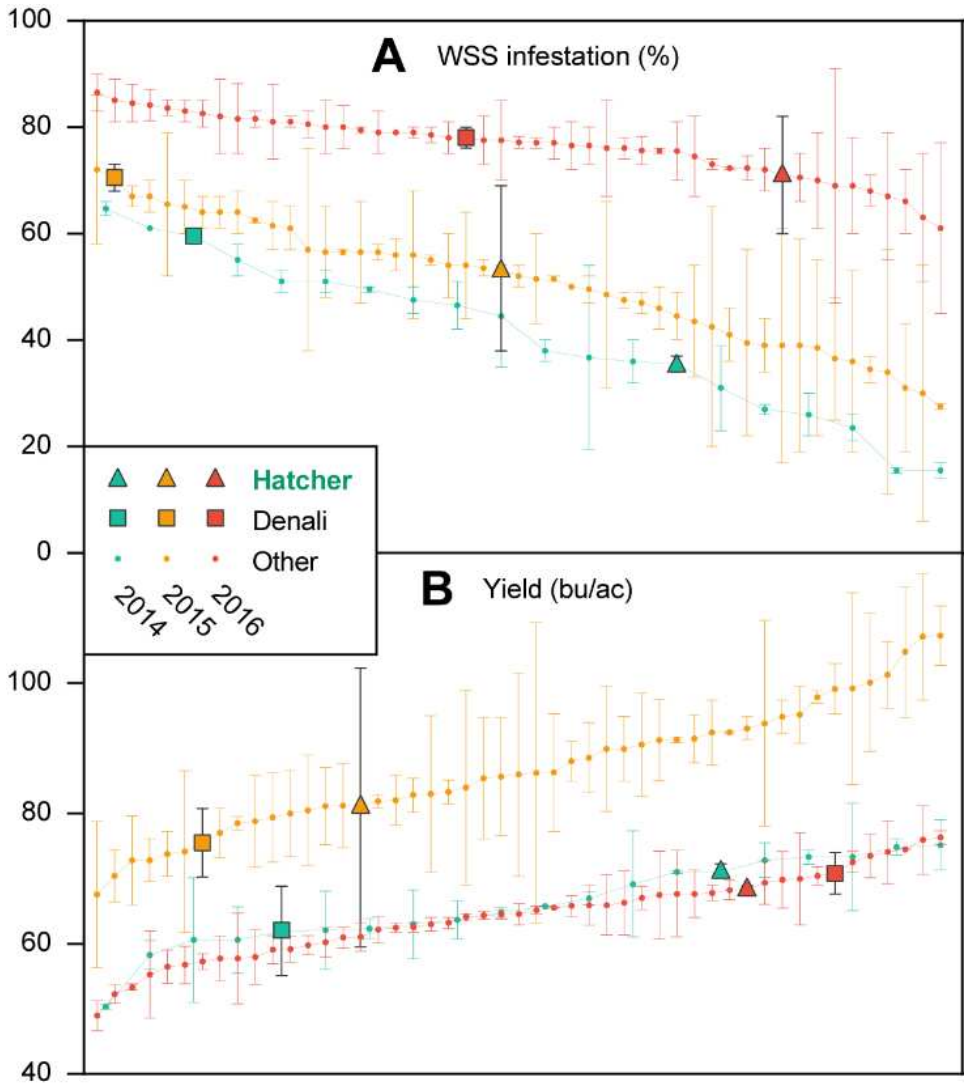

Figure 12. Distribution for WSS infestation and yield for several cultivars of hollow-stem winter wheat. A total of 20 cultivars were evaluated in 2014 and 50 in 2015 and 2016. **(A)** Sawfly infestation percentages of 91 cultivars from a three-year trial within an infested field. For each cultivar, infestation percentage was calculated as such: % = (infested tillers/total number of tillers) × 100. **(B)** Grain yield from the three-year trial expressed as bushels per acre (one bushel = 60 pounds of wheat). Symbols are used to denote the two winter wheat cultivars chosen for metabolic analysis due to consistent differences in infestation and yield: Denali (square; poor response to infestation), Hatcher (triangle; better response to infestation). Dots denote the mean value ± standard error of the mean between two plot replicates of a single cultivar (n = 2). Abbreviations/Notations: bu/ac = bushels per acre; % = percentage of wheat stems infested with WSS.

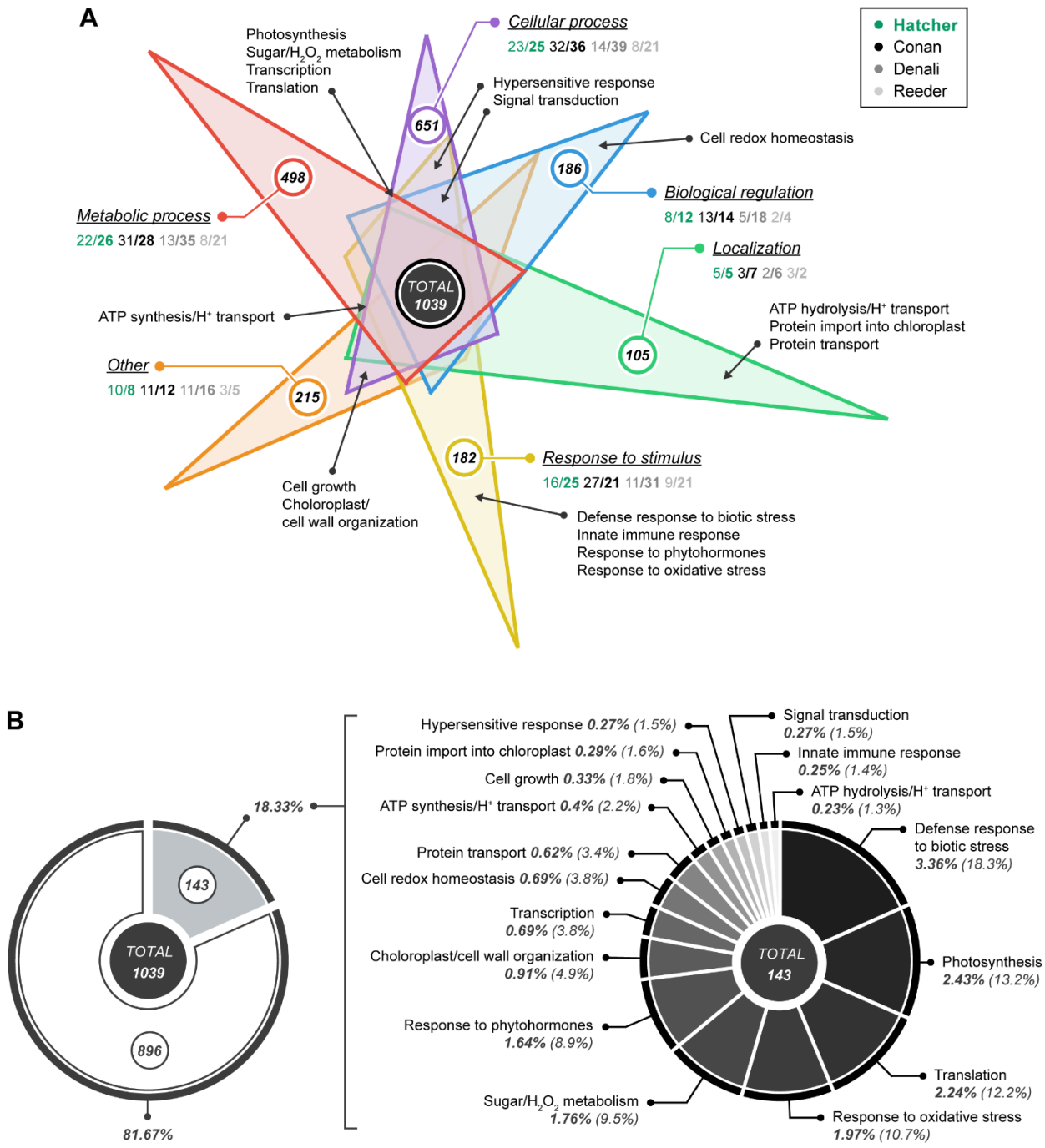

Figure 13. Overview of the wheat stem proteome. **(A)** Venn diagram showing major GO biological processes represented in the wheat stem proteome and overlap of proteins involved in more than one process. Numbers in colored circles represent unique low-level GO biological processes (e.g., 498 are related to metabolic processes), and the black circle is the total number of low-level GO biological processes from detected proteins. Low-level processes of biological relevance in the study and largely represented among detected proteins are indicated. As an example, hypersensitive response points towards the area of overlap between cellular process and response to stimuli because it is associated with both these biological processes. For

significant proteins in each cultivar, the number of occurrences for a given biological process is provided (1/**1** represents the number of occurrences in controls and infested plants, respectively). **(B)** Pie chart of highly represented GO biological processes. Each slice represents the percentage of occurrence for a given process, calculated as such: (# of occurrences of the biological process/Total # of occurrences across the dataset) × 100. Among the 1039 unique low-level processes identified, 143 were further grouped within 17 important processes, including photosynthesis and response to biotic stress. These accounted for 18.33% of occurrences across the proteomics dataset. Bold italic and regular italic numbers in the right panel represent occurrence within the whole dataset and within the 17 subgroups of processes, respectively.

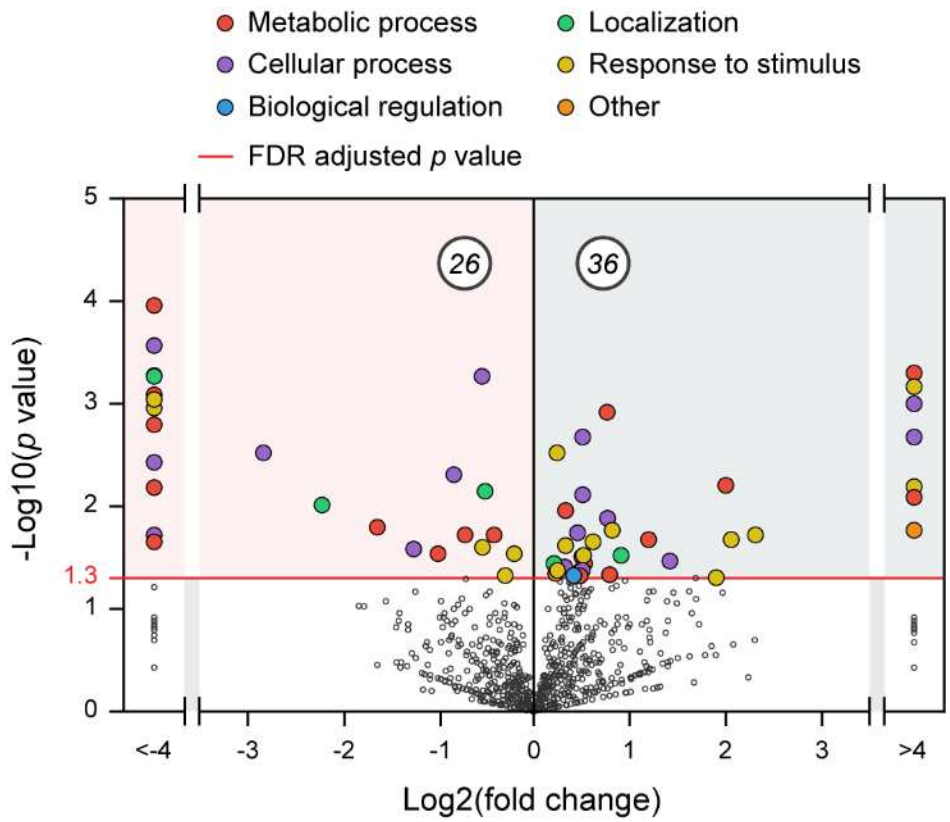

Figure 14. Stem proteins that varied due to infestation within Hatcher. The volcano plot shows significant down- (red square, left plot side) and up-regulated (blue square, right side) proteins after infestation, at the FDR adjusted $p < 0.05$ level for comparisons of $n = 3$ replicates per treatment. Circled numbers indicate the total number of down- and up-regulated proteins. Changes were calculated as such: (mean WSS)/(mean No WSS) treatments and centered around zero using $\log_2$ transformation. WSS corresponds to infested plants, No WSS represents controls. Dots in extended regions of the graph indicate presence/absence of the detected protein. Corresponding significant proteins are described in Table 4A.

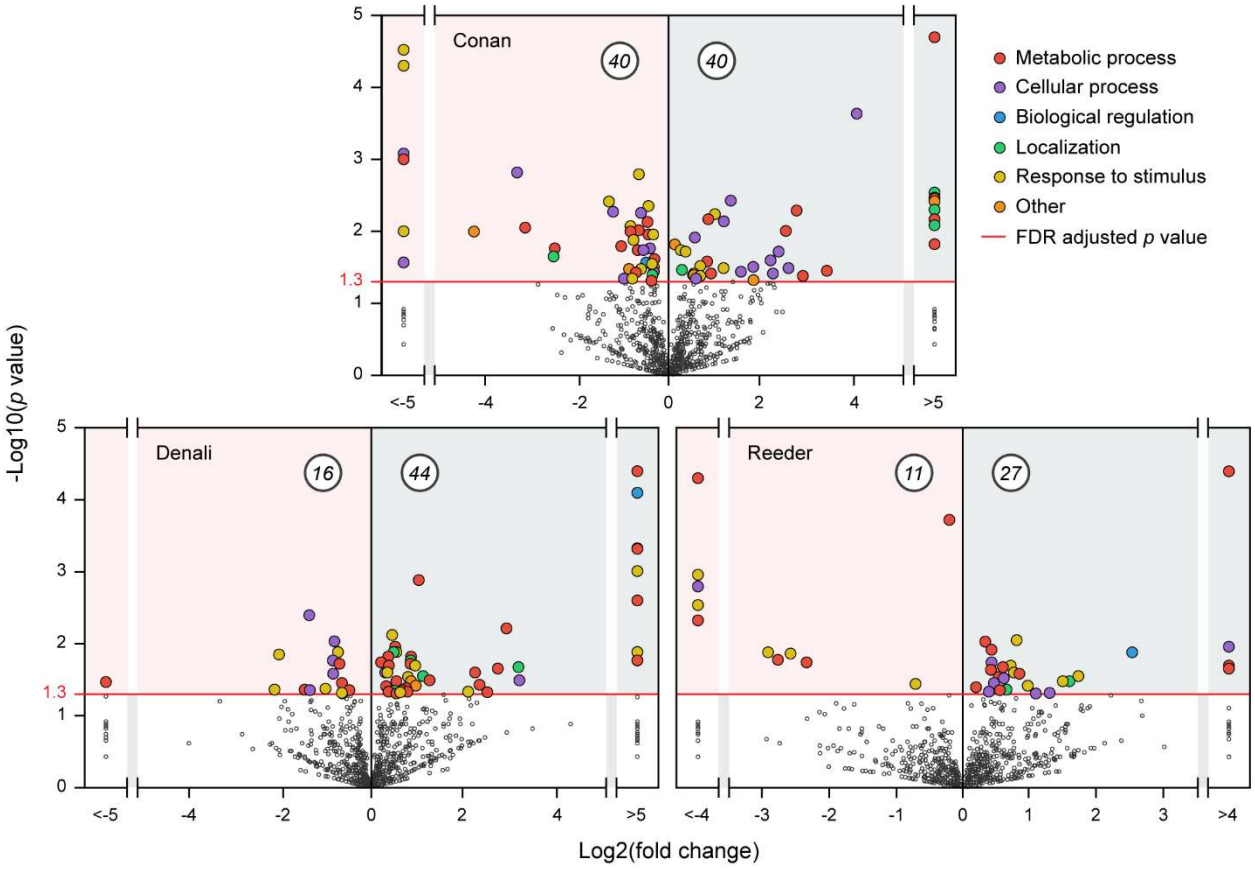

Figure 15. Stem proteins that varied due to infestation within Conan, Denali, and Reeder. Volcano plots show significant down- (red square, left plot side) and up-regulated (blue square, right side) proteins after infestation, at the FDR adjusted $p < 0.05$ level for comparisons of $n = 3$ replicates per treatment. Circled numbers indicate the total number of down- and up-regulated proteins. Changes were calculated as such: (mean WSS)/(mean No WSS) treatments and centered around zero using $\log_2$ transformation. WSS corresponds to infested plants, No WSS represents controls. Dots in extended regions of the graph indicate presence/absence of the detected protein.

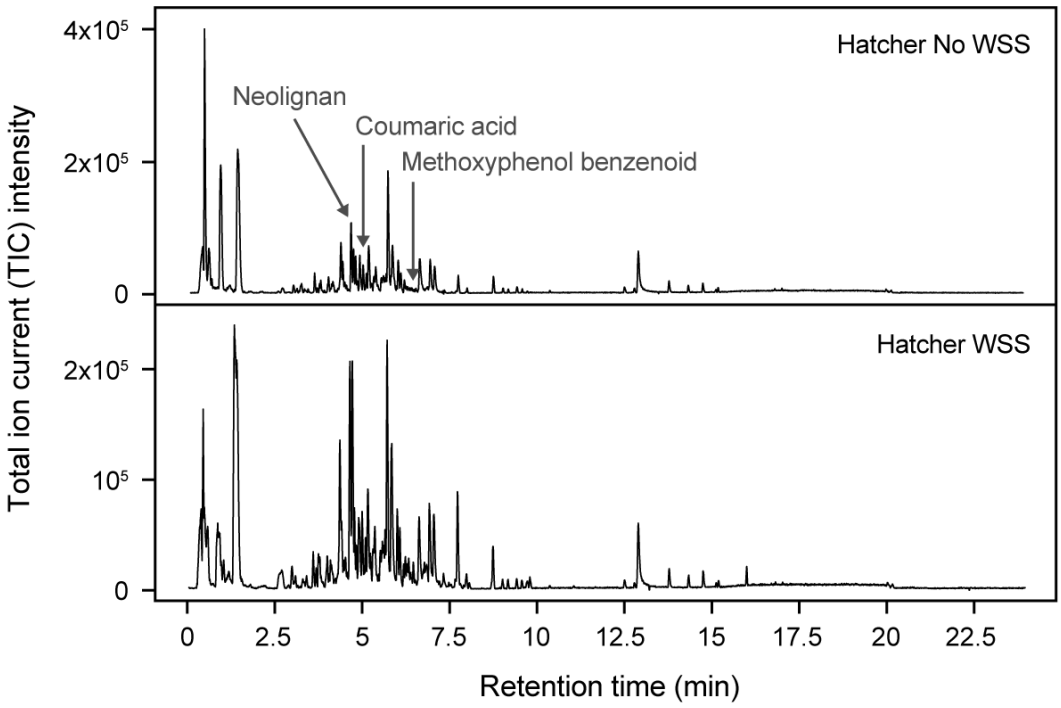

Figure 16. Example LC-MS chromatograms from the WSS resistant cultivar Hatcher. Chromatograms are provided to demonstrate global changes in metabolites observed in Hatcher, with and without WSS infestation. Arrows indicate peaks of example compounds that were more abundant in the WSS treatment, at the respective retention times. Abbreviations/Notations: cmps. = compounds; No WSS = control, no treatment; WSS = treatment, infestation.

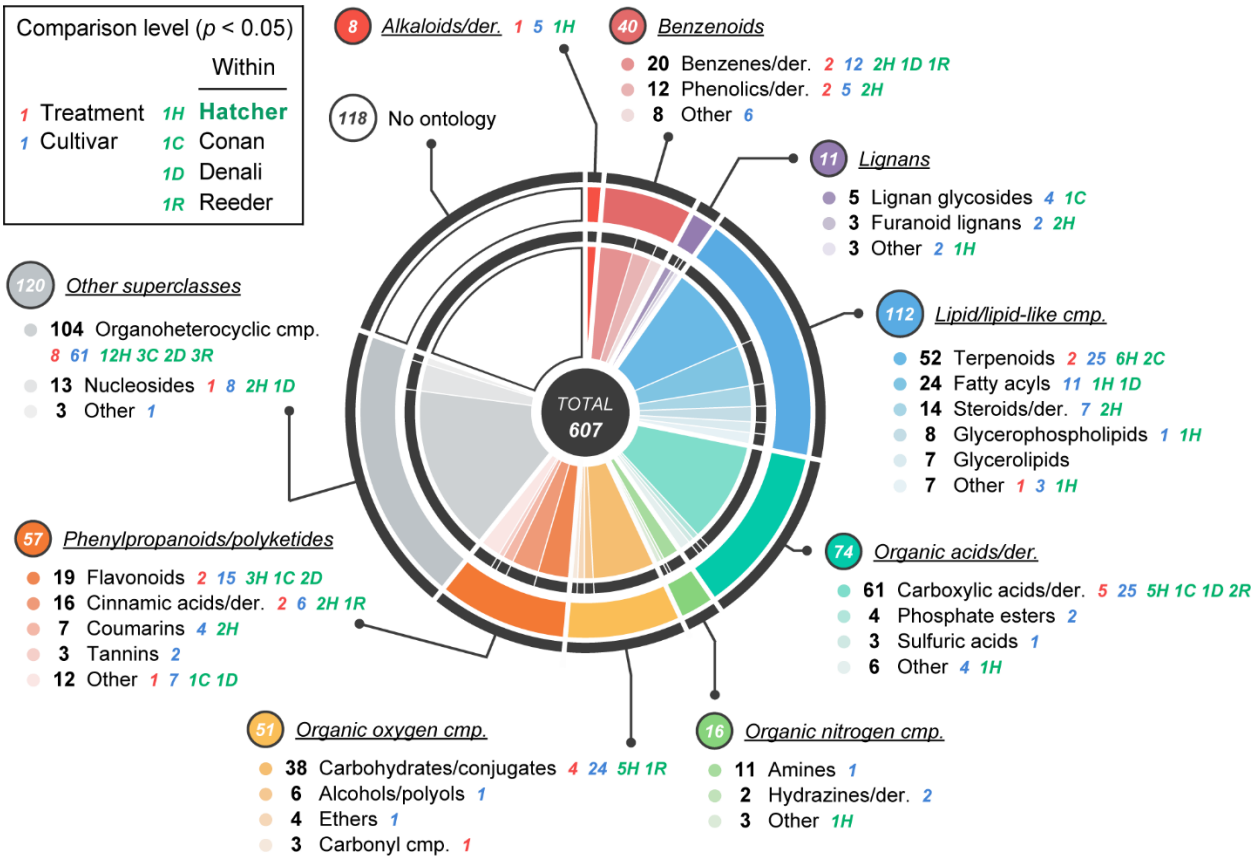

Figure 17. Overview of the wheat stem metabolome. Pie chart illustrating the distribution of metabolites, classified based on chemical ontology (Figure S1). A total of 607 metabolites (center of the chart) were annotated in the metabolomics data. Each colored segment represents the proportion of a chemical superclass among the 607 annotated compounds, and shades within a segment color indicate the proportion of each class/subclass within a superclass. Chemical superclasses included the benzenoids (light red segment), lignans (purple segment), and lipids (blue segment). Minor superclasses ("other") and metabolites with no ontology were reported in the grey and white segments, respectively. Number of metabolites within each superclass are indicated inside colored bubbles. Example classes/subclasses within each superclass are provided and their total amount is indicated as bold black numbers. Colored italic numbers indicate how many compounds were significant at the $p < 0.05$ level: red for treatment comparisons (No WSS/WSS), blue for cultivars, and green for comparisons of treatment within cultivar. Number of biological replicates varied based on the comparison: $n = 18–20$ for treatment comparisons, $n = 10$ for cultivar comparisons (except Denali for which $n = 8$), and $n = 5$ for treatment within cultivar (except Denali untreated plants for which $n = 3$). *t* tests and one-way ANOVAs were conducted between treatments and among cultivars, respectively. Abbreviations/Notations: der. = derivative; cmp. = compound; H = Hatcher; C = Conan; D = Denali; R = Reeder; No WSS = control, no treatment; WSS = treatment, infestation.

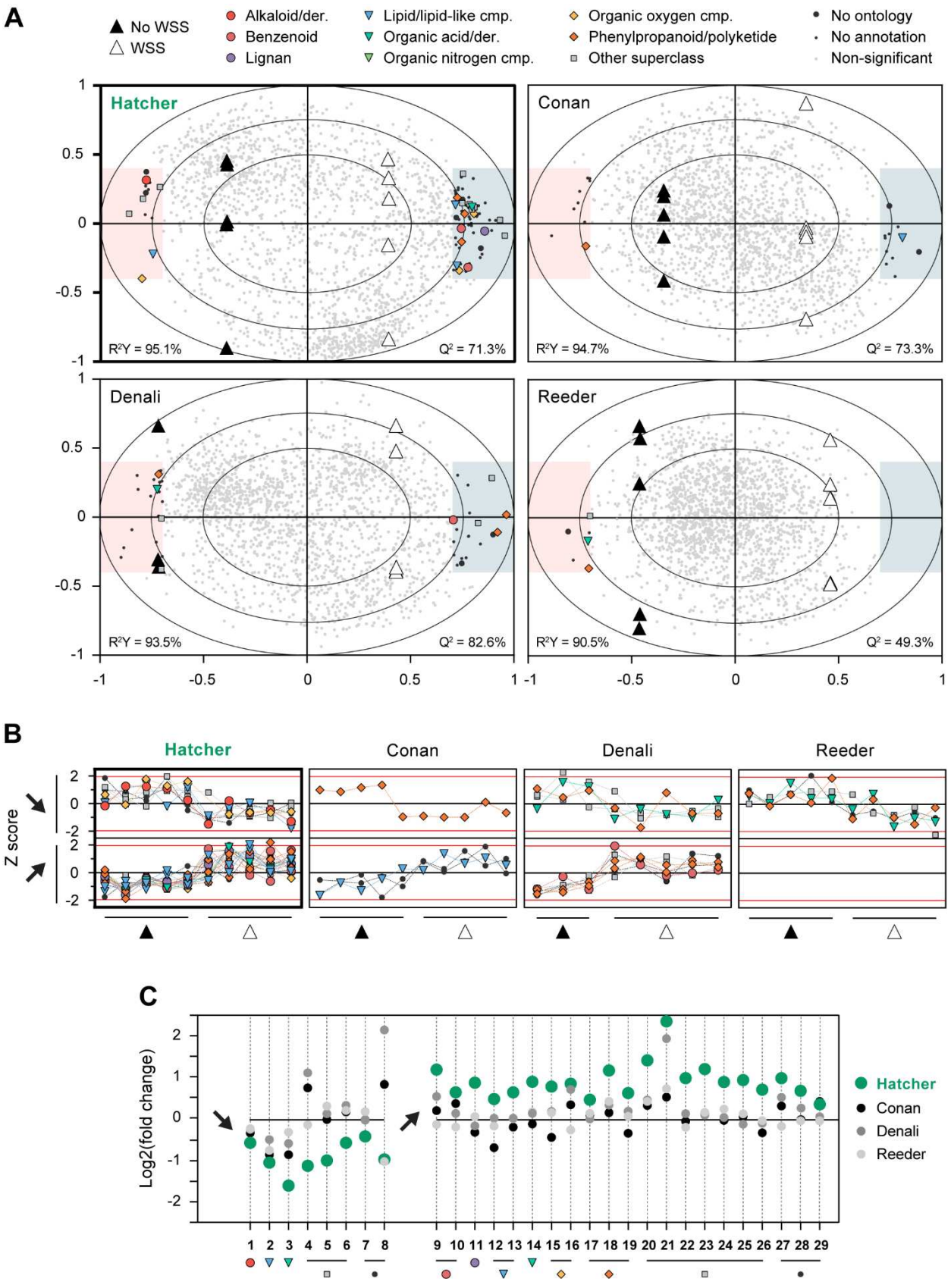
A
No WSS
WSS
Alkaloid/der.
Benzenoid
Lignan
Lipid/lipid-like cmp.
Organic acid/der.
Organic nitrogen cmp.
Organic oxygen cmp.
Phenylpropanoid/polyketide
Other superclass
No ontology
No annotation
Non-significant
Hatcher
R²Y = 95.1%
Q² = 71.3%
Conan
R²Y = 94.7%
Q² = 73.3%
Denali
R²Y = 93.5%
Q² = 82.6%
Reeder
R²Y = 90.5%
Q² = 49.3%
B
Hatcher
Conan
Denali
Reeder
Z score
C
Log2(fold change)
Hatcher
Conan
Denali
Reeder

Figure 18. Stem metabolites that varied due to infestation within each of the four wheat cultivars. **(A)** OPLS-DA biplot of correlation scaled scores (triangles) and loadings (all other shapes). Color shaded regions indicate metabolites that most strongly varied due to the WSS treatment: red corresponds to down-regulation, and blue means up-regulation of metabolites upon WSS infestation, respectively. **(B)** Variable trend plots show z scores of metabolite abundances within the red and blue shaded regions, and z-transformation was based on the mean abundance and standard deviation of the metabolite within each model. **(C)** Fold change plot of metabolite abundances between control and infested plants. X-axis numbers correspond to metabolites listed in Table 6, which are strongly varying in the Hatcher model. Fold changes were calculated as such: (mean WSS)/(mean No WSS) treatments and centered around zero using $\log_2$ transformation. WSS corresponds to infested plants, No WSS represents controls. For each cultivar, $n = 5$ replicates per treatment except Denali controls ($n = 3$ replicates). Abbreviations/Notations: No WSS = control, no treatment; WSS = treatment, infestation; der. = derivative; cmp. = compound; R^2Y = fraction of y (i.e., sample classes) variance explained by the model; Q^2 = cross-validation estimate for the predictive ability of the model; ↘ = down-regulated in the WSS treatment; ↗ = up-regulated in the WSS treatment.

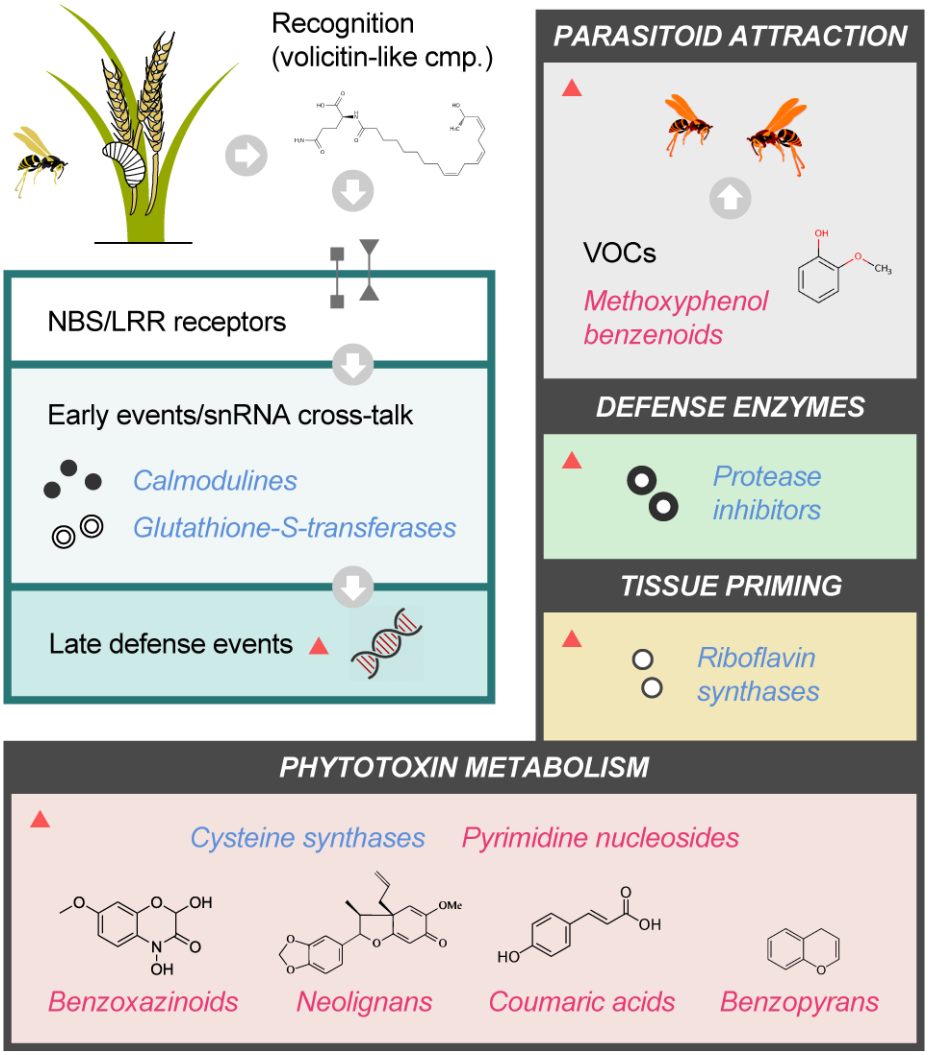

Figure 19. Putative model for the molecular basis of WSS resistance in Hatcher. Metabolites are indicated using their common name in italic pink and structural formula. Proteins are represented by their name in italic blue and schematic circles. Red triangles indicate late molecular defense mechanisms. Abbreviations: cmp. = compound; VOCs = volatile organic compounds.

REFERENCES

1. Beres, B.L.; Dosdall, L.M.; Weaver, D.K.; Cárcamo, H.A.; Spaner, D.M. Biology and integrated management of wheat stem sawfly and the need for continuing research. *Can. Entomol.* **2011**, *143*, 105–125.

2. Norton, E. Notes on North American Tenthredinidae, with descriptions of new species. *T. A. Entomol. Soc.* **1872**, *4*, 77–86.

3. Shanower, T.G.; Hoelmer, K.A. Biological control of wheat stem sawflies: past and future. *J. Agric. Urban Entomol.* **2004**, *21*, 197–221.

4. Lesieur, V.; Martin, J.F.; Weaver, D.K.; Hoelmer, K.A.; Smith, D.R.; Morrill, W.L.; Kadiri, N.; Peairs, F.B.; Cockrell, D.M.; Randolph, T.L.; Waters, D.K.; Bon, M.C. Phylogeography of the Wheat Stem Sawfly, *Cephus cinctus* Norton (Hymenoptera: Cephidae): implications for pest management. *PLoS One* **2016**, *11*, e0168370.

5. Cockrell, D.M.; Griffin-Nolan, R.J.; Rand, T.A.; Altilmisani, N.; Ode, P.J.; Peairs, F. Host plants of the wheat stem sawfly (Hymenoptera: Cephidae). *Environ. Entomol.* **2017**, *46*, 847–854.

6. Nilsen, K.T.; Clarke, J.M.; Beres, B.L.; Pozniak, C.J. Sowing density and cultivar effects on pith expression in solid-stemmed durum wheat. *Agron. J.* **2016**, *108*, 219–228.

7. Holmes, N.D. The effect of light on the resistance of hard red spring wheats to the wheat stem sawfly, *Cephus cinctus* (Hymenoptera: Cephidae). *Can. Entomol.* **1984**, *116*, 677–684.

8. Macedo, T.B.; Weaver, D.K.; Peterson, R.K.D. Photosynthesis in wheat at the grain filling stage is altered by larval wheat stem sawfly (Hymenoptera: Cephidae) injury and reduced water availability. *J. Entomol. Sci.* **2007**, *42*, 228–238.

9. Morrill, W.L.; Gabor, J.W.; Kushnak, G.D. Wheat stem sawfly (Hymenoptera: Cephidae): damage and detection. *J. Econ. Entomol.* **1992**, *85*, 2413–2417.

10. Weiss, M.J.; Morrill, W.L. Wheat stem sawfly (Hymenoptera: Cephidae) revisited. *Am. Entomol.* **1992**, *38*, 241–245.

11. Sherman, J.D.; Blake, N.K.; Martin, J.M.; Kephart, K.D.; Smith, J.; Clark, D.R.; Hofland, M.L.; Weaver, D.K.; Lanning, S.P.; Heo, H.-Y.; Pumphrey, M.; Chen, J.; Talbert, L.E. Agronomic impact of a stem solidness gene in near-isogenic lines of wheat. *Crop Sci.* **2015**, *55*, 514–520.

12. Szczepaniec, A.; Glover, K.D.; Berzonsky, W. Impact of solid and hollow varieties of winter and spring wheat on severity of wheat stem sawfly (Hymenoptera: Cephidae) infestations and yield and quality of grain. *J. Econ. Entomol.* **2015**, *108*, 2316–2323.

13. Cook, J.P.; Wichman, D.M.; Martin, J.M.; Bruckner, P.L.; Talbert, L.E. Identification of microsatellite markers associated with a stem solidness locus in wheat. *Crop Sci.* **2004**, *44*, 1397–1402.

14. Varella, A.C.; Talbert, L.E.; Hofland, M.L.; Buteler, M.; Sherman, J.D.; Blake, N.K.; Heo, H.-Y.; Martin, J.M.; Weaver, D.K. Alleles at a quantitative trait locus for stem solidness in wheat affect

temporal patterns of pith expression and level of resistance to the wheat stem sawfly. *Plant Breeding* **2016**, *135*, 546–551.

15. War, A.R.; Paulraj, M.G.; Ahmad, T.; Buhroo, A.A.; Hussain, B.; Ignacimuthu, S.; Sharma, H.C. Mechanisms of plant defense against insect herbivores. *Plant Signal Behav.* **2012**, *7*, 1306–1320.

16. Baldwin, I.T.; Halitschke, R.; Kessler, A.; Schittko, U. Merging molecular and ecological approaches in plant–insect interactions. *Curr. Opin. Plant Biol.* **2001**, *4*, 351–358.

17. Stotz, H.U.; Kroymann, J.; Mitchell-Olds, T. Plant–insect interactions. *Curr. Opin. Plant Biol.* **1999**, *2*, 268–272.

18. Fürstenberg-Hägg, J.; Zagrobelny, M.; Bak, S. Plant defense against insect herbivores. *Int. J. Mol. Sci.* **2013**, *14*, 10242–10297.

19. Banfield, M.J. Perturbation of host ubiquitin systems by plant pathogen/pest effector proteins. *Cell. Microbiol.* **2015**, *17*, 18–25.

20. Dubreuil-Maurizi, C.; Poinssot, B. Role of glutathione in plant signaling under biotic stress. *Plant Signal Behav.* **2012**, *7*, 210–212.

21. Vandenborre, G.; Smagghe, G.; Van Damme, E.J. Plant lectins as defense proteins against phytophagous insects. *Phytochemistry* **2011**, *72*, 1538–1550.

22. Lefebvre, B.; Timmers, T.; Mbengue, M.; Moreau, S.; Herve, C.; Toth, K.; Bittencourt-Silvestre, J.; Klaus, D.; Deslandes, L.; Godiard, L.; Murray, J.D.; Udvardi, M.K.; Raffaele, S.; Mongrand, S.; Cullimore, J.; Gamas, P.; Niebel, A.; Ott, T. A remorin protein interacts with symbiotic receptors and regulates bacterial infection. *Proc. Natl. Acad. Sci. USA* **2010**, *107*, 2343–2348.

23. Wouters, F.C.; Blanchette, B.; Gershenzon, J.; Vassão, D.G. Plant defense and herbivore counter-defense: benzoxazinoids and insect herbivores. *Phytochem. Rev.* **2016**, *15*, 1127–1151.

24. Cagirici, H.B.; Biyiklioglu, S.; Budak, H. Assembly and annotation of transcriptome provided evidence of miRNA mobility between wheat and wheat stem sawfly. *Front. Plant Sci.* **2017**, *8*, 1653.

25. Tzin, V.; Hojo, Y.; Strickler, S.R.; Bartsch, L.J.; Archer, C.M.; Ahern, K.R.; Zhou, S.; Christensen, S.A.; Galis, I.; Mueller, L.A.; Jander, G. Rapid defense responses in maize leaves induced by *Spodoptera exigua* caterpillar feeding. *J. Exp. Bot.* **2017**, *68*, 4709–4723.

26. Vélez-Bermúdez, I.C.; Salazar-Henao, J.E.; Fornalé, S.; López-Vidriero, I.; Franco-Zorrilla, J.M.; Grotewold, E.; Gray, J.; Solano, R.; Schmidt, W.; Pagés, M.; Riera, M.; Caparros-Ruiz, D. A MYB/ZML complex regulates wound-induced lignin genes in maize. *Plant Cell* **2015**, *27*, 3245–3259.

27. Kaur, H.; Salh, P.K.; Singh, B. Role of defense enzymes and phenolics in resistance of wheat crop (*Triticum aestivum* L.) towards aphid complex. *J. Plant Interact.* **2017**, *12*, 304–311.

28. Biyiklioglu, S.; Alptekin, B.; Akpinar, B.A.; Varella, A.C.; Hofland, M.L.; Weaver, D.K.; Bothner, B.; Budak, H. A large-scale multiomics analysis of wheat stem solidness and the wheat stem sawfly feeding response, and syntenic associations in barley, *Brachypodium*, and rice. *Funct. Integr. Genomics* **2018**, *18*, 241–259.

29. Talbert, L.E.; Sherman, J.D.; Hofland, M.L.; Lanning, S.P.; Blake, N.K.; Grabbe, R.; Lamb, P.F.; Martin, J.M.; Weaver, D.K.; Bürstmayr, H. Resistance to *Cephus cinctus* Norton, the wheat stem sawfly, in a recombinant inbred line population of wheat derived from two resistance sources. *Plant Breeding* **2014**, *133*, 427–432.

30. Varella, A.C.; Weaver, D.K.; Peterson, R.K.; Sherman, J.D.; Hofland, M.L.; Blake, N.K.; Martin, J.M.; Talbert, L.E. Host plant quantitative trait loci affect specific behavioral sequences in oviposition by a stem-mining insect. *Theor. Appl. Genet.* **2017**, *130*, 187–197.

31. Haley, S.D.; Quick, J.S.; Johnson, J.J.; Peairs, F.B.; Stromberger, A.; Clayshulte, S.R.; Clifford, B.L.; Rudolf, J.B.; Seabourn, B.W.; Chung, O.K.; Jin, Y.; Kolmer, J. Registration of 'Hatcher' wheat. *Crop Sci.* **2005**, *45*, 2654–2656.

32. Haley, S.D.; Johnson, J.J.; Peairs, F.B.; Stromberger, J.A.; Hudson, E.E.; Seifert, S.A.; Kottke, R.A.; Valdez, V.A.; Rudolph, J.B.; Martin, T.J.; Bai, G.; Chen, X.; Bowden, R.L.; Jin, Y.; Kolmer, J.A.; Chen, M.-S.; Seabourn, B.W. Registration of 'Denali' wheat. *J. Plant Regist.* **2012**, *6*, 311–314.

33. Holmes, N.D. The effect of the wheat stem sawfly, *Cephus cinctus* (Hymenoptera: Cephidae), on the yield and quality of wheat. *Can. Entomol.* **1977**, *109*, 1591–1598.

34. Zadoks, J.C.; Chang, T.T.; Konzak, C.F. A decimal code for the growth stages of cereals. *Weed Res.* **1974**, *14*, 415–421.

35. Schauer, K.L.; Freund, D.M.; Prenni, J.E.; Curthoys, N.P. Proteomic profiling and pathway analysis of the response of rat renal proximal convoluted tubules to metabolic acidosis. *Am. J. Physiol. Renal Physiol.* **2013**, *305*, 628–640.

36. Scopes, R.K. Measurement of protein by spectrophotometry at 205 nm. *Anal. Biochem.* **1974**, *59*, 277–282.

37. Bereman, M.S.; Beri, J.; Sharma, V.; Nathe, C.; Eckels, J.; MacLean, B.; MacCoss, M.J. An automated pipeline to monitor system performance in liquid chromatography-tandem mass spectrometry proteomic experiments. *J. Proteome Res.* **2016**, *15*, 4763–4769.

38. Keller, A.; Nesvizhskii, A.I.; Kolker, E.; Aebersold, R. Empirical statistical model to estimate the accuracy of peptide identifications. *Anal. Chem.* **2002**, *74*, 5383–5392.

39. Searle, B.C.; Turner, M.; Nesvizhskii, A.I. Improving sensitivity by probabilistically combining results from multiple MS/MS search methodologies. *J. Proteome Res.* **2008**, *7*, 245–253.

40. Käll, L.; Storey, J.D.; MacCoss, M.J.; Noble, W.S. Assigning significance to peptides identified by tandem mass spectrometry using decoy databases. *J. Proteome Res.* **2008**, *7*, 29–34.

41. Nesvizhskii, A.I.; Keller, A.; Kolker, E.; Aebersold, R. A statistical model for identifying proteins by tandem mass spectrometry. *Anal. Chem.* **2003**, *75*, 4646–4658.

42. Wheat Protein Database. Available online: http://wheatproteome.org/.

43. UniProt database. Available online: http://www.uniprot.org/.

44. Broeckling, C.D.; Prenni, J.E. Stacked injections of biphasic extractions for improved metabolomic coverage and sample throughput. *Anal. Chem.* **2018**, *90*, 1147–1153.

45. Smith, C.A.; Want, E.J.; O'Maille, G.; Abagyan, R.; Siuzdak, G. XCMS: processing mass spectrometry data for metabolite profiling using nonlinear peak alignment, matching, and identification. *Anal. Chem.* **2006**, *78*, 779–787.

46. R Core Team. R: a language and environment for statistical computing. **2017**, R Foundation for Statistical Computing, Vienna, Austria (https://www.R-project.org/).

47. Broeckling, C.D.; Afsar, F.A.; Neumann, S.; Ben-Hur, A.; Prenni, J.E. RAMClust: a novel feature clustering method enables spectral-matching-based annotation for metabolomics data. *Anal. Chem.* **2014**, *86*, 6812–6817.

48. METLIN database. Available online: http://metlin.scripps.edu/.

49. Tautenhahn, R.; Cho, K.; Uritboonthai, W.; Zhu, Z.; Patti, G.J.; Siuzdak, G. An accelerated workflow for untargeted metabolomics using the METLIN database. *Nat. Biotechnol.* **2012**, *30*, 826–828.

50. Human Metabolome Database. Available online: http://www.hmdb.ca/.

51. Tsugawa, H.; Kind, T.; Nakabayashi, R.; Yukihira, D.; Tanaka, W.; Cajka, T.; Saito, K.; Fiehn, O.; Arita, M. Hydrogen rearrangement rules: computational MS/MS fragmentation and structure elucidation using MS-FINDER software. *Anal. Chem.* **2016**, *88*, 7946–7958.

52. Lai, Z.; Tsugawa, H.; Wohlgemuth, G.; Mehta, S.; Mueller, M.; Zheng, Y.; Ogiwara, A.; Meissen, J.; Showalter, M.; Takeuchi, K.; Kind, T.; Beal, P.; Arita, M.; Fiehn, O. Identifying metabolites by integrating metabolome databases with mass spectrometry cheminformatics. *Nat. Methods* **2018**, *15*, 53–56.

53. Feunang, Y.D.; Eisner, R.; Knox, C.; Chepelev, L.; Hastings, J.; Owen, G.; Fahy, E.; Steinbeck, C.; Subramanian, S.; Bolton, E.; Greiner, R.; Wishart, D.S. ClassyFire: automated chemical classification with a comprehensive, computable taxonomy. *J. Cheminform.* **2016**, *8*, 61.

54. Sumner, L.W.; Amberg, A.; Barrett, D.; Beale, M.H.; Beger, R.; Daykin, C.A.; Fan, T.W.; Fiehn, O.; Goodacre, R.; Griffin, J.L.; Hankemeier, T.; Hardy, N.; Harnly, J.; Higashi, R.; Kopka, J.; Lane, A.N.; Lindon, J.C.; Marriott, P.; Nicholls, A.W.; Reily, M.D.; Thaden, J.J.; Viant, M.R. Proposed minimum reporting standards for chemical analysis. *Metabolomics* **2007**, *3*, 211–221.

55. Benjamini, Y.; Hochberg, Y. Controlling the false discovery rate: a practical and powerful approach to multiple testing. *J. R. Stat. Soc.* **1995**, *57*, 289–300.

56. Gene Ontology and GO Annotations website. Available online: http://www.ebi.ac.uk/QuickGO/term/.

57. Nebraska crop improvement association website. Available online: http://www.necrop.org/.

58. Bayram, A.; Tonğa, A. *cis*-jasmone treatments affect pests and beneficial insects of wheat (*Triticum aestivum* L.): the influence of doses and plant growth stages. *Crop Prot.* **2018**, *105*, 70–79.

59. Kärkönen, A.; Murigneux, A.; Martinant, J.-P.; Pepey, E.; Tatout, C.; Dudley, B.J.; Fry, S.C. UDP-glucose dehydrogenases of maize: a role in cell wall pentose biosynthesis. *Biochem. J.* **2005**, *391*, 409–415.

60. Kawasaki, T.; Koita, H.; Nakatsubo, T.; Hasegawa, K.; Wakabayashi, K.; Takahashi, H.; Umemura, K.; Umezawa, T.; Shimamoto, K. Cinnamoyl-CoA reductase, a key enzyme in lignin

biosynthesis, is an effector of small GTPase Rac in defense signaling in rice. *Proc. Natl. Acad. Sci. USA* **2006**, *103*, 230–235.

61. Al-Whaibi, M.H. Plant heat-shock proteins: a mini review. *JKSUS* **2011**, *23*, 139–150.

62. Barre, A.; Bourne, Y.; Van Damme, E.J.M.; Peumans, W.J.; Rougé, P. Mannose-binding plant lectins: different structural scaffolds for a common sugar-recognition process. *Biochimie* **2001**, *83*, 645–651.

63. Yamauchi, Y.; Hasegawa, A.; Mizutani, M.; Sugimoto, Y. Chloroplastic NADPH-dependent alkenal/one oxidoreductase contributes to the detoxification of reactive carbonyls produced under oxidative stress. *FEBS Lett.* **2012**, *586*, 1208–1213.

64. Álvarez, C.; Bermúdez, M.A.; Romero, L.C.; Gotor, C.; García, I. Cysteine homeostasis plays an essential role in plant immunity. *New Phytol.* **2012**, *193*, 165–177.

65. Zhang, S.; Yang, X.; Sun, M.; Sun, F.; Deng, S.; Dong, H. Riboflavin-induced priming for pathogen defense in *Arabidopsis thaliana*. *J. Integr. Plant Biol.* **2009**, *51*, 167–174.

66. Ranty, B.; Aldon, D.; Galaud, J.-P. Plant calmodulins and calmodulin-related proteins: multifaceted relays to decode calcium signals. *Plant Signal Behav.* **2006**, *1*, 96–104.

67. Anderson, V.A.; Haley, S.D.; Peairs, F.B.; van Eck, L.; Leach, J.E.; Lapitan, N.L. Virus-induced gene silencing suggests (1,3;1,4)-β-glucanase is a susceptibility factor in the compatible Russian wheat aphid-wheat interaction. *Mol. Plant Microbe Interact.* **2014**, *27*, 913–922.

68. Moreira, X.; Lundborg, L.; Zas, R.; Carrillo-Gavilán, A.; Borg-Karlson, A.-K.; Sampedro, L. Inducibility of chemical defences by two chewing insect herbivores in pine trees is specific to targeted plant tissue, particular herbivore and defensive trait. *Phytochemistry* **2013**, *94*, 113–122.

69. Huot, B.; Yao, J.; Montgomery, B.L.; He, S.Y. Growth-defense tradeoffs in plants: a balancing act to optimize fitness. *Mol. Plant* **2014**, *7*, 1267–1287.

70. Lu, H.; Rate, D.N.; Song, J.T.; Greenberg, J.T. ACD6, a novel ankyrin protein, is a regulator and an effector of salicylic acid signaling in the *Arabidopsis* defense response. *Plant Cell* **2003**, *15*, 2408–2420.

71. Frey, M.; Schullehner, K.; Dick, R.; Fiesselmann, A.; Gierl, A. Benzoxazinoid biosynthesis, a model for evolution of secondary metabolic pathways in plants. *Phytochemistry* **2009**, *70*, 1645–1651.

72. Ramachandran, R.; Norris, D.M.; Phillips, J.K.; Phillips, T.W. Volatiles mediating plant-herbivore-natural enemy interactions: soybean looper frass volatiles, 3-octanone and guaiacol, as kairomones for the parasitoid *Microplitis demolitor*. *J. Agric. Food Chem.* **1991**, *39*, 2310–2317.

73. Nitao, J.K.; Johnson, K.S.; Scriber, J.M.; Nair, M.G. *Magnolia virginiana* neolignan compounds as chemical barriers to swallowtail butterfly host use. *J. Chem. Ecol.* **1992**, *18*, 1661–1671.

74. Sambangi, P.; Rani, P.U. Physiological effects of resveratrol and coumaric acid on two major groundnut pests and their egg parasitoid behavior. *Arch. Insect Biochem. Physiol.* **2016**, *91*, 230–245.

75. Sangeetha, S.; Sarada, D.V. Phenyl derivative of pyranocoumarin precludes *Fusarium oxysporum* f.sp. *Lycopersici* infection in *Lycopersicon esculentum* via induction of enzymes of the phenylpropanoid pathway. *Appl. Biochem. Biotechnol.* **2015**, *175*, 1168–1180.

76. Fung, S.Y.; Herrebout, W.M.; Verpoorte, R.; Fischer, F.C. Butenolides in small ermine moths, *Yponomeuta* spp. (Lepidoptera: Yponomeutidae), and spindle-tree, *Euonymus europaeus* (Celestraceae). *J. Chem. Ecol.* **1988**, *14*, 1099–1111.

77. Wang, W.-X.; Kusari, S.; Laatsch, H.; Golz, C.; Kusari, P.; Strohmann, C.; Kayser, O.; Spiteller, M. Antibacterial azaphilones from an endophytic fungus, *Colletotrichum* sp. BS4. *J. Nat. Prod.* **2016**, *79*, 704−710.

78. de Matos Nunes, J.; Bertodo, L.O.O.; da Rosa, L.M.G.; Von Poser, G.L.; Rech, S.B. Stress induction of valuable secondary metabolites in *Hypericum polyanthemum* acclimatized plants. *S. Afr. J. Bot.* **2014**, *94*, 182–189.

79. Kafer, C.; Zhou, L.; Santoso, D.; Guirgis, A.; Weers, B.; Park, S.; Thornburg, R. Regulation fo pyrimidine metabolism in plants. *Front. Biosci.* **2004**, *9*, 1611–1625.

80. Piesik, D.; Weaver, D.K.; Runyon, J.B.; Buteler, M.; Peck, G.E.; Morrill, W.L. Behavioural responses of wheat stem sawflies to wheat volatiles. *Agr. Forest Entomol.* **2008**, *10*, 245–253.

81. Weaver, D.K.; Buteler, M.; Hofland, M.L.; Runyon, J.B.; Nansen, C.; Talbert, L.E.; Lamb, P.; Carlson, G.R. Cultivar preferences of ovipositing wheat stem sawflies as influenced by the amount of volatile attractant. *J. Econ. Entomol.* **2009**, *102*, 1009–1017.

82. Buteler, M.; Weaver, D.K.; Peterson, R.K.D. Oviposition behavior of the wheat stem sawfly when encountering plants infested with cryptic conspecifics. *Environ. Entomol.* **2009**, *38*, 1707–1715.

83. Schröder, R.; Cristescu, S.M.; Harren, F.J.; Hilker, M. Reduction of ethylene emission from Scots pine elicited by insect egg secretion. *J. Exp. Bot.* **2007**, *58*, 1835–1842.

84. Hogenhout, S.A.; Bos, J.I. Effector proteins that modulate plant–insect interactions. *Curr. Opin. Plant Biol.* **2011**, *14*, 422–428.

85. Acevedo, F.E.; Rivera-Vega, L.J.; Chung, S.H.; Ray, S.; Felton, G.W. Cues from chewing insects — the intersection of DAMPs, HAMPs, MAMPs and effectors. *Curr. Opin. Plant Biol.* **2015**, *26*, 80–86.

86. Alborn, H.T.; Jones, T.H.; Stenhagen, G.S.; Tumlinson, J.H. Identification and synthesis of volicitin and related components. *J. Chem. Ecol.* **2000**, *26*, 203–220.

87. Uauy, C.; Wulff, B.B.H.; Dubcovsky, J. Combining traditional mutagenesis with new high-throughput sequencing and genome editing to reveal hidden variation in polyploid wheat. *Annu. Rev. Genet.* **2017**, *51*, 435–454.

CHAPTER 4 – CONCLUSION AND FUTURE PERSPECTIVES

4.1. Conclusion

The advanced mass spectrometry-based methods used here enabled the understanding of passive and active defense of wheat to a broad range of stresses, including chewing pest pressure. Non-targeted GC-MS metabolomics data demonstrated that variation in cuticular wax composition and crystal microstructures related to plant defense exists among tissues and cultivars of common wheat. Leaf surfaces were characterized by high levels of alcohols and stem surfaces showed higher content in β-diketones. While most of the detected compounds were equally distributed among cultivars, two Conan wax alcohols were higher in content than the other cultivars. Further, SEM imaging provided insights in wheat wax microstructural topography and allowed for the identification of two types of epicuticular wax crystals in wheat: platelets and tubules. Taken together, these results indicate that Conan epicuticular features potentially contribute to stress resistance.

Mass spectrometry-based proteomics and metabolomics data demonstrated active defense responses to insect infestation in the hollow-stemmed and WSS resistant cultivar Hatcher. Hatcher up-regulated proteins upon WSS feeding included detoxification, Ca^{2+} flux, proteinase inhibitor, and systemic signaling activities. Increased metabolites upon infestation included anti-herbivory compounds and associated precursors. Semi-solid-stemmed and resistant Conan displayed a different set of protein and metabolic changes after exposure to WSS, suggesting that pith expression is the major means of resistance in this cultivar and Hatcher resistance relies upon alternative molecular mechanisms that have been largely unexplored.

Two cultivars that have been shown for high yield performances under abiotic and/or biotic pressure, Conan and Hatcher, were assayed in this research and displayed unique combinations of proteins and metabolites with demonstrated roles in defense to stress.

4.2. Limitations

Omics datasets described in this manuscript were relatively rich and contained numerous proteins and metabolites that varied between cultivars of wheat and that have been described as pest resistance facilitators. However, the molecular approaches used here rely upon instruments that allow for the detection of a limited set of proteins and metabolites. Compound databases as well as annotation algorithms are upgraded on a regular basis, however, none provide complete accuracy of annotation. All proteins and metabolites detected in our research were annotated with high confidence using advanced software, yet, it is critical to acknowledge the possibility of erroneous annotation (e.g., mismatch with a compound or protein with very close structure and chemical properties) or important proteins that could not be detected. Likewise, the use of upgraded, improved versions of the wheat genome database (IWGSC refSeqv1.0 was released on Jul. 17, 2018) will need to be integrated for further interrogation of proteomics datasets [1]. Future work is needed to validate our results by way of genomics and transcriptomics, and section 4.3.2. describes a potential workflow for model validation using example molecules detected in our study.

4.3. Current and Future Work

4.3.1. Current Work

The present manuscript describes molecular variation in four cultivars of wheat that were grown in the greenhouse. Data that is currently being interrogated will assess the quantitative

nature of plant defense to WSS through detection of metabolites in a population of wheat varieties (cultivars and advanced breeding lines), grown in the field. These include hollow-stem cultivars Hatcher and Denali, as well as a variety with high performance in the field and constitutive presence of trichomes on its epicuticle, CO11D1397 (data not shown). Plant growth, data collection for two consecutive years and three time points per year, and detection of metabolites using LC-MS across the population have already been conducted. Preliminary results indicate the presence of anti-herbivory metabolites in wheat leaves and stems (e.g., terpenoids, glycosides; Appendix 1). Multivariate analyses (PCA) show clear separation of samples based on metabolite content for dates of harvesting. This suggests variation in time for defense metabolite contents and potential correlation of WSS wheat resistance with growth stage. Further data analysis will determine the metabolite content of each variety and comparisons will be made between plants with differential levels of resistance to *C. cinctus* to establish correlations.

4.3.2. Model Validation Using Genomics and Transcriptomics Approaches

Based on our results, novel aspects of wheat molecular and genetic defense could be exploited to increase yields and meet the demand of the rapidly growing human population. Omics methods allow for the identification and description of complex molecular networks underlying plant defense to stress. These data will be invaluable for wheat geneticists and breeders, because candidate genes that code for critical actors in passive and active defense responses, and that have been detected in our study, can be targeted for crop improvement.

Recent advances in wheat functional genomics, genome editing, and breeding techniques open new avenues for rapid identification and introgression (i.e., transfer of genetic information to another wheat line or cultivar) of desirable traits [2]. Bread wheat (*T. aestivum*) is a hexaploid species and usually has three homoeologous copies of each gene. This drastically reduces the

potential for improvement through genetic mutations because of the complex relationship between gene copies [2]. However, tremendous progress in wheat genetics during the last decade now enables protocols that circumvent major limitations. First, the most current annotated genome assemblies allow for more reliable interpretation of wheat sequencing data and identification of candidate genes and their allelic variants [1]. Observing a gene's function usually requires functional genomics techniques and large mutant populations are available to observe phenotypes that result from knocked-out genes [3]. Since it is very unlikely to induce mutations in the three copies of a gene within the same plant, it is recommended to proceed with crossings of different plants that each carry one mutation. Together with the use of *Triticum durum* wheat (tetraploid) instead of *T. aestivum* plants, speed breeding techniques allow for reduced time and effort for plant growth, and phenotypes are available more quickly [4]. Knock-outs and mutations are achieved through the use of RNAi or CRISPR constructs [5,6].

In the context of wheat resistance to *Cephus cinctus*, the example of increases in proteinase inhibitors in resistant plants may be of major interest for breeders. The introgression of allelic variants in elite lines using the abovementioned techniques would increase their resistance through antibiosis of feeding larvae. Likewise, wheat specialists would benefit from a better understanding of the wax biosynthesis genes (e.g., *TaFAR* genes), that could be mutated to alter the plant epicuticle and reinforce this natural barrier against insect pests [7,8]. A follow-up study can integrate transcriptomics to quantify levels of mRNA associated with resistance to WSS in wheat, including *PR* and *TaFAR* genes. While several *FAR* genes potentially involved in high leaf alcohol content of resistant cultivar Conan have been characterized in wheat, the PR-6 proteinase inhibitor overexpressed in resistant Hatcher was in fact a protein with very high orthology (*e* value = 8×10^{-8}) with a protein from *Arabidopsis thaliana*. Let us focus on two

genes/allelic variants to be introgressed: *T. aestivum* homolog for *AT2G38870* (i.e., encodes a PR peptide that belongs to the PR-6 proteinase inhibitor family) and *TaFAR2* (i.e., wax biosynthetic gene encoding a fatty acyl-coenzyme A reductase that is predominantly responsible for the accumulation of $C_{18:0}$ primary alcohols).

In Colorado, spring wheat is largely supplanted by winter varieties, and desirable traits from resistant cultivar Conan therefore need to be introgressed into a winter cultivar. Likewise, resistant Hatcher shows satisfactory yield rates in the field, but several winter wheat cultivars exceed that performance. In the eventuality that the WSS resistance phenotypes observed in Conan and Hatcher are validated using transcriptomics, and candidate genes have been identified, there is a need to cross these cultivars with another one with superior field performance. A well-performing and widely used line that has been developed by the Colorado wheat breeding program is Byrd. Byrd is a hollow-stem and WSS susceptible wheat cultivar. As mentioned before, the function of candidate genes need to be assessed using functional genomics techniques (e.g., use of TILLING mutant populations to observe knocked-out genes and resulting phenotypes) before crossing.

The next step is to breed for a potentially marketable line. Once genes/allelic variants responsible for the trait of interest are validated, they are introgressed in Byrd. Successive back-crossings (6 to 9) are performed, and at each generation, only the recombinant lines that carry the gene(s)/allele(s) of interest are backcrossed with Byrd to progressively eliminate the genetic background of the WSS resistant line. Then, an advanced near isogenic line (NIL) with Byrd's genetic background, except for the gene/allele of interest, is obtained. In the greenhouse and with novel methods such as speed breeding, three generations per year can be bred, to obtain an advanced line within three years. It takes more time if both the *AT2G38870* homolog and

TaFAR2 are simultaneously introgressed. The advanced line is then grown in the field to assess performance in outdoor conditions. Resistance phenotype of the advanced line is assessed in field trials and molecular studies are conducted to evaluate stem proteinase inhibitor and leaf primary alcohol contents. Wheat breeders ultimately have access to an advanced wheat line with superior yield and high resistance to an economically important pest of wheat in Colorado.

4.3.3. Identification of New Actors in the Wheat/WSS Interaction

Another promising line of research on plant–insect interactions is the study of small non-coding RNA sequences (ncRNAs) such as lncRNAs (long non-coding RNAs) and miRNAs (micro RNAs) using transcriptomics methods. Recent literature describes ncRNAs as key actors of mRNA regulation with implications in plant–pest communication and the response to herbivory [9]. Thousands of lnc/miRNAs from WSS larvae were characterized by Cagirici et al. (2017) and included miR-277, a short RNA sequence that targets several loci on chromosome 3B (region that contains the major stem-solidness QTL *Qss.msub-3BL*). Predicted targets of miR-277 in wheat showed significant similarity to ankyrin-like proteins with known functions in biotic resistance [10]. It is hypothesized that sawfly larvae actively express ncRNAs to suppress the defense response in wheat. Given the great diversity in small non-coding RNA sequences, their involvement in plant resistance is also expected. Future work on the response of wheat to WSS infestations warrants the integration of transcriptomics tools to elucidate the role of ncRNA cross-talk between plants and insects and provide novel targets for wheat breeding.

REFERENCES

1. Clavijo, B.J.; Venturini, L.; Schudoma, C.; Accinelli, G.G.; Kaithakottil, G.; Wright, J.; Borrill, P.; Kettleborough, G.; Heavens, D.; Chapman, H.; Lipscombe, J.; Barker, T.; Lu, F.H.; McKenzie, N.; Raats, D.; Ramirez-Gonzalez, R.H.; Coince, A.; Peel, N.; Percival-Alwyn, L.; Duncan, O.; Trosch, J.; Yu, G.; Bolser, D.M.; Namaati, G.; Kerhornou, A.; Spannagl, M.; Gundlach, H.; Haberer, G.; Davey, R.P.; Fosker, C.; Palma, F.D.; Phillips, A.L.; Millar, A.H.; Kersey, P.J.; Uauy, C.; Krasileva, K.V.; Swarbreck, D.; Bevan, M.W.; Clark, M.D. An improved assembly and annotation of the allohexaploid wheat genome identifies complete families of agronomic genes and provides genomic evidence for chromosomal translocations. *Genome Res.* **2017**, *27*, 885–896.

2. Uauy, C.; Wulff, B.B.H.; Dubcovsky, J. Combining traditional mutagenesis with new high-throughput sequencing and genome editing to reveal hidden variation in polyploid wheat. *Annu. Rev. Genet.* **2017**, *51*, 435–454.

3. Wheat TILLING resource. Available online: http://www.wheat-tilling.com/.

4. Watson, A.; Ghosh, S.; Williams, M.J.; Cuddy, W.S.; Simmonds, J.; Rey, M.D.; Asyraf Md Hatta, M.; Hinchliffe, A.; Steed, A.; Reynolds, D.; Adamski, N.M.; Breakspear, A.; Korolev, A.; Rayner, T.; Dixon, L.E.; Riaz, A.; Martin, W.; Ryan, M.; Edwards, D.; Batley, J.; Raman, H.; Carter, J.; Rogers, C.; Domoney, C.; Moore, G.; Harwood, W.; Nicholson, P.; Dieters, M.J.; DeLacy, I.H.; Zhou, J.; Uauy, C.; Boden, S.A.; Park, R.F.; Wulff, B.B.H.; Hickey, L.T. Speed breeding is a powerful tool to accelerate crop research and breeding. *Nat. Plants* **2018**, *4*, 23–29.

5. Uauy, C.; Distelfeld, A.; Fahima, T.; Blechl, A.; Dubcovsky, J. A NAC gene regulating senescence improves grain protein. *Science* **2006**, *314*, 1298–1301.

6. Zhang, Y.; Bai, Y.; Wu, G.; Zou, S.; Chen, Y.; Gao, C.; Tang, D. Simultaneous modification of three homoeologs of *TaEDR1* by genome editing enhances powdery mildew resistance in wheat. *Plant J.* **2017**, *91*, 714–724.

7. Zhang, Z.; Wei, W.; Zhu, H.; Challa, G.S.; Bi, C.; Trick, H.N.; Li, W. *W3* is a new wax locus that is essential for biosynthesis of β-diketone, development of glaucousness, and reduction of cuticle permeability in common wheat. *PLoS One* **2015**, *10*, e0140524.

8. Wang, M.; Wang, Y.; Wu, H.; Xu, J.; Li, T.; Hegebarth, D.; Jetter, R.; Chen, L.; Wang, Z. Three *TaFAR* genes function in the biosynthesis of primary alcohols and the response to abiotic stresses in *Triticum aestivum*. *Sci. Rep.* **2016**, *6*, 25008.

9. Cagirici, H.B.; Biyiklioglu, S.; Budak, H. Assembly and annotation of transcriptome provided evidence of miRNA mobility between wheat and wheat stem sawfly. *Front. Plant Sci.* **2017**, *8*, 1653.

10. Lu, H.; Rate, D.N.; Song, J.T.; Greenberg, J.T. ACD6, a novel ankyrin protein, is a regulator and an effector of salicylic acid signaling in the *Arabidopsis* defense response. *Plant Cell* **2003**, *15*, 2408–2420.

APPENDIX 1 – FIELD WHEAT EXPERIMENT

A.1. Summary

Increasing incidence and severity of Wheat Stem Sawfly (*Cephus cinctus*, WSS) infestations in Colorado wheat (*Triticum aestivum* L.) support the need to understand metabolic variation related to herbivore defense in field-grown plants. A study was performed that evaluated leaf and stem tissue collected from a population of 100 wheat varieties (a mixture of both cultivars and advanced breeding lines) in a WSS-infested field. Leaves and stems were collected at six time points over the course of two years (2015 and 2016). Metabolites were extracted and detected using LC-MS non-targeted metabolomics. A total of 669 metabolites were detected between tissues and among varieties, of which 160 were annotated. The LC-MS data was associated to measures of plant resistance including yield components (test weight, grain yield) and infestation rates per plot (percent infestation, live larvae, dead larvae, frass without larvae), using multivariate regression modeling. Preliminary results provide evidence of a molecular basis of field resistance to WSS.

A.2. Methodology

A.2.1. Plant Material

Metabolite profiles were obtained from a total of 100 wheat varieties (*Triticum aestivum* L., Poaceae). Wheat plants were grown in the field (New Raymer, CO, USA) under conventional conditions (e.g., precipitation, temperature, photoperiod). Data was collected for two consecutive years and three harvesting time points per year (Figure 20). The total number of cultivars and advanced breeding lines planted in 2015 (n = 100) was assessed, and only those that were planted in both years were assessed for the 2016 data (n = 36). The three harvesting dates of each

year were relatively close across years to improve reproducibility of the results, and corresponded to, respectively, jointing (approximately Zadoks growth stage 30), heading (approximately Zadoks 55), and flowering stages (approximately Zadoks 65) [1]. All plants were planted the year prior to harvest for obligate vernalization, that is Sep. 18, 2014, for wheat harvested in 2015 and Sep. 18, 2015, for wheat harvested in 2016. Wheat varieties were harvested on Jul. 30, 2015, and Jul. 14, 2016, for 2015 and 2016 measurements, respectively. Plants were grouped in randomized complete block designs.

A.2.2. Field Measurements

For each variety, plots were 5 feet wide by 12 feet long and seeded at an approximate density of 700,000 seeds per acre, in 6 rows per plot with 9-inch spacing between rows. Plots were harvested using a Wintersteiger Elite combine with a Grainguage weighing system. An area of 60 square feet was used for yield calculations and adjusted to 12% moisture basis according to the moisture value provided by the combine. Test weight was determined from the Grainguage weighing system on an uncleaned sample of the grain. Soil fertility amendments were applied by the cooperating farmer based on soil fertility recommendations appropriate for the area.

Wheat Stem Sawfly adult counts in the field were measured for the years 2015 and 2016 by doing one hundred 180-degree sweeps at 7 different sites (New Raymer, CO, USA) and various sampling dates (= 100 sweeps per site per date; Figure 20). Insect sweeps were conducted along the field edge bordering the wheat/fallow border. Mean WSS infestation per sampling date was calculated as follows: (total WSS adults across all sites × 100 sweeps)/(number of sampled sites × 100 sweeps). Field infestation indicators (i.e., percent infestation, live larvae, dead larvae, frass without larvae) were determined by collecting wheat stubble after harvest from the middle of plots using a shovel. One hundred tillers were randomly

selected for each variety and bisected in the lab using a scalpel to determine presence/absence and state of WSS larvae. Infestation percentages were calculated as such: % = (infested tillers/total number of tillers) × 100.

A.2.3. Tissue Collection from Field Sites and Metabolite Extraction

For metabolomics analysis, 1091 tissue samples were collected from 624 plants (with either one or two biological replicates per plant per harvesting date per year) and used for metabolite extraction. One leaf and one stem were collected from three plants within a plot (one single variety) and pooled in a single tube, and each variety was planted in either one or two plots (50 varieties planted in one plot, 50 varieties planted in two plots). Replicated plots were not pooled and thus a total of 50 + 50 × 2 = 150 samples were collected per time point (harvesting date). Plants were harvested at three time points per year, during two years (2015 and 2016) and for both tissues, except 2016 where stems were only collected at two time points (Figure 20). Leaves and stems from each sample were then separated for metabolomics analysis. In total, 150 samples × 3 times points × 2 years × 2 tissues = 1800 samples collected from 900 plants in theory, but some were lost in the sample preparation process (e.g., tube cracking during tissue grinding) or did not contain enough tissue material for extraction.

Equivalent positions were probed in all cultivars: the fourth leaf of each plant (starting from the flag leaf), and stems at the third and fourth internodes (starting from the first internode, also termed peduncle), were collected and separated, flash frozen in liquid nitrogen, temporarily stored on dry ice in the field, and transferred to –80 °C for storage (Figure 21). Samples were lyophilized for 72 h. Dried, frozen separated leaves and stems were then placed in 5 mL conical centrifuge tubes and ground to a fine powder using a mix of 3.2 mm and 11 mm diameter

stainless steel beads (Next Advance, Troy, NY, USA) and a Buller Blender Storm 5 tissue homogenizer (Next Advance).

Non-volatile metabolites were extracted as previously described with the following modifications [2]. Briefly, 25 mg of powdered leaves and stems were transferred to 2 mL glass vials and immersed in 1 mL of a cold methanol:methyl tert-butyl ether (MTBE) solution (2:1, 75% methanol:MTBE; Sigma-Aldrich). Samples were vortexed for 1 h at 4 °C and 300 µL of cold liquid chromatography grade water (Sigma-Aldrich) were then added to the mixture. Samples were centrifuged for 15 min (4 °C, 2850 g), and the isolated aqueous layer was transferred to a new glass vial. Water-soluble extracts were then evaporated under a continuous gas nitrogen flow and reconstituted in 100 µL of methanol:water (1:1, v/v).

A.2.4. Metabolite Detection by LC-MS

Non-targeted metabolite profiling was performed using LC-MS as previously described [2]. Briefly, 2 µL of extracts were injected onto an Acquity UPLC system (Waters Corporation, Milford, MA, USA) in discrete, randomized blocks with a pooled QC injection after every seven sample injections. Compounds were separated using an Acquity UPLC CSH phenyl hexyl column (1.7 µm, 1.0 × 100 mm; Waters Corporation), using a gradient from solvent A (2 mM ammonium hydroxide, 0.1% formic acid) to solvent B (acetonitrile, 0.1% formic acid). Injections were made in 100% A, held for 1 min, ramped to 98% B over 12 min, held at 98% B for 3 min, and then returned to starting conditions over 0.05 min and allowed to re-equilibrate for 3.95 min, with a 200 µL/min constant flow rate. The column and samples were held at 65 °C and 6 °C, respectively. The column eluent was infused into a Xevo G2 Q-TOF mass spectrometer (Waters Corporation) with an electrospray source in positive ion mode, scanning 50-2000 *m*/*z* at a rate of five scans per s, alternating between MS (6 V collision energy) and MS^E mode (15–30 V ramp).

Calibration was performed prior to sample analysis using sodium iodide with 1 ppm mass accuracy. The capillary voltage was held at 2200 V, the source temperature at 150 °C, and nitrogen desolvation temperature at 350 °C with a gas flow rate of 800 L/h. Experimental data was collected using an indiscriminate approach (data independent MS/MS = idMS/MS), and two spectral clusters for each detected compound were used – one for low energy MS and one for high energy MS/MS.

A.2.5. Data Processing and Annotation

A matrix of molecular features as defined by retention time and mass (m/z) was created from LC-MS data files after conversion to .cdf format and processing by XCMS [3] in R v3.4.4 [4]. The R package RAMClust was used to deconvolute data into spectral clusters [5]. Molecular features were normalized to total ion current (TIC), the relative quantity of each feature was determined by the mean area of the chromatographic peak among two replicate injections (n = 2), and spectral clusters were quantified as a weighted abundance of all molecular features in the cluster. Identification of metabolites was performed manually by matching mass spectra and retention times to in-house and external databases including METLIN [6,7] and the Human Metabolome Database (HMDB) [8], as well as using custom R scripts. In short, the R package InterpretMSSpectrum was used to infer molecular weights, the MS-FINDER program v2.40 [9,10] allowed for inference of chemical formulas and structures, the Chemical Translation Service web application program interface (API) was used to retrieve chemical names of compounds with available International Chemical Identifiers (InChIKey), and the ClassyFire web API was used to look up full chemical ontology [11]. Confidence levels were all assigned based upon classification of metabolite annotation by Sumner et al. (2007) [12]. All annotated metabolites in this study were assigned a level 1 or 2 confidence.

A.2.6. Statistical Analysis

Metabolite contents were compared using Student's *t* tests and ANOVA with *p* thresholds of 0.05. Differences in content identified using ANOVA were further compared with Tukey HSD pairwise comparisons. Benjamini–Hochberg correction was systematically applied across all *t* tests and ANOVA output [12]. Principal component analysis (PCA) modeling was conducted on the LC-MS data after log-transforming, mean-centering and unit variance (UV)-scaling using SIMCA v14.1 (MKS Data Analytics, Umea, Sweden).

A.3. Results

A.3.1. Description of Detected Metabolites

A total of 669 putative compounds were detected using LC-MS metabolomics. Of these, 635 (95%) were assigned a chemical formula. One hundred and sixty (24% of total) compounds were tentatively annotated and were assigned a level 1 or 2 annotation confidence. Classification of annotated metabolites based on chemical structures yielded ontology trees for 128 compounds (19% of total; Table S2). Metabolites were sorted within ten chemical superclasses (i.e., alkaloids, benzenoids, hydrocarbons, lignans, lipids, nucleosides, organic acids, organic nitrogen/oxygen compounds, phenylpropanoids). Nine ontology levels were used in the classification, from chemical kingdom (highest chemical hierarchy, i.e., organic compounds) to parent level 5 (lowest hierarchy, e.g., α amino acids). In the metabolomics dataset, the classification analysis revealed the presence of one alkaloid or derivative, ten benzenoids (including a methoxyphenol structure described in Chapter 3 as being potentially involved in WSS parasitoid attraction), seven hydrocarbons and derivatives, one lignan, 58 lipids, one nucleoside, 11 organic acids and derivatives including seven carboxylic acids, two organic nitrogen compounds, 11 organic oxygen compounds (e.g., two carbohydrates and conjugates,

and three alcohols and polyols), 15 organoheterocyclic compounds, and ten phenylpropanoids and polyketides including three flavonoids and two coumarins. Metabolomics output and data from the field were further compiled in a matrix that includes relative abundances of all putative compounds, for all samples, as well as measures of plant resistance including yield components (test weight, grain yield) and infestation rates per plot (percent infestation, live larvae, dead larvae, frass without larvae; Table S3).

A.3.2. Metabolites Varied between Tissues of Wheat

564 putative compounds (84% of total) varied between leaves and stems of wheat based on univariate statistics results (*t* test, FDR adjusted $p < 0.05$). Multivariate statistics were also conducted and revealed separation of leaf and stem samples based on metabolite content (Figure 22).

A.3.3. Metabolites Varied among Harvesting Dates

303 putative compounds (45% of total) varied between 2015 and 2016 (*t* test, FDR adjusted $p < 0.05$), 563 compounds (84% of total) varied among harvesting dates of 2015 (ANOVA, FDR adjusted $p < 0.05$), and 518 compounds (77% of total) varied among harvesting dates of 2016 (ANOVA, FDR adjusted $p < 0.05$). Multivariate modeling showed separation of samples based on date of harvest (Figure 23). Principal component analysis conducted on leaves of the 100 wheat varieties revealed grouping of samples with similar harvesting dates between years (e.g., samples collected on Mar. 31, 2015 and Mar. 29, 2016 are relatively close in the PCA model, denoting similar metabolite contents; Figure 23A). Similar results were obtained when comparing stem samples (Figure 23B).

A.3.4. Preliminary Conclusions

Taken together, preliminary results using multivariate analyses (PCA) show clear separation of samples based on metabolite content for dates of harvesting. This suggests variation in time for defense metabolite contents and potential correlation of WSS wheat resistance with growth stage. Further data analysis will determine the metabolite content of each line/cultivar and comparisons will be made between plants with differential levels of resistance to *C. cinctus* to establish correlations. The tremendous efforts made in our lab to decipher the molecular basis of wheat resistance to a major insect pest will ultimately contribute to the identification of candidate genes and QTLs that will further be assessed and introgressed for their role in the defense response to herbivory.

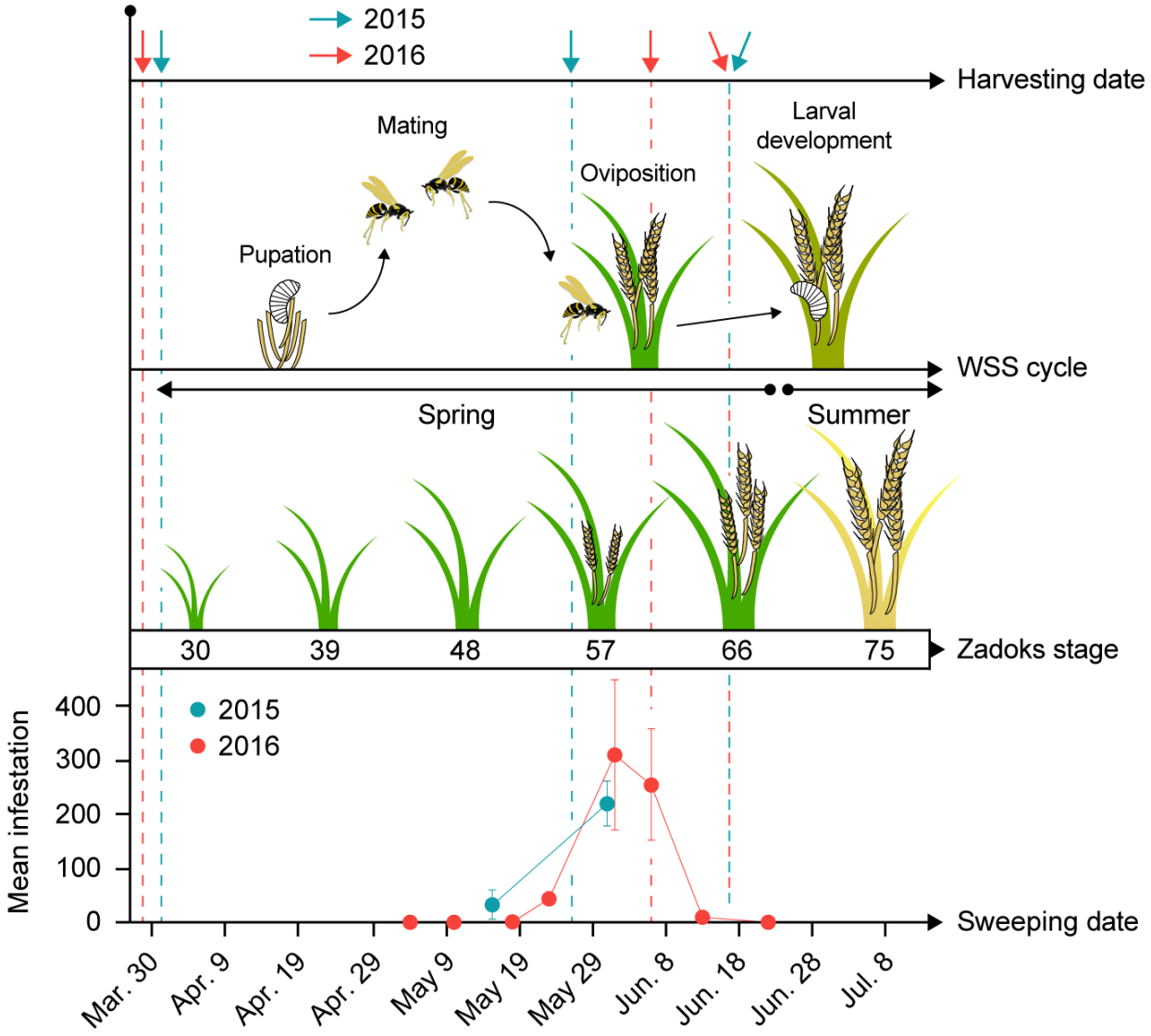

Figure 20. Wheat tissue harvesting dates in relationship with WSS infestation periods. Wheat leaves and stems were harvested at dates indicated by colored arrows and dashed lines. Corresponding wheat Zadoks stage and WSS cycle period and field infestation are also illustrated. For both years, each infestation data point was calculated as follows: (total WSS adults across all sites × 100 sweeps)/(number of sampled sites × 100 sweeps) ± standard error of the mean.

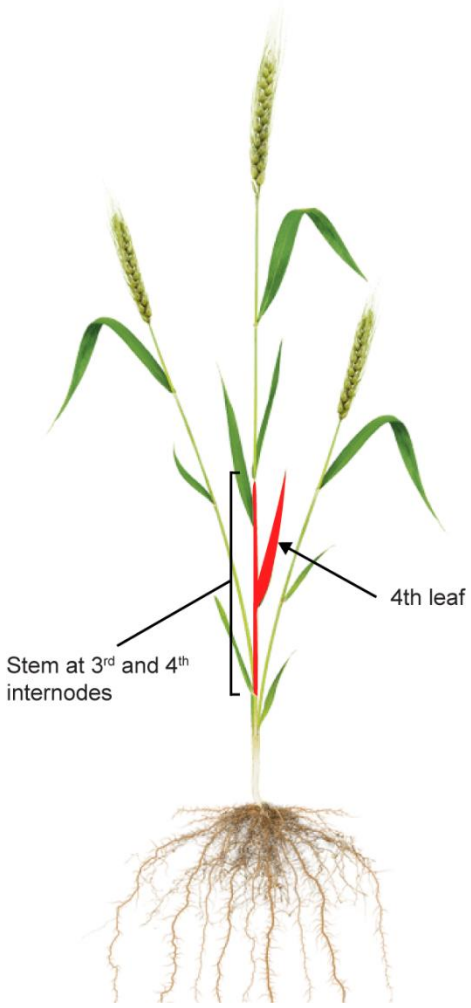

Figure 21. Probing position of wheat tissue during field sampling. The fourth leaf of each plant (starting from the flag leaf), and stems at the third and fourth internodes (starting from the first internode, also termed peduncle), were collected and separated for metabolomics analysis.

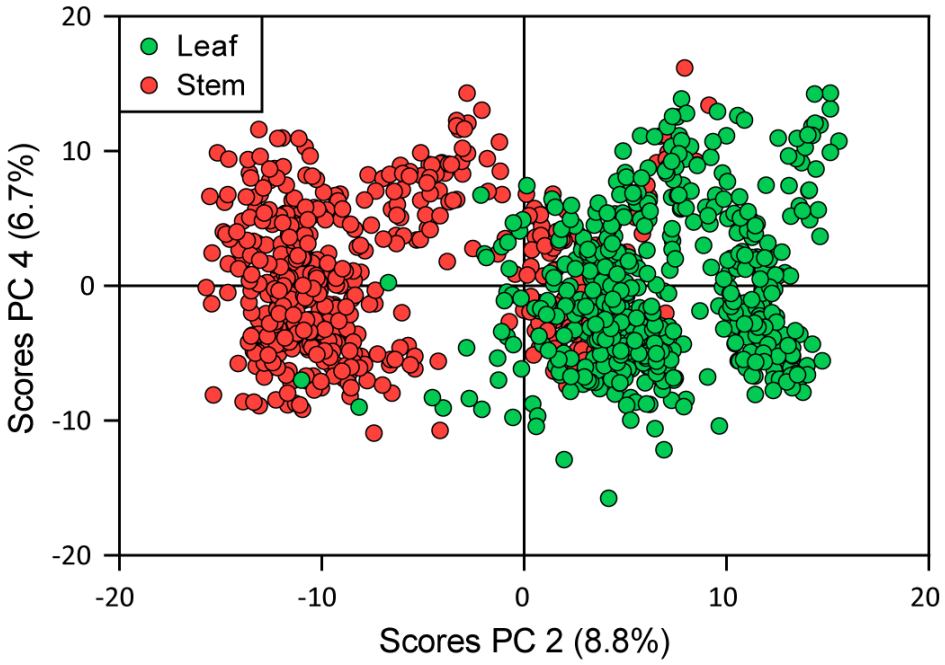

Figure 22. Metabolite distribution in leaf and stem tissue. Multivariate analysis demonstrating specific composition in cuticular wax chemistry between leaves and stems of wheat. Principal component analysis (PCA) of the 100 varieties showed that most metabolite variation was due to differences between leaves and stems. Each PC score point represents the metabolite profile for a single biological replicate (n = 1–12 replicates per variety). Abbreviation: PC = principal component.

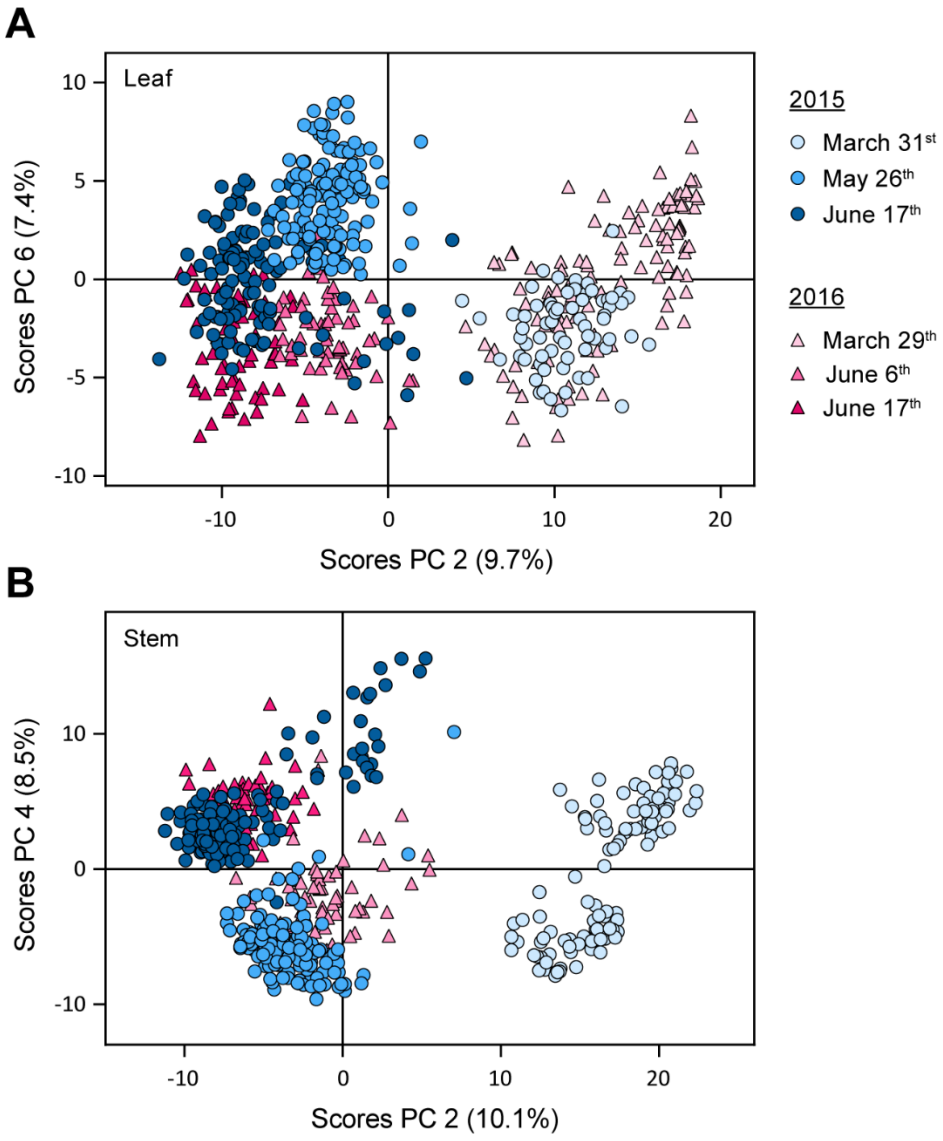

Figure 23. Metabolite levels among dates of harvest within leaves and stems of wheat. Principal component analysis showed variation for different dates of harvest (including growth stage and year) within leaf **(A)** and stem **(B)** tissue. Abbreviation: PC = principal component.

REFERENCES

1. Zadoks, J.C.; Chang, T.T.; Konzak, C.F. A decimal code for the growth stages of cereals. *Weed Res.* **1974**, *14*, 415–421.

2. Broeckling, C.D.; Prenni, J.E. Stacked injections of biphasic extractions for improved metabolomic coverage and sample throughput. *Anal. Chem.* **2018**, *90*, 1147–1153.

3. Smith, C.A.; Want, E.J.; O'Maille, G.; Abagyan, R.; Siuzdak, G. XCMS: processing mass spectrometry data for metabolite profiling using nonlinear peak alignment, matching, and identification. *Anal. Chem.* **2006**, *78*, 779–787.

4. R Core Team. R: a language and environment for statistical computing. **2017**, R Foundation for Statistical Computing, Vienna, Austria (https://www.R-project.org/).

5. Broeckling, C.D.; Afsar, F.A.; Neumann, S.; Ben-Hur, A.; Prenni, J.E. RAMClust: a novel feature clustering method enables spectral-matching-based annotation for metabolomics data. *Anal. Chem.* **2014**, *86*, 6812–6817.

6. METLIN database. Available online: http://metlin.scripps.edu/.

7. Tautenhahn, R.; Cho, K.; Uritboonthai, W.; Zhu, Z.; Patti, G.J.; Siuzdak, G. An accelerated workflow for untargeted metabolomics using the METLIN database. *Nat. Biotechnol.* **2012**, *30*, 826–828.

8. Human Metabolome Database. Available online: http://www.hmdb.ca/.

9. Tsugawa, H.; Kind, T.; Nakabayashi, R.; Yukihira, D.; Tanaka, W.; Cajka, T.; Saito, K.; Fiehn, O.; Arita, M. Hydrogen rearrangement rules: computational MS/MS fragmentation and structure elucidation using MS-FINDER software. *Anal. Chem.* **2016**, *88*, 7946–7958.

10. Lai, Z.; Tsugawa, H.; Wohlgemuth, G.; Mehta, S.; Mueller, M.; Zheng, Y.; Ogiwara, A.; Meissen, J.; Showalter, M.; Takeuchi, K.; Kind, T.; Beal, P.; Arita, M.; Fiehn, O. Identifying metabolites by integrating metabolome databases with mass spectrometry cheminformatics. *Nat. Methods* **2018**, *15*, 53–56.

11. Feunang, Y.D.; Eisner, R.; Knox, C.; Chepelev, L.; Hastings, J.; Owen, G.; Fahy, E.; Steinbeck, C.; Subramanian, S.; Bolton, E.; Greiner, R.; Wishart, D.S. ClassyFire: automated chemical classification with a comprehensive, computable taxonomy. *J. Cheminform.* **2016**, *8*, 61.

12. Sumner, L.W.; Amberg, A.; Barrett, D.; Beale, M.H.; Beger, R.; Daykin, C.A.; Fan, T.W.; Fiehn, O.; Goodacre, R.; Griffin, J.L.; Hankemeier, T.; Hardy, N.; Harnly, J.; Higashi, R.; Kopka, J.; Lane, A.N.; Lindon, J.C.; Marriott, P.; Nicholls, A.W.; Reily, M.D.; Thaden, J.J.; Viant, M.R. Proposed minimum reporting standards for chemical analysis. *Metabolomics* **2007**, *3*, 211–221.